Mixed-conducting perovskite membranes for oxygen separation

Towards the development of a supported thin-film membrane

Marco van der Haar

Mixed-conducting perovskite membranes for oxygen separation
towards the development of a supported thin-film membrane

MIXED-CONDUCTING PEROVSKITE MEMBRANES FOR OXYGEN SEPARATION

TOWARDS THE DEVELOPMENT OF A
SUPPORTED THIN-FILM MEMBRANE

PROEFSCHRIFT

ter verkrijging van

de graad van doctor aan de Universiteit Twente,

op gezag van de rector magnificus,

prof. dr. F.A. van Vught,

volgens besluit van het College voor Promoties

in het openbaar te verdedigen

op donderdag 21 juni 2001 te 13:15 uur

door

Lubertus Marco van der Haar

geboren op 15 september 1972

te Ermelo

Dit proefschrift is goedgekeurd door de promotor

prof. dr. ir. H. Verweij

en de assistent promotor

dr. H.J.M. Bouwmeester

*Education is an admirable thing, but it is well
to remember from time to time
that nothing that is worth knowing can be taught*

Oscar Wilde

Aan mijn ouders

Contents

1

Introduction

1.1   Application of dense ceramic membranes

A bright application perspective has developed for dense mixed conducting membranes. Since the mid 1980s, the scientific and industrial interest in these membranes has grown extensively. Currently, their possible use as oxygen separation membranes is regarded as a cost-effective, clean and flexible route for the production of oxygen from air.

Since oxygen is one of the most widely used chemicals, in power generation, industry and healthcare, there is vast economical interest in developing more efficient production facilities. Up till now, oxygen is mainly produced through cryogenic destillation of air. The major drawback of this process lies in its high energy costs, making it economically feasible only on large production scales. Another, more flexible way of producing oxygen is based on selective gas adsorption. In this process, called Pressure Swing Adsorption (PSA), nitrogen is selectively adsorbed on a zeolite or a carbon molecular sieve, resulting in oxygen enrichment of the gas phase [1]. This technique is suitable for small-scale oxygen production, but it has the disadvantage of being discontinuous. Furthermore, the production costs sharply rise when oxygen purities higher than 95% are required. Compared to these conventional techniques, oxygen production via dense membranes can offer substantial advantages. Owing to the nature of the separation process, oxygen can be obtained with infinite selectivity. Besides their application in oxygen production, the integration of dense membranes into membrane reactors is considered very promising. These reactors, combining separation and catalytic conversion, are considered an attractive route for partial hydrocarbon oxidation of which the production of syngas from methane is the most prominent example. It is therefore not surprising that the first pioneering studies have triggered extensive scientific and technological interest in dense ceramic membranes, which has resulted in a considerable number of patent applications [2-8]. This chapter provides a concise introduction into the main topics concerning dense ceramic membranes

for oxygen separation. For a comprehensive overview of the recent developments in dense ceramic membrane research, the reader is referred to Bouwmeester and Burggraaf [9].

1.2   Membrane concepts

Dense membranes derive their capability for oxygen separation from the presence of oxygen vacancies in the crystal lattice of the membrane material. Oxygen is incorporated and released from the lattice at the high and low oxygen chemical potential side respectively, according to the reaction:

$$O_2 + 2V_O^{\cdot\cdot} \leftrightarrows 2O_O^x + 4h^{\cdot} \tag{1.1}$$

Since the membrane is dense, passage of molecular oxygen through pores is not possible. Yet, the vacancies enable anionic oxygen to be selectively transported through the lattice via a hopping mechanism, providing there is a driving force, i.e. a gradient in oxygen chemical potential. This is feasible only when the oxygen ions possess enough thermal energy to overcome the energy barrier to hop from one crystallographic site to the other. This requires elevated membrane operation temperatures, typically in the range from 700°C to 1100°C. Furthermore, since the oxygen *ions* are transported, counter-transport of electronic charge carriers is required to maintain charge neutrality.

As schematically shown in figure 1.1, several membrane concepts are possible, all of them employing a dense ceramic oxygen ion conducting material. Concept (a), called an *oxygen pump* [10], is based on a material conductive only for oxygen ions, i.e. a solid electrolyte. Electrodes and wiring are required for the (external) counter transport of electrons. The electrodes need to be porous since oxygen can only be incorporated into or released from the oxide lattice at the triple phase boundary between the electrolyte, electrode and gas phase. The driving force for oxygen transport is applied as a potential difference between the electrodes. In concept (b) the external wiring is replaced by a metallic phase being dispersed in the solid electrolyte, thereby forming a percolative network. The driving force for diffusion is the difference in oxygen partial pressure applied across this *dual phase membrane* [11]. Similar to the previous concept, oxygen can only be incorporated or released at the triple phase boundary. Employing a single phase *mixed electron and ion conducting oxide* as illustrated in concept (c) relieves this restriction. These materials show both a high ionic and electronic conductivity and therefore allow large oxygen fluxes, as firstly reported by Teraoka *et al.* [12]. These mixed conducting materials are in the focal point of this thesis.
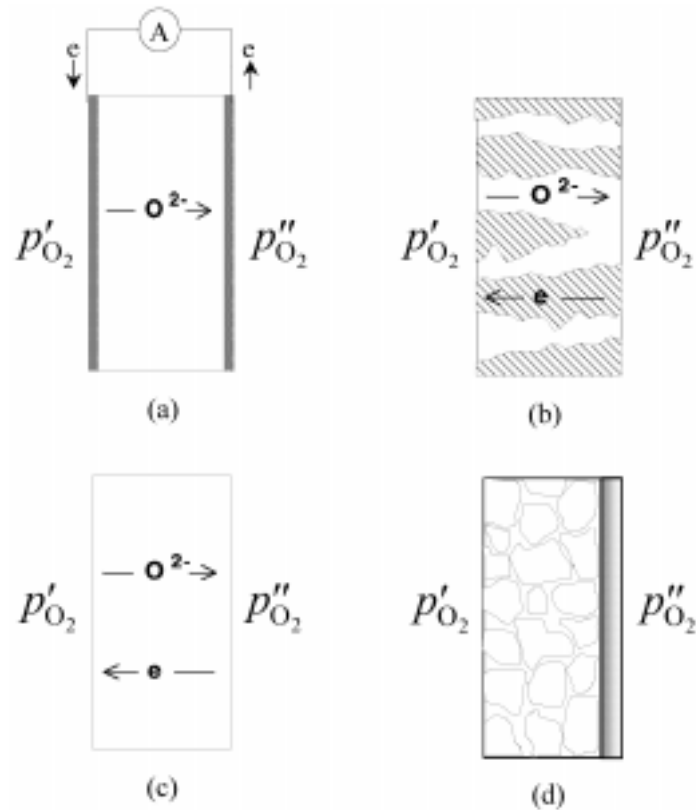
Figure 1.1: Various membrane concepts employing a dense oxygen ion conducting material: (a) oxygen pump, (b) dual-phase membrane, (c) mixed conducting oxide and (d) thin supported mixed oxide.

1.3 Mixed conducting perovskites

Currently, the acceptor-doped perovskite-type oxides with general formula $La_{1-x}A_xCo_{1-y}B_yO_{3-\delta}$ (A = Sr, Ba, Ca and B = Fe, Cu, Ni) are ranked among the most promising materials for oxygen separation membranes. In these compounds, which show excellent electronic and ionic conductivity, the substitution of La^{3+} with alkaline earth metal ions at the A-site strongly increases the formation of oxygen vacancies. For instance, the incorporation of Sr^{2+} in a $LaCoO_3$ host lattice is represented in Kröger-Vink notation as:

$$SrCoO_3 \xrightarrow{\text{LaCoO}_3} Sr_{La}^{'} + Co_{Co}^{\cdot} + 3O_O^{x} \qquad (1.2)$$
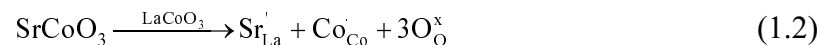
Charge compensation takes place through an increase in the net valency of the transition metal at the B-site[*]. Equation (1.2) represents the first of two possible charge

---

[*] In-depth studies [13] have shown that in $La_{1-x}Sr_xCoO_{3-\delta}$ the charge is not localised on the Co-ions, but is in fact delocalised in a broad conduction band. However, this does not change the essence of the presented mechanism for oxygen vacancy formation.

compensation mechanisms. The second mechanism involves the actual formation of oxygen vacancies:

$$2Co_{Co}^{\cdot} + \tfrac{1}{2}O_O^x \leftrightarrows Co_{Co}^x + V_O^{\cdot\cdot} + \tfrac{1}{2}O_2 \qquad (1.3)$$
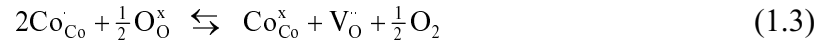
Which of these charge compensation mechanisms prevails depends on temperature and oxygen partial pressure. In La$_{1-x}$Sr$_x$CoO$_{3-\delta}$, δ can attain values up to 0.35. This illustrates the stability of the perovskite structure: it allows both high dopant concentrations and the accompanying high degree of oxygen non-stoichiometry.

1.4   Oxygen transport through mixed conducting membranes

When a gradient in oxygen chemical potential is applied across a dense mixed conducting membrane, vacancy-mediated oxygen transport occurs from the high to the low oxygen chemical potential side accompanied by a counter flux of electrons or electron holes. Besides bulk transport, oxygen transfer occurs across the interface between the gas phase and the oxide.

1.4.1   Bulk transport

In general, when cross terms between fluxes are neglected, the flux of the charged species under an electrochemical potential gradient is given by [14]:

$$j_i = \frac{-\sigma_i}{z_i^2 F^2}\nabla\eta_i \qquad (1.4)$$

in which σ_i is the conductivity, z_i the charge number and F the Faraday constant. For each species, the gradient in electrochemical potential is given by:

$$\nabla\eta_i = \nabla\mu_i + z_i F \nabla\phi \qquad (1.5)$$

In this expression $\nabla\mu_i$ and $\nabla\phi_i$ represent the gradient in chemical and electrical potential, respectively. Under steady state conditions, the counter flux of electronic charge carriers balances the oxygen anion flux, thereby preventing charge accumulation:

$$2j_{O^{2-}} = j_{h^{\cdot}} - j_{e^{'}} \qquad (1.6)$$

Assuming local chemical equilibrium and using $j_{O_2} = \tfrac{1}{2}j_{O^{2-}}$, an expression for the oxygen flux through the membrane can be derived by combining equations (1.4) to (1.6):

$$j_{O_2} = -\frac{t_{el}\sigma_{ion}}{16F^2}\nabla\mu_{O_2} \qquad (1.7)$$

where t_{el} and σ_{ion} are the electronic transference number and ionic conductivity respectively. Integrating equation (1.7) over the membrane thickness L, using $\nabla\mu_i = RT\dfrac{\partial \ln P_{O_2}}{\partial x}$, yields the Wagner equation [15]:

$$j_{O_2} = -\frac{RT}{16F^2 L} \int\limits_{\ln P'_{O_2}}^{\ln P''_{O_2}} t_{el}\sigma_{ion} d\ln P_{O_2} \tag{1.8}$$

in which the prime and double prime denote the high and low oxygen partial pressure side of the membrane respectively. It is important to note that according to equation (1.8) the flux is inversely proportional to the membrane thickness.

1.4.2 Influence of surface processes

Equation (1.8) is valid only when the bulk transport of oxygen rate limits the oxygen permeation. In practice, the surface exchange reactions proceeding at the gas-oxide interface always, to some degree, exert control over the permeation rate [16]. As a consequence, part of the chemical potential difference is consumed by interfacial oxygen exchange, as illustrated in figure 1.2. Decreasing the membrane thickness increases the part of the driving force consumed by the surface processes, finally rendering the rate of oxygen permeation independent of membrane thickness.
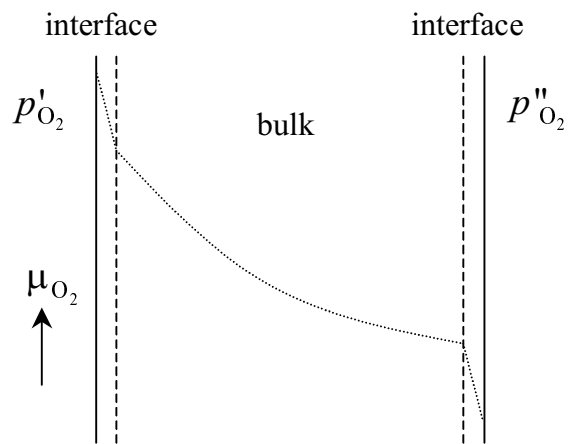
Figure 1.2: Schematic representation of the oxygen chemical potential profile during steady state permeation through a symmetric membrane

To derive a parameter that distinguishes between surface exchange and bulk diffusion controlled kinetics, the case of mixed rate control is considered. In this situation the surface and bulk processes consume an equal amount of the total driving force:

$$\Delta\mu_{O_2}^{bulk} = \Delta\mu_{O_2}^{surface} \tag{1.9}$$

When an *asymmetric* membrane is considered in which the surface reaction is rate limiting only at *one* surface, $\Delta\mu_{O_2}^{surface}$ comprises the total chemical potential drop over this interface. Using Wagner's equation for the bulk transport and Onsager's relation for the surface exchange, the flux balance reads:

$$\frac{\overline{t_{el}\sigma_{ion}}}{16F^2 L}\Delta\mu_{O_2}^{bulk} = j_{ex}^0 \frac{\Delta\mu_{O_2}^{surface}}{RT} \tag{1.10}$$

The parameter j_{ex}^0 represents the exchange flux in the absence of a chemical potential gradient and is related to the surface exchange coefficient k_s through [9]:

$$j_{ex}^0 = \tfrac{1}{4} k_s c_o \qquad (1.11)$$

which is accessible via ^{18}O-^{16}O exchange experiments. Combination of equations (1.9) and (1.10) yields an expression for the characteristic membrane thickness L_c at which the surface and the diffusion process consume an equal share of the total driving force:

$$L_c = \frac{RT}{16F^2} \frac{t_{el}\sigma_{ion}}{j_{ex}^0} \qquad (1.12)$$

In equation (1.12) the averaging bar over $t_{el}\sigma_{ion}$ is omitted since small p_{O_2} gradients are considered. In the case of a symmetrical membrane, the overall flux equation can be written as [9]:

$$j_{O_2} = -\frac{1}{1+(2L_c/L)} \frac{t_{el}\sigma_{ion}}{16F^2} \frac{\Delta\mu_{O_2}^{total}}{L} \qquad (1.13)$$

The factor 2 in the denominator is introduced since in the case of a symmetrical membrane the exchange processes at *both* surfaces can be rate limiting. In this case the membrane thickness at which the surface and the diffusion process consume an equal share of the total driving force is $2L_c$. For large membrane thicknesses, equation (1.13) transforms into Wagner's equation for bulk transport with the flux proportional to L^{-1}. For membrane thicknesses well below $2L_c$ the flux is independent of L. Therefore, the value of L_c is a convenient parameter in determining the influence of bulk and surface processes on the rate of oxygen permeation. In general, it can be stated that decreasing the membrane thickness below approximately $0.1L_c$ is not useful, since no significant gain in flux can be achieved anymore.

1.4.3   Determination of L_c

When it is assumed that the ionic conductivity is much smaller than the electronic conductivity, which is generally true for the acceptor-doped cobaltites and ferrites, equation (1.12) can be simplified by making use of the Nernst-Einstein relation:

$$\sigma_{ion} = \frac{c_O D_c z_{O^{2-}}^2 F^2}{RT} \qquad (1.14)$$

in which D_c represents the component-diffusion coefficient of the oxygen anions with valence charge $z_{O^{2-}} = -2$. Substitution reduces the expression for L_c to:

$$L_c = \frac{D_c}{k_s} \qquad (1.15)$$

When correlation effects and effects due to mass difference between the component and a corresponding tracer component are neglected, the component-diffusion coefficient D_c is equal to the tracer diffusion coefficient D^* [17]. Both D^* and k_s can readily be determined with [18]O-^{16}O exchange experiments [18,19], by fitting the isotope diffusion profiles with the appropriate diffusion model.

Another convenient method for determining L_c is provided by chemical relaxation-type experiments [20,21,22]. In these experiments a physical material property, e.g. mass or electrical conductivity is monitored during re-equilibration after a stepwise change in oxygen partial pressure. By fitting the relaxation profile with the appropriate model, the values for the chemical diffusion coefficient $\widetilde{D}$ and the apparent surface exchange coefficient K_s are obtained. $\widetilde{D}$ and K_s relate to D_c and k_s, respectively, via:

$$\widetilde{D} = D_c \gamma \tag{1.16}$$

$$K_s = k_s \gamma \tag{1.17}$$

where γ is the thermodynamic factor:

$$\gamma = \frac{1}{2} \frac{\partial \ln p_{O_2}}{\partial \ln \delta} \tag{1.18}$$

1.5 Improvement of the membrane performance

Although the industrial interests in dense membranes are large by virtue of their vast possible application area, several aspects still have to be addressed before industrial application becomes feasible. Important factors that still have to be optimised are the magnitude of the oxygen flux in correlation with the operating temperature and the mechanical and chemical membrane stability [23].

1.5.1 Thin supported membranes

As far as the magnitude of the oxygen flux is considered, the maximum fluxes that have been reported are typically 1 μmole cm^{-2}s^{-1} for 0.5 mm thick membranes at 850°C under an air/helium gradient [12]. For large-scale technical applications the membrane flux needs to increase further by approximately a factor 10. An obvious method to increase the oxygen flux and/or reduce the operating temperatures is lowering the membrane thickness to the micrometer range. An important aspect in this approach, which is schematically shown as concept (d) in figure 1.1, is the necessity of supporting the membranes on porous substrates to provide sufficient mechanical strength. The expansion behaviour of these supports should match with that of the membrane as a function of temperature and oxygen partial pressure. The supports should further be able to withstand the membrane operation

temperature for an extended period of time without chemical and structural changes taking place. Mass transfer through the support should not rate limit the permeation through the membrane top layer. Furthermore, a low surface roughness and a narrow pore size distribution near the support/membrane interface are crucial requirements for successfully depositing a dense membrane top-layer.

1.5.2   Pulsed laser deposition

To realise the concept of a thin supported membrane, various modern thin-film techniques can be employed. Prominent examples are chemical vapour deposition, electrochemical vapour deposition, sol-gel processing, sputtering and laser ablation [24-26]. Of these methods, Laser ablation or Pulsed Laser Deposition (PLD) has recently emerged as one of the more suitable techniques for the deposition of a wide variety of materials with complex stoichiometry [27,28]. Using PLD, high quality layers can be fabricated with excellent texture and various crystallographic orientations. It can be employed to deposit layers of high-Tc superconductors, ferrites, ferro-electrics, opto-electronics, tribological coatings, metals, insulators, and biomaterials. The technique combines stoichiometric material transfer from target to substrate with process simplicity. High-quality films can be grown at high deposition rates compared with other techniques. Up till now, research has been focused primarily on deposition of (epitaxial) films on nonporous substrates, mostly single-crystals. Therefore, the deposition of thin dense oxygen separation membranes on porous supports clearly represents a new and challenging application of PLD.

1.5.3   Surface modification

As explained in the previous section, the approach of decreasing the membrane thickness by developing thin supported dense membranes only then results in a flux enhancement when bulk transport of oxygen rate limits the permeation. However, for membrane thicknesses below 0.5 mm, the influence of the surface exchange kinetics most likely has to be addressed too. For example, the L_c values that are reported in literature for various acceptor-doped cobaltites and ferrites vary from several microns to millimeters [16,29]. Therefore, the development of micrometer-thin dense membranes should include a strategy to enhance the surface exchange reactions. Obvious possibilities to improve the surface reaction rate are modification of the surface by depositing either a porous surface layer or an exchange-active layer, containing exchange catalysts.

1.6   Scope of this thesis

The main objective of the research described in this thesis is the development and the characterisation of dense supported $La_{1-x}Sr_xCoO_{3-\delta}$ layers. First the permeation properties

of unsupported bulk $La_{1-x}Sr_xCoO_{3-\delta}$ membranes are presented in chapter 2. In this chapter the dependence of the permeation on the applied pressure difference, temperature, Sr content and membrane thickness are discussed. The influence of bulk and surface processes is evaluated. In chapter 3 conductivity relaxation data of $La_{1-x}Sr_xCoO_{3-\delta}$ with varying Sr content are presented. The observed trends in $\tilde{D}$ and K_s and the associated values for L_c are presented and the results are compared with data obtained from permeation measurements. Chapter 4 describes the synthesis of porous $La_{1-x}Sr_xCoO_{3-\delta}$ supports. This chapter, which mainly focuses on perovskite powder processing, includes an excursion to the centrifugal casting of dense perovskite tubes. Chapter 5 describes the deposition of thin supported membranes by means of PLD on both porous α-Al_2O_3 and perovskite support materials. The oxygen permeation properties of the perovskite-supported membranes are presented and discussed in chapter 6. In chapter 7, the permeation and transport properties of non-supported $La_{0.5}Sr_{0.5}CoO_{3-\delta}$ membranes are studied as a function of the degree of B-site substitution of cobalt with either copper or nickel. Permeation and conductivity relaxation experiments are employed to study the oxygen transport. Finally, in chapter 8 an evaluation of the results of the previous chapters is presented, including recommendations for future research and proposals to obtain further improvement in membrane performance.

1.7   References

1. R.M. Thorogood, "Developments in air separation", *Gas Sep. Purif.*, **5** 83 (1991)
2. E.A. Hazbun, "Ceramic Membrane for Hydrocarbon Conversion," US Patent 4,791,079, 1988
3. A.G. Dixon, W.R. Moser and Y.H. Ma, "Waste Reduction and Recovery using O2-permeable Membrane Reactors," Ind. Eng. Chem. Res., **33** 3015 (1994)
4. T.J. Mazanec, "Novel solid multi-component membranes, electrochemical reactors and use of membranes and reactor for oxidation reactions," European Patent Application 0,399,833, 1990
5. R.M. Thorogood, R. Srinivasan, T.F. Yee and M.P. Drake, "Composite mixed conductor membranes for producing oxygen," US Patent 5,240,480, 1993
6. M. Liu, A.V. Joshi and Y. Shen "Mixed ionic-electronic conductors for oxygen separation and electrocatalysis," US Patent 5,273,628, 1993
7. A.J.Burggraaf and Y.S. Lin, "Method for manufacturing ultrathin inorganic membranes," US Patent 5,160,618, 1992
8. M.F. Carolan, P.N. Dyer, J.M. LaBar, Sr., and R.M. Thorogood "Process for recovering oxygen from gaseous mixtures containing water or carbon dioxide which process employs ion transport membranes," US Patent 5,261,932, 1993
9. H.J.M. Bouwmeester, A.J. Burggraaf, "Dense ceramic membranes for oxygen separation", in: CRC Handbook of Solid State Electrochemistry, ed. P.J. Gellings and H.J.M. Bouwmeester, CRC Press, Boca Raton 1997
10. J.W. Suitor, D.J. Clark, R.W. Losey, Development of an alternative oxygen production source using a zirconia solid electrolyte membrane, in: Technical progress report for fiscal years 1987, 1988 and 1990, Jet Propulsion Laboratory International Document D7790, 1990
11. T.J. Mazanec, T.L. Cable, J.G. Frye, Electrocatalytic cells for chemical reaction, Solid Sate Ionics, **53-56** 111 (1992)
12. Y. Teraoka, H.M. Zhang, S. Furukawa, N. Yamazoe, "Oxygen Permeation Through Perovskite-Type Oxides", *Chem. Lett.*, 1743 (1985)

13. M.H.R. Lankhorst, H.J.M. Bouwmeester and H. Verweij, "High-temperature coulometric titration of $La_{1-x}Sr_xCoO_{3-\delta}$: Evidence for the effect of electronic band structure on nonstoichiometry behavior," J. Solid State Chem. **133** 555-67 (1997)

14. H. Schmalzried, Solid Sate Reactions, Verlag Chemie, Weinheim 1981

15. C. Wagner, W. Schottky, "Beitrag zur Theorie des Anlaufvorganges", *Z. Phys. Chem*, **B11** 25 (1930)

16. H.J.M. Bouwmeester, H. Kruidhof and A.J. Burggraaf, "Importance of the surface exchange kinetics as rate limiting step in oxygen permeation through mixed-conducting oxides", *Solid State Ionics*, **72** 185 (1994)

17. N.E. Benes, H.J.M. Bouwmeester, H. Verweij, "Multi-component diffusion on a three dimensional lattice gas", submitted for publication

18. B.A. Boukamp, I.C. Vinke, K.J. de Vries, A.J. Burggraaf, "Surface oxygen exchange properties of bismuth oxide-based solid electrolytes and electrode materials", *Solid State Ionics*, **32/33** 918 (1989)

19. J. Kilner, "Isotopic exchange in mixed and ionically conducting membranes", in: *Proc. 2nd Int. Symp. Ionic and Mixed Conducting Oxide Ceramics*, **94-12**, T.A. Ramanarayanan, W.L. Worrell, Hl.L. Tuller Eds. The Electrochemical Society, Pennington, NJ, 174 (1994)

20. J.E. ten Elshof, M.H.R. Lankhorst, H.J.M. Bouwmeester, "Oxygen Exchange and Diffusion Coefficients of Strontium-Doped Lanthanum Ferrites by Electrical Conductivity Relaxation", *J. Electrochem. Soc.* **144** 1060 (1997)

21. I. Yasuda, T. Hikita, "Precise Determination of the Chemical Diffusion Coefficient of Calcium-Doped Lanthanum Chromites by Means of Electrical Conductivity Relaxation", *J. Electrochem. Soc.*, 141 1268 (1994)

22. H. Kanai, T. Hashimoto, H. Tagawa, J. Mizusaki, "Diffusion coefficient of oxygen in $La_{1.7}Sr_{0.3}CuO_{4-\delta}$, *Solid State Ionics* **99** 193 (1997)

23. P.V. Hendriksen, P.H. Larsen, M. Mogensen, F.W. Poulsen, K. Wiik, "Prospects and problems of dense oxygen permeable membranes", *Catalysis Today*, **56** 283 (2000)

24. C.H. Chen, H.J.M. Bouwmeester, H. Kruidhof, J.E. ten Elshof, A.J. Burggraaf, "Fabrication of $La_{1-x}Sr_xCoO_{3-\delta}$ thin layers on porous supports by a polymeric sol-gel process," *J. Mater. Chem.*, **6** 815 (1996)

25. B. McCool, G. Xomeritakis and Y.S. Lin, "Composition control and permeation properties of sputter deposited palladium silver membranes", *J. Membr. Sci.* **161** 67 (1999)

26. E.A.F. Span, F.J.G. Roesthuis, D.H.A. Blank, H. Rogalla, "Structural and electrical properties of $La_{0.5}Sr_{0.5}CoO_3$ films on $SrTiO_3$ and porous α-Al_2O_3 substrates", *Applied Physics A*, **69** 783 (1999)

27. D.H.A. Blank, R.P.J. IJsselsteijn, P.G. Out, H.J.H. Kuiper, J. Flokstra, H. Rogalla, "High Tc-thin prepared by laser ablation: Material distribution and droplet problem", *Mat. Science & Eng. B*, **B13** 67 (1992)

28. G. Koster, G.J.H.M. Rijnders, D.H.A. Blank, H. Rogalla, "Imposed layer by layer growth by pulsed laser interval deposition", *Appl. Phys. Lett.*, **74** 3729 (1999)

29. S. Carter, A. Selcuk, R.J. Chater, J. Kajda, J.A. Kilner, B.C.H. Steele, "Oxygen Transport in Selected Nonstoichiometric Perovskite-Structure Oxides", *Solid State Ionics*, **53** 597 (1992)

2

Oxygen permeation through La$_{1-x}$Sr$_x$CoO$_{3-\delta}$ membranes

Abstract

The kinetics of oxygen transport through dense La$_{1-x}$Sr$_x$CoO$_{3-\delta}$ membranes (x = 0.2, 0.5 and 0.7) was investigated using oxygen permeation measurements in the temperature range of 750-1000°C, oxygen partial pressure range of 0.001-0.21 bar and membrane thickness range of 0.5-2mm. Results showed a clear influence of surface exchange in rate limiting the oxygen flux. However, even for the thinnest specimens in this study the oxygen fluxes remain predominantly controlled by bulk oxygen diffusion through the membrane. The calculated characteristic membrane thickness L$_c$, below which oxygen transport is predominantly rate limited by surface exchange, varies approximately between 70 and 230 μm. From the oxygen pressure dependence of oxygen permeation it follows that the ionic conductivity of the different compositions La$_{1-x}$Sr$_x$CoO$_{3-\delta}$ is unfavourably affected with lowering oxygen partial pressure and temperature, which is attributed to vacancy trapping effects associated with the ordering of oxygen vacancies. The results of this study are in excellent agreement with recent observations from conductivity relaxation experiments.

2.1   Introduction

Mixed oxygen anion and electronic conducting perovskite materials have received increasing academic and industrial interest in recent years due to their possible technological applications [1-7]. The advantage of their use, provided that the ceramic membrane can be prepared free of cracks or connected-through porosity, is its ability to separate oxygen from an air supply with infinite selectivity. Besides oxygen production, a promising use is in a membrane reactor, integrating oxygen separation and catalytic reaction into a single step. To realise the potential benefits of such membranes, however, a number of technical hurdles still needs to be taken [8].

The partial substitution of A- and B-cations in the ABO_3 perovskite structure by other metal cations with lower valencies increases oxygen semi-permeability, due to the formation of oxygen vacancies. The positively charged oxygen vacancies tend to become disordered at high temperatures, which gives rise to high values for the ionic conductivity [9]. Under the influence of a gradient of oxygen partial pressure the oxygen anions are transported across the membrane, which motion is charge-compensated by a simultaneous transport of electronic charge carriers. In contrast with fuel cells and oxygen pumps, the dense ceramic membrane operates without the need of electrodes and external circuitry. The presence of the high electronic conductivity usually exhibited by the perovskites acts as an internal short-circuit for the return path of electrons.

In the selection of perovskite membranes, the most obvious criterion is the magnitude of the oxygen flux and its dependence on temperature and oxygen partial pressure differential across the membrane. The transport of oxygen through the perovskite membrane is usually described in the framework of Wagner's theory [10]. The assumption made is that lattice oxygen diffusion determines the overall permeation process. However, the real oxygen flux may be controlled by the rate of the surface exchange reaction, the extent of which can vary with membrane thickness, temperature and gradient in oxygen partial pressure [11]. Moreover, immobilisation of oxygen vacancies due to clustering or ordering can have a detrimental effect on the magnitude of the oxygen flux. In a recent study on perovskite materials $La_{1-x}Sr_xCoO_{3-\delta}$, the chemical diffusion coefficient and the surface exchange coefficient were measured at temperatures 600-850°C [12,13]. Both parameters were found to decrease profoundly with decreasing p_{O_2} below about 10^{-2} bar, at all temperatures. Concordant with data from high temperature ^{17}O-NMR on related perovskite structures [14], the results were rationalised by ordering of oxygen vacancies into nano-sized microdomains at low enough oxygen partial pressures.

Understanding the oxygen permeation mechanism can help to identify membrane materials with improved performance characteristics. In the present work, a detailed permeation study is presented of the system La$_{1-x}$Sr$_x$CoO$_{3-\delta}$. The oxygen permeation rates were measured as functions of temperature, membrane thickness and oxygen partial pressures with the aim to clarify the rate-limiting step.

2.2   Theory

The oxygen flux through a dense membrane is generally described by Wagner's equation, assuming bulk oxygen diffusion to be rate limiting:

$$j_{O_2} = -\frac{RT}{4^2 F^2 L} \int_{\ln p'_{O_2}}^{\ln p''_{O_2}} t_{el} \sigma_{ion} \, d\ln p_{O_2} \tag{2.1}$$

Here σ_{ion} is the ionic conductivity, L the membrane thickness, and p'_{O_2} and p''_{O_2} are the oxygen partial pressures at the oxygen-rich and oxygen-lean side of the membrane, respectively. Other parameters have their usual significance. As La$_{1-x}$Sr$_x$CoO$_{3-\delta}$ shows predominant electronic conductivity, the electronic transference number, t_{el}, may conveniently taken to be unity. In the case of non-interacting, fully ionised oxygen vacancies, all contributing to transport, the ionic conductivity can be described by:

$$\sigma_{ion} = \frac{4F^2 [V_O^{\bullet\bullet}] D_V}{RTV_m} \tag{2.2}$$

where D_v is the vacancy diffusion coefficient, V_m the perovskite molar volume and $[V_O^{\bullet\bullet}]$ ($\equiv \delta$) the mole fraction of oxygen vacancies. Following data of oxygen nonstoichiometry exhibited by phases La$_{1-x}$Sr$_x$CoO$_{3-\delta}$ as measured by Mizusaki *et al.* [15] using thermogravimetry, equation. (2.2) can be transformed into the power law expression:

$$\sigma_{ion} = \sigma_{ion}^0 p_{O_2}^n \tag{2.3}$$

assuming that the vacancy diffusion coefficient, D_v, does not vary with oxygen partial pressure. Based on this analysis, the oxygen permeation flux can be obtained by integrating equation (2.1):

$$j_{O_2} = \frac{\sigma_{ion}^0 RT}{4^2 nF^2 L} \left[p'^n_{O_2} - p''^n_{O_2} \right] \tag{2.4}$$

Fitting experimental oxygen flux data to equation (2.4) yields values for the two parameters n and σ_{ion}^0. Figure 2.1 schematically shows the influence of the power index n

on j_{O_2} - $\log(p''_{O_2})$ curves. If the ionic conductivity increases with decreasing p_{O_2}, i.e. $n < 0$, the obtained curve is concave. This would be the case if the number of oxygen vacancies contributing to ionic transport in $La_{1-x}Sr_xCoO_{3-\delta}$ would increase with decreasing oxygen partial pressure. A straight line is obtained if the ionic conductivity were invariant with p_{O_2}, that is for $n = 0$, whereas a convex curve is obtained for $n > 0$. In the latter case, the oxygen ionic conductivity decreases with decreasing oxygen partial pressure. Alternatively, values for the ionic conductivity, at a given p_{O_2}, can be calculated from the slope of isothermal oxygen flux data, using:

$$\left(\frac{\partial j_{O_2}}{\partial \ln p''_{O_2}} \right)_{p'_{O_2}} = -t_{el} \sigma_{ion} \frac{RT}{4^2 F^2 L} \tag{2.5}$$

which is obtained by differentiation of equation (2.1).
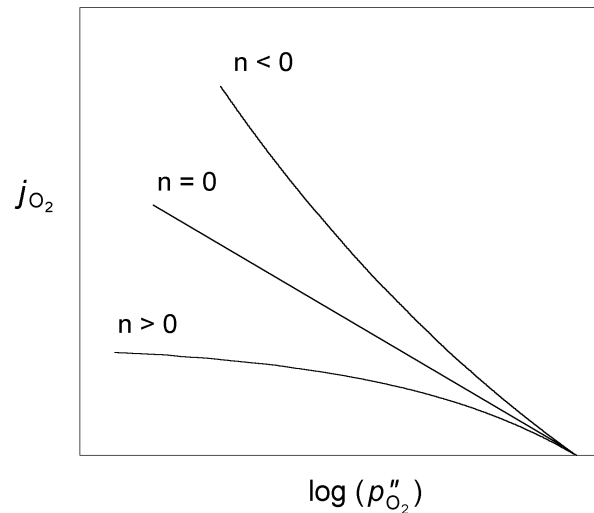
Figure 2.1 Oxygen flux as a function of $\log(p''_{O_2})$ for $p'_{O_2} > p''_{O_2}$, calculated using equation (2.4), using different values for *n*.

Until now, lattice diffusion of oxygen vacancies has been considered as rate limiting step in the oxygen permeation mechanism. However, oxygen surface exchange may exert a partial or dominant control on oxygen permeation. A logical approach to discriminate between these steps would be measurement of the oxygen permeation as a function of membrane thickness *L*. Bouwmeester *et al.* [11,16] proposed to use a characteristic length, L_c, to describe the possible involvement of surface exchange in limiting the oxygen flux,

$$j_{O_2} = -\frac{1}{1 + (2 L_c / L)} \frac{\overline{t_{el} \sigma_{ion}}}{16 F^2} \frac{\Delta \mu_{O_2}^{total}}{L} \tag{2.6}$$

where $\Delta\mu_{O_2}^{total}$ $(= RT\ln(p_{O_2}'' / p_{O_2}'))$ is the total oxygen chemical potential drop across the membrane and $\overline{t_{el}\sigma_{ion}}$ the average value of the product of the transference number and ionic conductivity over the applied oxygen partial pressure differential. Below L_c, the oxygen flux is predominantly controlled by the surface exchange rate. The only assumption made in the derivation of equation (2.6) is that of linear transport kinetics for diffusion and interfacial exchange. With the additional assumption of small p_{O_2} gradients appearing across the membrane, it follows that

$$L_c = \frac{RT}{4F^2} \frac{t_{el}\sigma_{ion}}{k_s c_O} \tag{2.7}$$

where k_s is the surface exchange coefficient and c_O the volume concentration of oxygen anions (at equilibrium). Using the classical Nernst-Einstein relationship, L_c can in the case of prevailing electronic conduction be expressed as:

$$L_c = \frac{D_s}{k_s}$$
$$= \frac{\widetilde{D}}{K_{tr}} \tag{2.8}$$

Determination of the values of the self-diffusion coefficient D_s (cm^2 s^{-1}) and the surface exchange coefficient k_s (cm s^{-1}) requires the use of ^{18}O-^{16}O isotopic exchange techniques. The chemical diffusion coefficient $\widetilde{D}$ (cm^2 s^{-1}) and the surface transfer coefficient K_{tr} (cm s^{-1}) follows from chemical equilibration techniques, such as conductivity relaxation. In the general case, L_c is a function of oxygen partial pressure and temperature.

2.3 Experimental

2.3.1 Sample preparation

La$_{1-x}$Sr$_x$CoO$_{3-\delta}$ ($x = 0.2$, 0.5 and 0.7) perovskite powders were prepared by thermal decomposition of precursor complexes derived from nitrate solutions using ethylene-diamine tetra-acetic acid (EDTA) as a complexing agent [17]. The powders were calcined in air at 940°C. The resulting powders were shown by X-ray powder diffraction to be single-phase perovskite. The powders were milled and isostatically pressed at 4000 bar followed by sintering at 1150°C for 10 h. The sintered bodies showed a relative density in excess of 96%. For permeation measurements disks with a diameter of 15 mm and a thickness ranging from 0.44 to 2.00 mm were cut from the sintered bodies. Prior to permeation measurements the disks were polished with 1000 MESH SiC and ultrasonically cleaned in ethanol.

2.3.2   Permeation measurements

Oxygen permeation experiments were performed in the range from 750 to 1000°C. The disks were sealed into a quartz reactor tube at 1000°C using glass rings[*]. One side of the sample disk was exposed to air (100 ml/min). The oxygen partial pressure at the other side was controlled by regulating the helium gas flow rate (0-56 ml/min), assuming ideal gas mixing conditions in that part of the reactor. The oxygen concentrations in both feed and permeate streams were monitored through home-made YSZ based oxygen sensors. Quantitative analysis of the oxygen concentration at the outlet of the reactor was performed by a gas chromatograph, which also measured the N_2 concentration in the sweep gas to check for inadequate sealing or membrane leakage. A schematic representation of the set-up is given in figure 2.2.
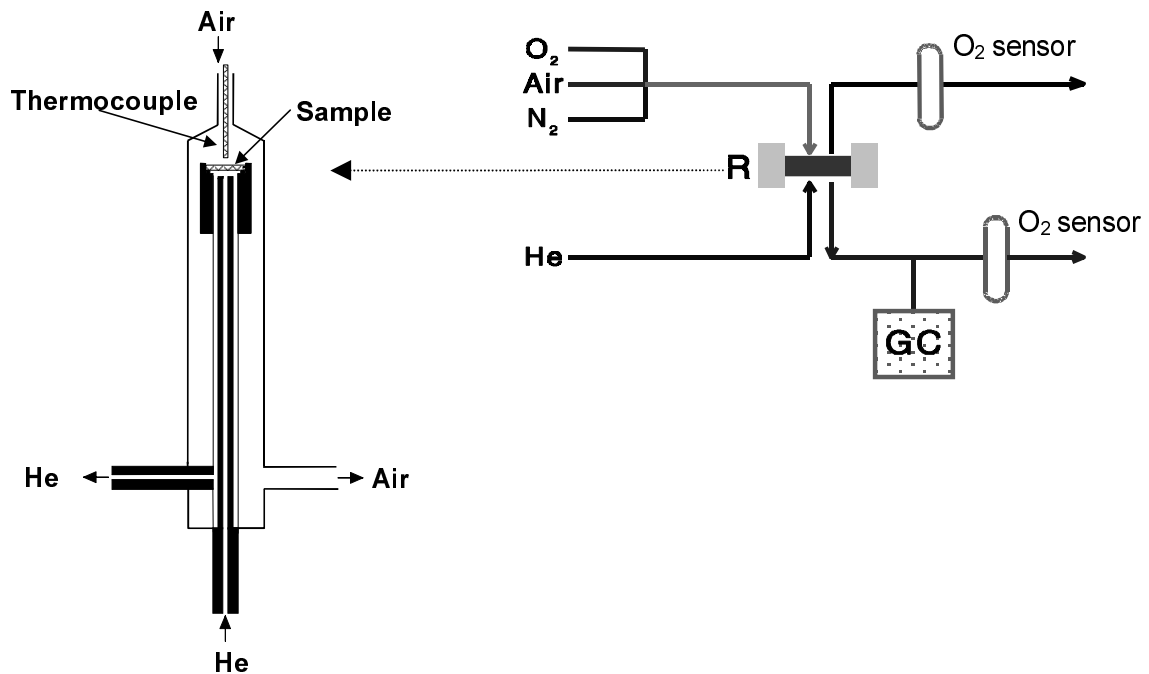
Figure 2.2   Schematic representation of the permeation reactor and set-up; GC = gas chromatograph.

Oxygen fluxes were corrected for non-axial contributions, according to:

$$j_{O_2} = \frac{1}{G} \frac{F c_O}{A} \tag{2.8}$$

where F is the flow rate at the outlet of the reactor, c_O the measured oxygen concentration and A the free surface area at the sealed side of the membrane. The correction factor G was calculated from a numerical solution of the steady-state diffusion equation based on Fick's second law, assuming a constant diffusion coefficient.

---

[*] 8252, Schott Netherlands B.V.

2.4   Results and discussion

2.4.1   Oxygen pressure dependence

Figure 2.3 shows the oxygen flux as a function of $\log(p''_{O_2})$ at different temperatures for 0.5 and 2 mm thick membranes with composition *x*=0.5. The drawn lines correspond to the best fit of the experimental data to equation (2.4), using *n* and σ^0_{ion} as fitting parameters, Error estimates of these parameters were obtained from a non-linear least square fitting of the data using a Marquardt algorithm, as outlined by Bevington [18]. In this method, it is assumed that the 'parent distribution' of variances for the data set may be replaced by the actual error differences. It should be noted that this method looses its validity when the errors are not purely random but contain a systematic component as well. All fitted curves were forced to pass the point where $p''_{O_2} = p'_{O_2}$ and, hence, the oxygen flux has reduced to zero. Table 2.1 gives a survey of the fit parameters for all investigated compositions. Note that for compositions x=0.7 and 0.5, only positive values for *n* are found.
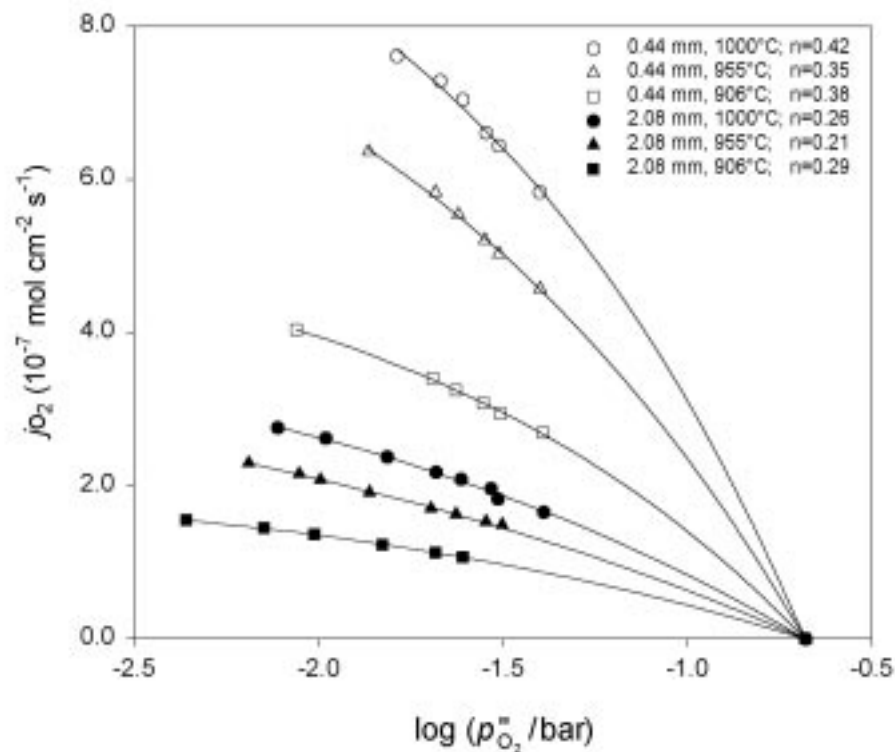
Figure 2.3:   Dependence of j_{O_2} on $\log(p''_{O_2})$ for the composition with *x*=0.5, measured using air as feed gas. The drawn lines represent the fit of the data to equation (2.4).

Based upon data of oxygen nonstoichiometry of phases La$_{1-x}$Sr$_x$CoO$_{3-\delta}$, *n* < 0 is expected. From table 2.1 is noted that for compositions *x*=0.5 and *x*=0.7, only positive values for *n* are found. For all three compositions the values deviate significantly from those obtained

in the thermogravimetric study by Mizusaki et al. [15]. In their study, the authors showed that the oxygen nonstoichiometry, at 800°C and at values of p_{O_2} similar to those used in the present study, varies approximately with $p_{O_2}{}^n$ with n equal to -0.25, -0.07 and -0.06 for samples with x=0.2, x=0.5 and x=0.7, respectively. Since analysis in terms of equation. (2.4) is based upon ionic diffusion through the bulk as the rate limiting step in oxygen permeation, a first consideration is to attribute the observed discrepancies to partial rate control by the surface exchange reactions. As discussed in the next section, in particular for the compositions with x=0.2 and x=0.5, the experimental data suggest a clear influence of surface exchange on permeation for the thinnest specimens in this study. For all compositions, however, oxygen permeation in the experimental range of thickness remains predominantly diffusion controlled.

Table 2.1:   Values of the power index n and the ionic conductivity σ_{ion}^0 obtained from fitting the j_{O_2} - $\log(p''_{O_2})$ curves to equation (2.4). Standard deviations are given in parenthesis.

Composition	L (mm)	T (°C)	n	σ_{ion}^0 (mS cm^{-1})
x = 0.2	0.44	1000	0.08 (0.01)	29.7 (2.1)
		955	-0.11 (0.04)	9.7 (1.6)
		906	0.13 (0.03)	10.2 (1.2)
		855	0.28 (0.07)	7.1 (1.7)
	0.98	1000	0.13 (0.04)	55.1 (7.7)
		955	-0.07 (0.02)	17.4 (1.0)
		906	0.10 (0.03)	14.7 (1.9)
		855	-0.01 (0.03)	4.4 (0.5)
	1.98	1000	-0.10 (0.03)	25.0 (2.8)
		955	0.01 (0.06)	22.4 (3.7)
		906	0.01 (0.01)	11.0 (0.7)
		855	0.05 (0.02)	4.9 (0.3)
x = 0.5	0.44	1000	0.42 (0.06)	587 (83)
		955	0.35 (0.03)	400 (32)
		906	0.38 (0.02)	267 (11)
		855	0.40 (0.02)	152 (75)
	0.74	1000	0.34 (0.02)	543 (27)
		955	0.35 (0.01)	493 (10)
		906	0.40 (0.02)	387 (23)
		855	0.34 (0.03)	216 (18)
	2.08	1000	0.26 (0.03)	551 (39)
		955	0.21 (0.02)	393 (20)
		906	0.29 (0.01)	333 (7)
x = 0.7	0.56	906	0.40 (0.04)	890 (89)
		802	0.46 (0.02)	465 (19)
	1.09	1000	0.22 (0.04)	1050 (90)
		906	0.18 (0.03)	565 (40)
	2.06	1000	0.33 (0.06)	1400 (200)
		906	0.22 (0.02)	669 (40)

Even for the thickest specimens in this study, which is around 2 mm, the power index n for samples with x=0.5 and x=0.7 is distinctly positive, at all temperatures. As for these specimens bulk diffusion is dominating the permeation, $n > 0$ implies that the oxygen ionic

conductivity of these samples decreases, rather than increases, with decreasing p_{O_2}. For both compositions, there is no clear trend in the behaviour of *n* with variation in temperature or sample thickness.

For the sample with x=0.2 and thickness 2.08 mm, the power index *n* increases with temperature from a value of –0.1 at 1000°C to +0.05 at 855°C. If bulk diffusion is assumed to prevail, the ionic conductivity can be calculated using equation (2.4). Corresponding results as a function of p_{O_2}, at various temperatures, are shown in figure 2.4. Also shown in this figure is a comparison of the ionic conductivities at 855°C with values calculated from chemical diffusion coefficients measured at 850°C using conductivity relaxation [9,13]. Thermodynamic factors needed for this calculation were evaluated from data of oxygen non-stoichiometry as a function of p_{O_2} [19]. As is evident from figure 2.4, the absolute values are in a very good agreement. The agreement in the overall trend is further improved if the ionic conductivity is not calculated using equation (2.4), but instead is determined from the experimental flux data using equation (2.5). To this end, the oxygen flux data were fitted with a third order polynomial, which was differentiated with respect to $\log(p_{O_2}'')$ to evaluate the slope at a given p_{O_2}. At other temperatures, as well as for other compositions, insufficient information was available to enable direct comparison of data obtained by using permeation and conductivity relaxation experiments.

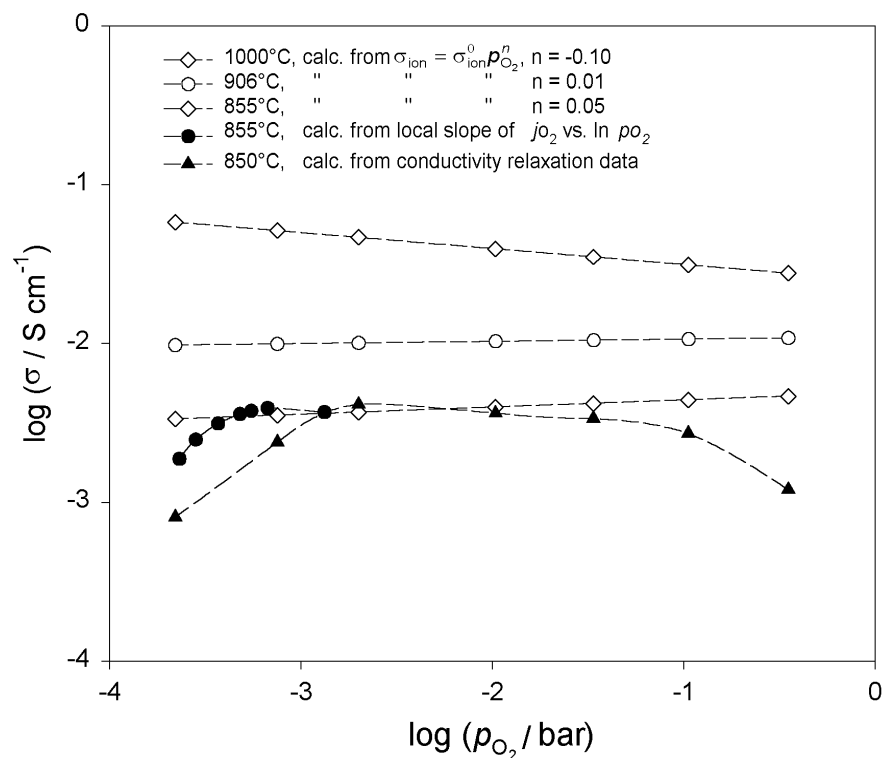Figure 2.4:   Ionic conductivity for the composition x=0.2, calculated from equation (2.3). In addition, for 850°C, the ionic conductivity calculated from equation (2.5) as well as from electrical conductivity relaxation data [9,13] is plotted.

In previous investigations on LaCoO$_{3-\delta}$ [20], the experimental results indicated a diffusion controlled oxygen flux at 1000°C. The ionic conductivity in the p_{O_2} range 1-10^{-2} bar was found to fit a $p_{O_2}{}^n$ dependence with $n = -0.46$ in good agreement with the data from oxygen nonstoichiometry measurements of LaCoO$_{3-\delta}$ ($\delta \propto p_{O_2}{}^{0.5}$). In the p_{O_2} range $10^{-2.8}$ - $10^{-3.4}$ bar, the value of n was found to be around -0.31. Comparison with the present data suggests that values of n for phases La$_{1-x}$Sr$_x$CoO$_{3-\delta}$, at 1000°C, depart more strongly from those obtained from data of oxygen nonstoichiometry as the strontium content increases. As with increasing strontium content the level of oxygen nonstoichiometry of phases La$_{1-x}$Sr$_x$CoO$_{3-\delta}$ increases, it is reasonable to assume that the observed discrepancies are due to increased interactions between oxygen vacancies. The resulting formation of extended defects or vacancy ordering effectively lowers the concentration of 'free' oxygen vacancies available for ionic transport. In particular, Adler *et al.* [14] have suggested that in the highly defective perovskites local ordering may occur in nano-sized microdomains. These phenomena are also held responsible for the decrease of the chemical diffusion coefficients with decreasing p_{O_2} in the temperature range 600-850°C, we have recently measured for phases La$_{1-x}$Sr$_x$CoO$_{3-\delta}$ (x=0.2, 0.5, 0.8) using conductivity relaxation [9,13].

The observation that the power index n is not significantly affected with variation of membrane thickness, in spite of partial surface control of the permeation kinetics for the thinnest specimens in this study (see next section), may indicate that common factors govern both the rates of oxygen diffusion and surface exchange. Here again, the results conform to those obtained from conductivity relaxation experiments, where it was found that the chemical diffusion coefficient $\tilde{D}$ and the surface exchange coefficient K_{tr} display similar oxygen partial pressure dependencies.

2.4.2   Membrane thickness dependence

Figure 2.6 shows the log-log plot of the oxygen flux versus membrane thickness, at given p_{O_2}'' and temperature, for compositions La$_{1-x}$Sr$_x$CoO$_{3-\delta}$. The experimental data were fitted to equation (2.6) to investigate the possible involvement of the surface exchange in limiting oxygen permeation. Fitting yields the characteristic membrane thickness L_c and an average value for the ionic conductivity $\overline{\sigma_{ion}}$ (assuming $t_{el} = 1$) over the applied p_{O_2} gradient. Some typical values found for L_c and $\overline{\sigma_{ion}}$ at temperatures of 1000°C and 900°C are listed in table 2.2. As can be seen from figure 2.6, the fits to the data are rather good. The dashed lines refer to the cases when there is no surface exchange limitation.

Equation (2.6) must be treated with care since linearised kinetics of surface exchange and bulk diffusion were assumed in its derivation. Any rate expression, if not linear by nature,

however, can be linearised close to equilibrium conditions. Strictly speaking, equation (2.6) is therefore only applicable for small p_{O_2} gradients across the membrane. Fitting of experimental data collected at constant p_{O_2} gradients in the range of $\log\left(p'_{O_2} / p''_{O_2}\right)$ from 0.7 to 2.0 gave however similar results for L_c. Values for L_c are considered to be in reasonable agreement with those obtained from conductivity relaxation experiments performed in the temperature range 600-850°C, yielding average values for compositions x=0.2, 0.5 and 0.7 of around 100 μm [9,13].
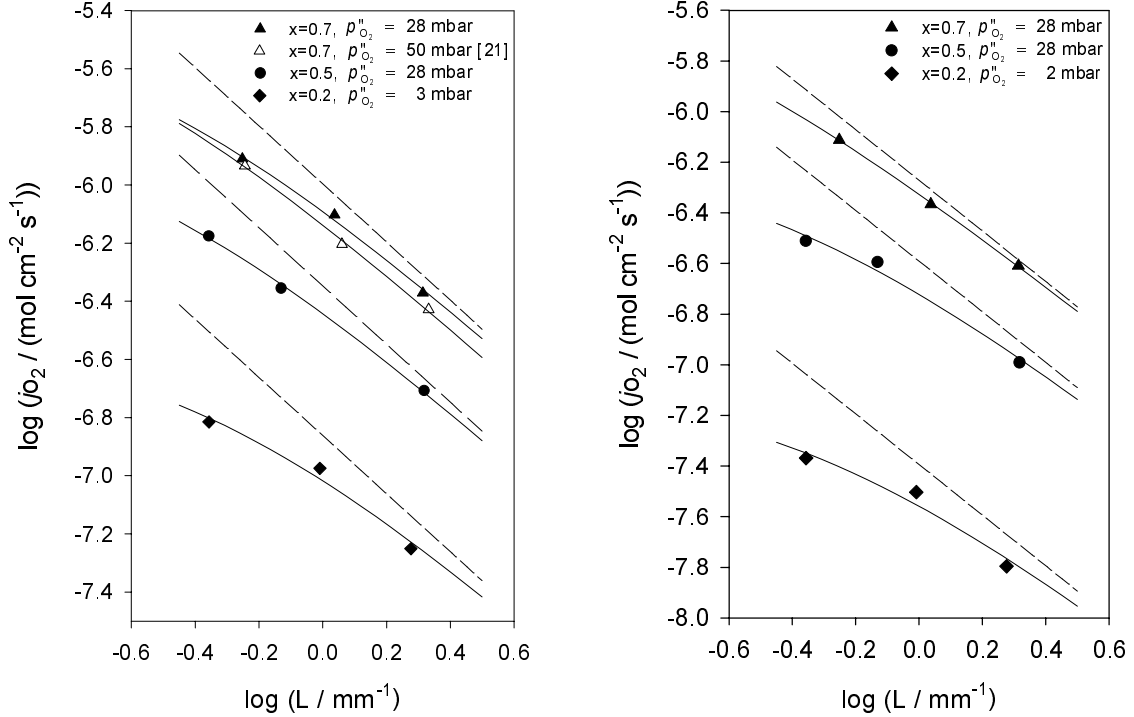
Figure 2.6: Membrane thickness dependence of the oxygen flux at 1000°C (left) and 900°C (right). The drawn lines indicate the fit to equation (2.6), the dashed lines indicate the situation in which there is no surface exchange limitation. Data from reference [20] are given for comparison.

Table 2.2: Values found for L_c and $\overline{\sigma_{ion}}$, calculated from the data shown in figure 2.6. The errors in both parameters are estimated at 30 μm and 10 mS cm^{-1}, respectively.

Temperature (°C)	x	p''_{O_2} (mbar)	L_c (μm)	$\overline{\sigma_{ion}}$ (mS cm^{-1})
1000	0.2	3	216	45
	0.5	28	123	315
	0.7	28	123	706
900	0.2	2	230	13
	0.5	28	177	194
	0.7	28	68	405

The factor $(1+2L_c/L)^{-1}$ in equation (2.6) gives the fraction to which the oxygen flux is reduced relative to that in the absence of surface exchange limitations. It is easily calculated that for a 2 mm thick sample with a value of L_c of 68 μm, as observed for La$_{0.3}$Sr$_{0.7}$CoO$_{3-\delta}$, this fraction is 0.94. Likewise, for a 0.5 mm thick sample, it is calculated

to be 0.79. For a value of L_c of 230 μm, as observed for the x=0.2 sample, the corresponding values are 0.81 and 0.52, respectively. The calculations confirm that for the thickest specimens used in this study, the oxygen flux is predominantly controlled by bulk oxygen diffusion through the membrane.

Figure 2.6 also shows previous results obtained for $La_{0.3}Sr_{0.7}CoO_{3-\delta}$, which was prepared by an aqueous sol-gel route [21]. The good agreement noted with data from the present study indicates that the different sample preparation procedure employed in the present study has little or no effect on the oxygen flux data neither on the relative role of surface exchange in the overall oxygen transport.

2.4.3   Temperature dependence

Arrhenius plots of oxygen permeation through $La_{1-x}Sr_xCoO_{3-\delta}$ ($x = 0.2$, 0.5 and 0.7) membranes in the temperature range 750-1000°C are given in figure 2.5. The measurements were conducted with a constant p_{O_2} gradient across the membrane. The plotted data refer to 0.5 mm thick membranes, but other membrane thicknesses gave similar results within experimental error. Activation energies for the different compositions calculated from the slopes of the plots are listed in the inset. A clear decrease of the activation energy is observed with increasing Sr-content, from 196 kJ/mole for x=0.2 to 89 kJ/mole for x=0.7. These values are in good agreement with those reported previously by van Doorn *et al.* [22]
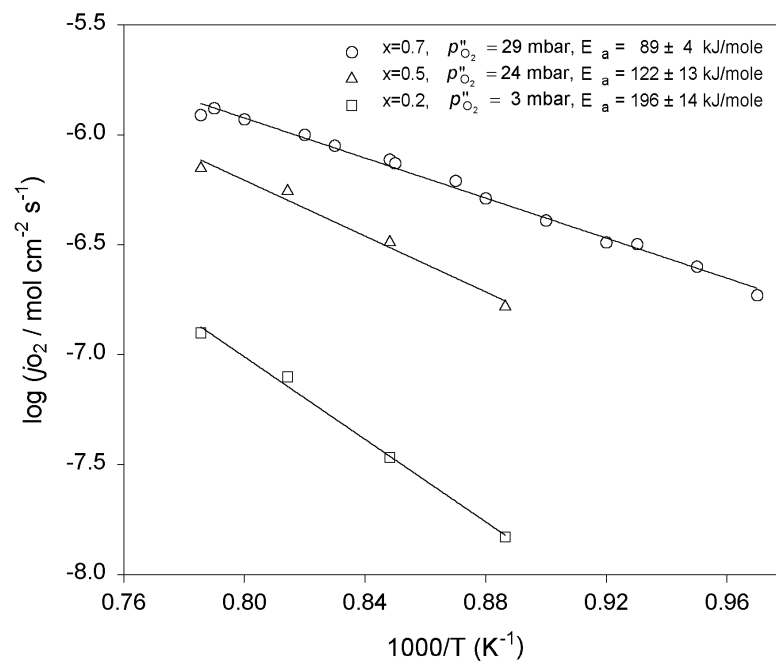

Figure 2.5:   Arrhenius plots of oxygen permeation through 0.5 mm thick $La_{1-x}Sr_xCoO_{3-\delta}$ membranes for different compositions. Air was used as feed gas. Values for the constant p''_{O_2} at the oxygen-lean side of the membrane and calculated activation energies are listed.

2.5   Summary and conclusions

Single phase samples of La$_{1-x}$Sr$_x$CoO$_{3-\delta}$ (x = 0.2, 0.5 and 0.7) were studied by permeation measurements. To learn more about the kinetics of oxygen permeation, *i.e.* the relative role of surface exchange and bulk diffusion in rate determining the transport of oxygen, measurements were conducted as a function of temperature, membrane thickness and oxygen partial pressure maintained at the oxygen-lean side of the membrane. Air was fed at the other side of the membrane in all cases. The results give clear evidence that for the thickest specimens in this study (~2 mm), the oxygen fluxes are predominantly controlled by bulk oxygen diffusion across the membrane. The calculated characteristic membrane thickness L_c, below which oxygen transport is predominantly rate limited by surface exchange, is found to vary between 68-230 μm at temperatures of 900 and 1000°C. The values are consistent with data collected using conductivity relaxation in the temperature range 600-850°C.

The experimental permeation rates are found to be proportional to $\left(p_{O_2}'^{\,n} - p_{O_2}''^{\,n} \right)$, where $p_{O_2}' > p_{O_2}''$. However, values observed for the power index *n* differ strongly from those expected form oxygen nonstoichiometry measurements of La$_{1-x}$Sr$_x$CoO$_{3-\delta}$. For samples with x=0.5 and x=0.7, power indexes 0.2>n>0.5 are obtained. While the trend for the oxygen nonstoichiometry of the perovskite phases is that δ increases with decreasing p_{O_2}, it follows from the present results that the ionic conductivity, being associated with the presence of mobile oxygen vacancies, decreases with decreasing p_{O_2}. For the thickest (~2 mm) specimen of the x=0.2 sample in this study, the value of *n* increases from –0.1 at 1000°C to +0.05 at 855°C. Concordant with data from conductivity relaxation, the observations are attributed to vacancy trapping effects associated with the ordering of vacancies at low temperatures and oxygen partial pressures.

2.6   References

1. E.A. Hazbun, "Ceramic Membrane for Hydrocarbon Conversion," US Patent 4,791,079, 1988
2. A.G. Dixon, W.R. Moser and Y.H. Ma, "Waste Reduction and Recovery using O2-permeable Membrane Reactors," *Ind. Eng. Chem. Res.*, **33** 3015 (1994)
3. T.J. Mazanec, "Novel solid multi-component membranes, electrochemical reactors and use of membranes and reactor for oxidation reactions," European Patent Application 0,399,833, 1990
4. R.M. Thorogood, R. Srinivasan, T.F. Yee and M.P. Drake, "Composite mixed conductor membranes for producing oxygen," US Patent 5,240,480, 1993
5. M. Liu, A.V. Joshi and Y. Shen "Mixed ionic-electronic conductors for oxygen separation and electrocatalysis," US Patent 5,273,628, 1993
6. A.J.Burggraaf and Y.S. Lin, "Method for manufacturing ultrathin inorganic membranes," US Patent 5,160,618, 1992
7. M.F. Carolan, P.N. Dyer, J.M. LaBar, Sr., and R.M. Thorogood "Process for recovering oxygen from gaseous mixtures containing water or carbon dioxide which process employs ion transport membranes," US Patent 5,261,932, 1993

8. P.N. Dyer, R.E. Richards, S.L. Russek, D.M. Taylor, "Ion Transport Membrane Technology For Oxygen Separation And Syngas Production", *Solid Sate Ionics* **134**, 21 (2000)

9. H. Kruidhof, H.J.M. Bouwmeester, R.H.E. van Doorn, A.J. Burggraaf, "Influence of order-disorder transitions on oxygen permeability through selected nonstoichiometric perovskite type oxides," *Solid State Ionics*, **63/65** 816 (1993)

10. C. Wagner, W. Schottky, "Beitrag zur Theorie des Anlaufvorganges", *Z. Phys. Chem*, **B11** 25 (1930)

11. H.J.M. Bouwmeester, H. Kruidhof and A.J. Burggraaf, "Importance of the surface exchange kinetics as rate limiting step in oxygen permeation through mixed-conducting oxides", *Solid State Ionics*, **72** 185 (1994)

12. L.M. van der Haar, M.W. den Otter, M. Morskate, H.J.M. Bouwmeester, H. Verweij, "Chemical diffusion and oxygen surface transfer of $La_{1-x}Sr_xCoO_{3-\delta}$ studied with electrical conductivity relaxation", *submitted*

13. Chapter 3 of this thesis

14. S. Adler, S. Russek, J Reimer, M. Fendorf, A. Stacy, Q. Huang, A. Santoro, J. Lynn, J. Baltisberger, U Werner, "Local structure and oxide-ion motion in defective perovskites", *Solid State Ionics* **68**, 193 (1994)

15. J. Mizusaki, Y. Mima, S. Yamauchi, K. Fueki, "Nonstoichiometry of the Perovskite-Type Oxides $La_{1-x}Sr_xCoO_{3-\delta}$", *J. Solid Sate Chem.* **80**, 102 (1989)

16. H.J.M. Bouwmeester, A.J. Burggraaf, "Dense ceramic membranes for oxygen separation", in: CRC Handbook of Solid State Electrochemistry, ed. P.J. Gellings and H.J.M. Bouwmeester, CRC Press, Boca Raton 1997

17. R.H.E. van Doorn, H. Kruidhof, A. Nijmeijer, L. Winnubst and A.J. Burggraaf, "Preparation of $La_{0.3}Sr_{0.7}CoO_{3-\delta}$ perovskite by thermal decomposition of metal-EDTA complexes," *J. Mater. Chem.*, **8** [9] 2109 (1998)

18. P.R. Bevington, "Data reduction and error analysis for the physical sciences", McGraw-Hill, New York, 1969

19. M.H.R. Lankhorst and H.J.M. Bouwmeester, "Determination of oxygen nonstoichiometry and diffusivity in mixed conducting oxides by oxygen coulometric titration, Part II: Oxygen non-stoichiometry and defect model for $La_{0.8}Sr_{0.2}CoO_{3-\delta}$ *J. Electrochem. Soc.* **144**, 1268 (1997)

20. C.H. Chen, H. Kruidhof, H.J.M. Bouwmeester and A.J. Burggraaf, "Ionic conductivity of perovskite $LaCoO_3$ measured by oxygen permeation technique," *J. Appl. Electrochem.*, **27** [1] 71-75 (1997)

21. C.H. Chen, H.J.M. Bouwmeester, R.H.E. van Doorn, H. Kruidhof and A.J. Burggraaf, "Oxygen permeation of $La_{0.3}Sr_{0.7}CoO_{3-\delta}$," *Solid State Ionics*, **98** [1-2] 7-13 (1997)

22. R.H.E. van Doorn, H. Kruidhof, H.J.M. Bouwmeester and A.J. Burggraaf, "Oxygen permeability of strontium-doped $LaCoO_{3-\delta}$ perovskites," Proceedings MRS Boston Fall meeting, november 1994, published in session Solid State Ionics

3

Chemical diffusion and oxygen surface transfer of $La_{1-x}Sr_xCoO_{3-\delta}$ studied with electrical conductivity relaxation

Abstract

The chemical diffusion coefficient and oxygen transfer coefficients of selected compositions in the series $La_{1-x}Sr_xCoO_{3-\delta}$ were studied using the conductivity relaxation technique. Measurements were performed in the temperature range 600-850°C and oxygen partial pressure 10^{-4}-1 bar. Chemical diffusivity and oxygen surface transfer in the $La_{1-x}Sr_xCoO_{3-\delta}$ perovskites appear to be highly correlated. The general trend displayed is that both parameters decrease with decreasing p_{O_2} below about 10^{-2} bar at all temperatures. This is attributed to ordering of induced vacancies at low enough oxygen partial pressures. The observation that the correlation between both parameters extends even to the lowest p_{O_2} values in this study, suggests a key role of the concentration of mobile oxygen vacancies, rather than of the extent of oxygen nonstoichiometry, in determining the rate of both processes. The characteristic thickness L_c, which equals the ratio of the chemical diffusion coefficient to the surface transfer coefficient, shows only a weak dependence on oxygen partial pressure and temperature. For different compositions $La_{1-x}Sr_xCoO_{3-\delta}$, L_c is found to vary between 50 and 150 μm.

3.1   Introduction

Oxygen transport through dense mixed ionic-electronic conducting perovskite-type membranes occurs as molecular oxygen is dissociated into oxygen ions, which migrate to the low pressure side of the membrane where they recombine to form oxygen molecules. Charge compensation takes place by a simultaneous flow of electronic charge carriers. The driving force for transport is the difference in oxygen partial pressure applied across the membrane. Both the transport through the oxide bulk and the interfacial gas-solid kinetic properties are of importance for the magnitude of the oxygen fluxes. Bulk diffusion in the ABO_3 perovskite structure occurs by the hopping of oxygen vacancies. The overall surface reaction may involve many steps such as adsorption, dissociation, transfer of charge to oxygen molecules, and incorporation of oxygen anions in the oxide bulk.

At first glance the oxygen fluxes can be maximised by reducing the membrane thickness to the μm-range, while providing sufficient mechanical strength through a suitable membrane support [1-8]. A suitable criterion for selection of appropriate materials for these thin-film membranes is the characteristic thickness L_c, indicating at which membrane thickness diffusion and surface reactions rate limit overall oxygen transport equally. Below L_c, no substantial gain in the oxygen flux can be achieved by further reduction of membrane thickness. For systems close to equilibrium, *i.e.* for small p_{O_2} -gradients, L_c is equal to the ratio of the chemical diffusion coefficient $\tilde{D}$ to the surface transfer coefficient K_{tr} [9].

High oxygen fluxes have been reported for $La_{1-x}Sr_xCoO_{3-\delta}$ perovskites [10,11]. In this material, divalent strontium as the A-site substituent causes the creation of oxygen vacancies. In the present study, electrical conductivity relaxation experiments are performed to determine $\tilde{D}$, K_{tr} and, hence, L_c for $La_{1-x}Sr_xCoO_{3-\delta}$ ($x = 0.2$, 0.5 and 0.7) as functions of oxygen partial pressure and temperature.

3.2   Theory

The conductivity relaxation technique involves measurement of the time variation of the electrical conductivity of a sample after a stepwise change in the oxygen partial pressure. The relaxation data are fitted to theoretical equations, as described below, using the chemical diffusion coefficient $\tilde{D}$ and the surface transfer coefficient K_{tr} as fitting parameters.

The change in electrical conductivity following the step change in oxygen partial pressure is governed by the reaction of the oxide with oxygen from the gas phase. In accordance with the Kröger-Vink notation, this reaction can be expressed by:

$$O_O^\times \to V_O^{\bullet\bullet} + \tfrac{1}{2}O_2 + 2e' \tag{1}$$

Hence, for each doubly ionised oxygen vacancy formed in the lattice, either two electrons are formed or two electron holes are annihilated. Assuming metallic conduction [12] for La$_{1-x}$Sr$_x$CoO$_{3-\delta}$, the electrons are transferred to a partially filled conduction band. In the ranges of temperature and oxygen partial pressure of interest to this study, the conductivity is found to be *p*-type, *i.e.*, decreasing with decreasing p_{O_2} [13].

In the analysis of the diffusion problem, a flat thin sheet is considered with thickness 2*b*. At $t < 0$, the sample is assumed to be in thermodynamic equilibrium with the surrounding atmosphere. At $t = 0$, the corresponding p_{O_2} is changed stepwise to a new value, associated with a new equilibrium oxygen concentration c_∞. Depending on the value of c_∞ relative to c_0, the oxygen concentration at $t < 0$, oxygen starts to diffuse into or out of the sample. Starting point in the derivation is Fick's second law:

$$\frac{\partial c}{\partial t} = \tilde{D}\frac{\partial^2 c}{\partial z^2} \tag{2}$$

where $\tilde{D}$ is the chemical diffusion coefficient. The surface reaction is assumed to proceed at a rate proportional to the difference between the actual concentration at the surface, c(±b), and c_∞. The boundary conditions at the surfaces $z = b$ and $z = -b$ are then given by

$$J(b) = -\tilde{D}\left.\frac{\partial c}{\partial z}\right|_{z=b} = K_{tr}\left[c(b) - c_\infty\right] \text{ and } J(-b) = -\tilde{D}\left.\frac{\partial c}{\partial z}\right|_{z=-b} = -K_{tr}\left[c(-b) - c_\infty\right] \tag{3}$$

where J denotes the flux density and K_{tr} the parameter controlling the rate of the surface reaction, called the surface transfer coefficient. The solution for the concentration profile as a function of time, *c(z,t)*, is obtained through an eigenfunction expansion of the initial oxygen concentration c_0 [14]:

$$\frac{c(z,t) - c_0}{c_\infty - c_0} = 1 - \sum_{n=1}^{\infty}\frac{2L_\beta\cos(\beta_n z/b)}{\left(\beta_n^2 + L_\beta^2 + L_\beta\right)\cos(\beta_n)}\exp\left(-\frac{t}{\tau_n}\right) \tag{4}$$

where the time constants τ_n are given by

$$\tau_n = \frac{b^2}{\tilde{D}\cdot\beta_n^2} \tag{5}$$

and the parameters β_n are obtained from:

$$\beta_n \tan \beta_n = \frac{bK_{tr}}{\tilde{D}} = L_\beta \; . \tag{6}$$

Equating the change in oxygen nonstoichiometry to changes in electrical conductivity it is possible to express the conductivity transient as:

$$\overline{\sigma} = \frac{\sigma(t) - \sigma_0}{\sigma_\infty - \sigma_0} = 1 - \sum_{n=1}^{\infty} \frac{2L_\beta^2}{\beta_n^2 \left(\beta_n^2 + L_\beta^2 + L_\beta \right)} \exp\left(-\frac{t}{\tau_n} \right) \tag{7}$$

which is valid only for small oxygen partial pressure steps, *i.e.* small changes in oxygen nonstoichiometry. Using equation (7) it is possible to obtain the parameters $\tilde{D}$ and K_{tr} from the experimental relaxation data provided that $0.03 < L_\beta < 30$. As outlined previously by Den Otter *et al.* [15], $\tilde{D}$ cannot be obtained from the relaxation data if $L_\beta < 0.03$. In that case the equilibration towards the new nonstoichiometry is entirely governed by the surface reactions. On the other hand, if $L_\beta > 30$, the transient is not affected by the surface reactions and only $\tilde{D}$ can be derived from the fitting procedure. A numerical method for calculation of the eigenvalues β_n is presented elsewhere [16].

3.3   Experimental

3.3.1   Sample preparation

$La_{1-x}Sr_xCoO_{3-\delta}$ ($x = 0.2$, 0.5 and 0.7) perovskite powders were prepared by thermal decomposition of precursor complexes derived from nitrate solutions using ethylene-diamine tetra-acetic acid (EDTA) as a complexing agent [17]. After calcination at 940°C the powders were isostatically pressed at 4000 bar and sintered at 1150°C for 10 h. The sintered bodies showed a relative density in excess of 96%. For conductivity relaxation experiments thin rectangular samples of 0.5 mm thickness, cut from the sintered bodies, were polished with 1000 MESH SiC and ultrasonically cleaned in ethanol prior to use.

3.3.2   Conductivity relaxation

The set-up used for conductivity relaxation experiments is shown schematically in figure 3.1. Relative changes in the electrical conductivity following a step change in p_{O_2}

were measured with a four-point technique using gold wires as electrodes. Gold paste[*] was used to attach the wires. The electrodes were fixed at their position after annealing in air at 900°C for 3 hours. Measurements were performed over the p_{O_2} range 10^{-4}-1 bar and temperature range 600-850°C. Step changes in p_{O_2} were achieved by using two separate nitrogen-diluted oxygen gas flows at 300 ml min^{-1}. Moisture filters[†] removed traces of water. With a fast electrical four-way valve the flows leading to the sample and the vent could be interchanged. The time constant for changing the p_{O_2} in the reactor was less than 0.75 s at 700°C. YSZ-based electrochemical oxygen pumps were used for achieving p_{O_2} values lower than 10^{-2} bar. The p_{O_2} in both gas streams was measured using a commercial oxygen sensor[‡]. The p_{O_2} in both oxidising and reducing runs was changed with a factor of three. Oxidising runs were carried out at a final p_{O_2} of 10^{-3} bar or higher to avoid mass transfer limitations in the gas phase.

1 Water absorber   3 Oxygen pump   5 Sample furnace
2 Mass flow controller   4 Four-way valve   6 Oxygen sensor
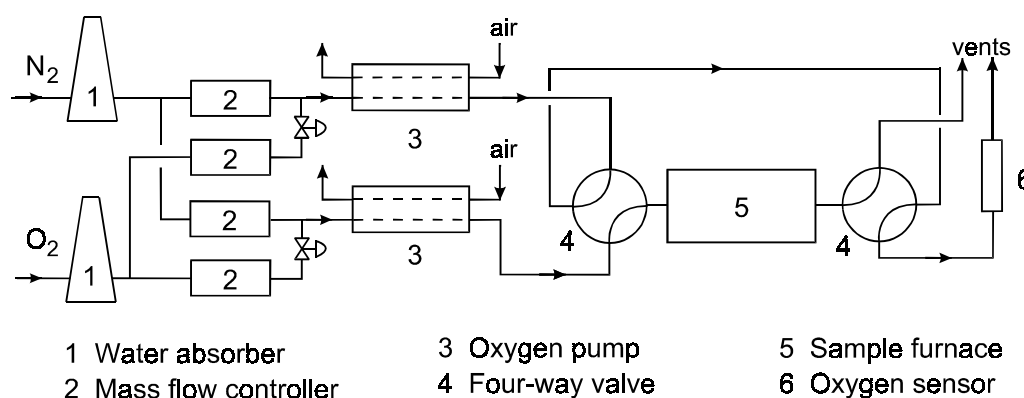
Figure 3.1:   Schematic representation of the conductivity relaxation set-up.

Four-point AC conductivity measurements were carried out using a lock-in amplifier[§]. The normalised change in conductivity with time after a step change in p_{O_2} was analysed using a computer program [18]. A more comprehensive description of the experimental set-up and details of the fitting routine are given elsewhere [19].

3.4   Results

Figure 3.2 shows typical conductivity relaxation data observed for different compositions La$_{1-x}$Sr$_x$CoO$_{3-\delta}$, following a p_{O_2} step change from 0.03 to 0.01 bar at 750°C. At high p_{O_2}, data from oxidation and reduction runs to the same final p_{O_2} were effectively identical. At

---

[*] Heraeus, Germany
[†] Gas Clean Moisture Filter 7971, Chrompack, The Netherlands
[‡] ZR893/4, Systech, The Netherlands
[§] EG&G Princeton Applied Research 5210, Ireland

p_{O_2} values below 0.03 bar, however, significant mass transfer limitations occurred in oxidation runs. For this reason only the fitted parameters obtained from data of reduction runs are presented below. The conductivity transients of the sample with composition $x = 0.2$ showed somewhat more noise, which is due to the higher electronic conductivity and, hence, smaller change in electrical conductivity with p_{O_2} relative to that observed for the other compositions in this study.
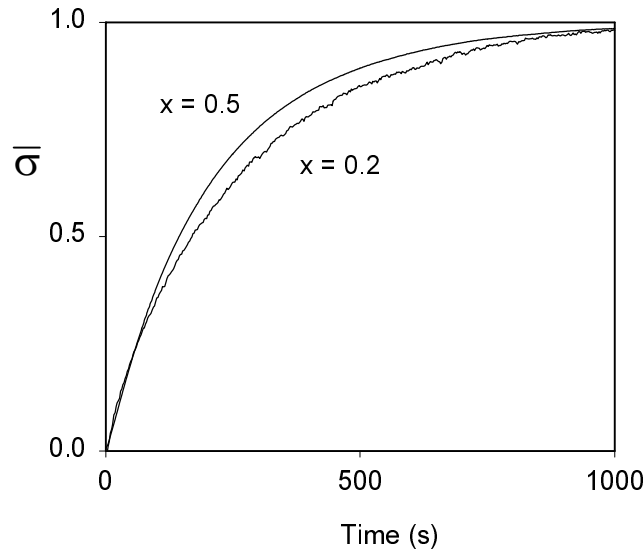
Figure 3.2: Typical relaxation transients for two different La$_{1-x}$Sr$_x$CoO$_{3-\delta}$ samples after a p_{O_2} step change from 0.03 to 0.01 bar at 750°C.

The chemical diffusion coefficient $\tilde{D}$ and surface transfer coefficient K_{tr} for La$_{1-x}$Sr$_x$CoO$_{3-\delta}$ as a function of p_{O_2} are shown in figure 3.3. The general trend observed is that both $\tilde{D}$ and K_{tr} remain fairly constant at high p_{O_2} values, but are significantly smaller at low p_{O_2}. Below a p_{O_2} of about 10^{-2} bar both parameters vary approximately with a $p_{O_2}{}^n$ dependence, with values of n as listed in table 3.1.

Arrhenius plots for $\tilde{D}$ and K_{tr} are given in figure 3.4 and figure 3.5. These plots were derived from relaxation data in which the final p_{O_2} was 0.011 bar. The same figures show the corresponding Arrhenius plots for the composition with $x = 0.7$ at several p_{O_2} values. Similar plots were obtained for the compositions with $x = 0.2$ and $x = 0.5$. A summary of activation energies obtained for $\tilde{D}$ and K_{tr} is given in table 3.2. The characteristic thickness L_c of La$_{1-x}$Sr$_x$CoO$_{3-\delta}$ varies between 50 and 150 μm and shows only a weak dependence on temperature and p_{O_2}. This is illustrated for the composition with $x = 0.7$ in figure 3.6.
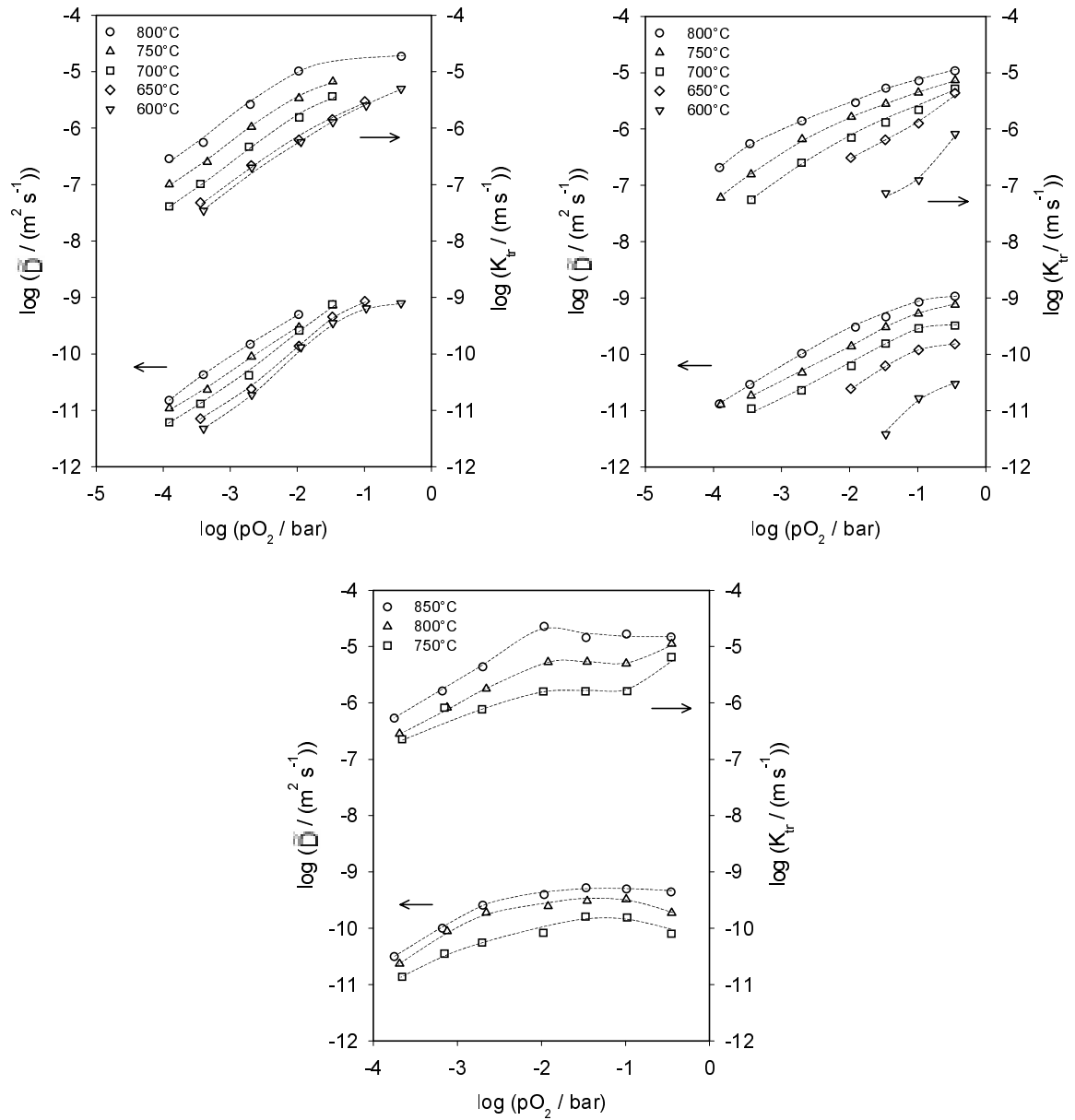
Figure 3.3: $\widetilde{D}$ and K_{tr} as a function of oxygen partial pressure for the La$_{1-x}$Sr$_x$CoO$_{3-\delta}$ compositions investigated: $x = 0.7$ (top left), 0.5 (top right) and 0.2 (bottom). The lines are an aid to link the data and have no theoretical significance.

Table 3.1:   Values of n for $\widetilde{D}$ and K_{tr} at various temperatures, determined for $p_{O_2} < 10^{-2}$ bar

T (°C)	La$_{0.3}$Sr$_{0.7}$CoO$_{3-\delta}$		La$_{0.5}$Sr$_{0.5}$CoO$_{3-\delta}$		La$_{0.8}$Sr$_{0.2}$CoO$_{3-\delta}$	
	$n_{\widetilde{D}}$	$n_{K_{tr}}$	$n_{\widetilde{D}}$	$n_{K_{tr}}$	$n_{\widetilde{D}}$	$n_{K_{tr}}$
600	0.99	0.80	-	-	-	-
650	0.94	0.81	-	-	-	-
700	0.89	0.80	0.53	0.72	-	-
750	0.76	0.80	0.56	0.72	0.41	0.43
800	0.78	0.84	0.68	0.55	0.49	0.70
850	-	-	-	-	0.57	0.92
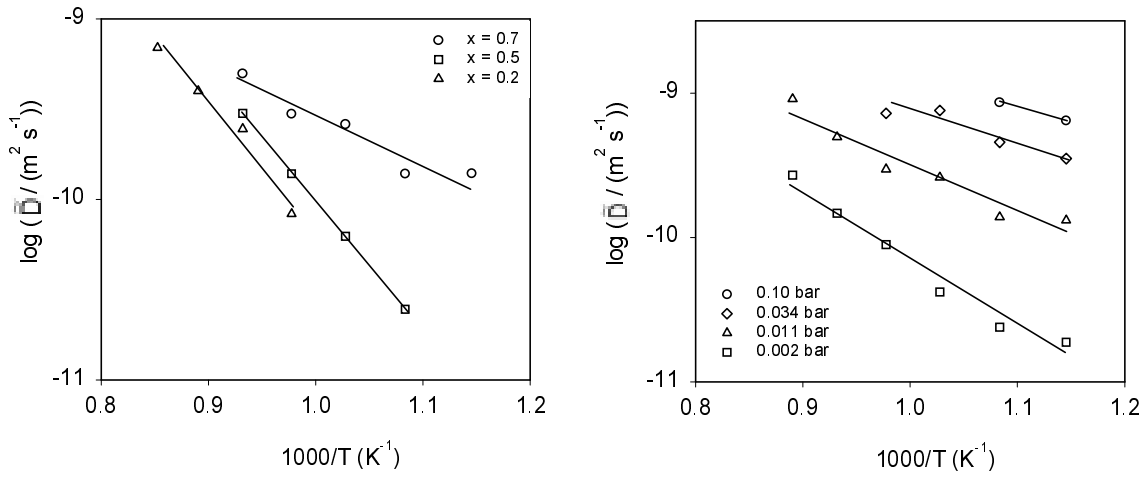
Figure 3.4:   Arrhenius plots of $\widetilde{D}$ for the $La_{1-x}Sr_xCoO_{3-\delta}$ compositions investigated at 0.011 bar (left) and for $x = 0.7$ at various oxygen partial pressures (right).
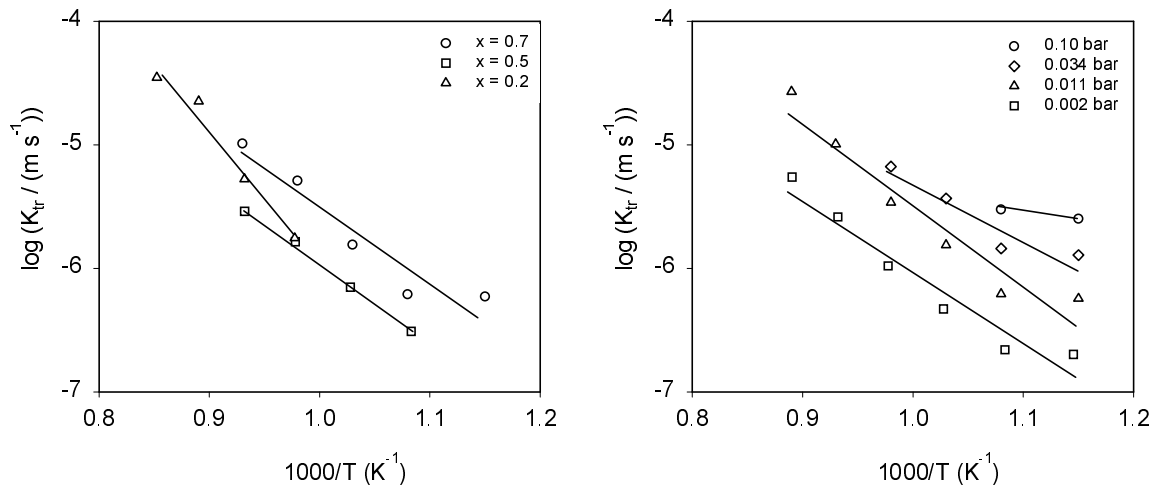
Figure 3.5:   Arrhenius plots of K_{tr} for the $La_{1-x}Sr_xCoO_{3-\delta}$ compositions investigated at 0.011 bar (right) and for $x = 0.7$ at various oxygen partial pressures (left).

Table 3.2: Activation energies of $\widetilde{D}$ and K_{tr} for $La_{1-x}Sr_xCoO_{3-\delta}$ at various p_{O_2}. Values are given in $kJ \cdot mol^{-1}$.

p_{O_2} (bar)	$La_{0.3}Sr_{0.7}CoO_{3-\delta}$		$La_{0.5}Sr_{0.5}CoO_{3-\delta}$		$La_{0.8}Sr_{0.2}CoO_{3-\delta}$	
	$E_{\widetilde{D}}^a$	$E_{K_{tr}}^a$	$E_{\widetilde{D}}^a$	$E_{K_{tr}}^a$	$E_{\widetilde{D}}^a$	$E_{K_{tr}}^a$
1.1×10^{-1}	65	105	106	97	108	198
3.4×10^{-2}	61	112	111	117	110	207
1.1×10^{-2}	63	134	136	126	136	216
2.0×10^{-3}	97	126	131	147	154	166
4.0×10^{-4}	91	117	-	-	-	-

3.5   Discussion

3.5.1   Chemical diffusion coefficient $\widetilde{D}$

Oxygen transport in defective perovskite oxides is generally considered to occur via a vacancy hopping mechanism. The diffusivity of oxygen is thus related to the extent of oxygen nonstoichiometry exhibited by the oxide. For a material with prevailing electronic conductivity, as observed for phases La$_{1-x}$Sr$_x$CoO$_{3-\delta}$, the following expression relates the chemical diffusion coefficient $\widetilde{D}$ to the vacancy diffusion coefficient D_V:

$$\widetilde{D} = D_V \cdot \gamma \tag{8}$$

where γ is the thermodynamic factor, defined by

$$\gamma = -\frac{1}{2}\frac{\partial \ln p_{O_2}}{\partial \ln \delta} \tag{9}$$

Strictly speaking, equation (8) holds only if oxygen vacancies are non-interacting and randomly distributed. The quantity γ is determined directly from experiment by measuring the oxygen nonstoichiometry as a function of p_{O_2}, either by thermogravimetry or coulometric titration. Utilising the nonstoichiometry data of Lankhorst and Bouwmeester [12] and Mizusaki *et al.* [20], it is found that γ for the phases La$_{1-x}$Sr$_x$CoO$_{3-\delta}$ is virtually independent of p_{O_2} at conditions covered by the experiments. For non-interacting defects the vacancy diffusion coefficient D_V is proportional to the fraction of regular lattice oxygen ions, $3-\delta \approx 3$, and is therefore expected to be approximately constant. When both γ and D_V are independent of p_{O_2} it follows from equation (8) that also $\widetilde{D}$ is invariant with p_{O_2}. It is seen in figure 3.3 that $\widetilde{D}$ decreases strongly with decreasing p_{O_2} below about 10^{-2} bar at
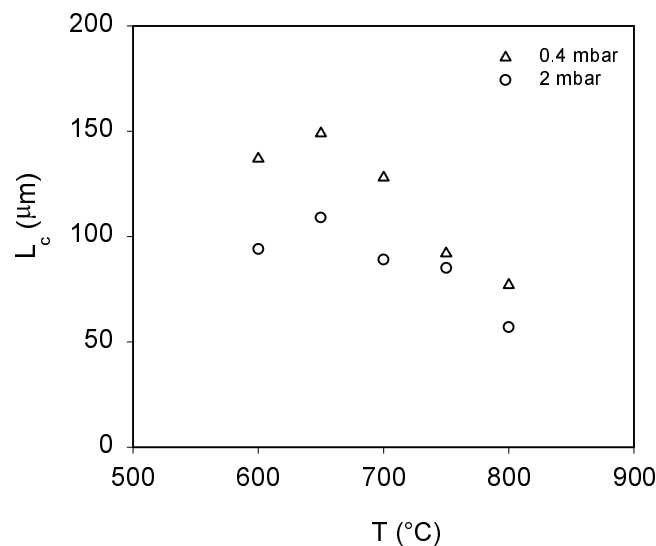

Figure 3.6:   Characteristic thickness L_c versus temperature for La$_{1-x}$Sr$_x$CoO$_{3-\delta}$ ($x = 0.7$).

all temperatures. The values measured for $\tilde{D}$ in the p_{O_2} range 0.01-1 bar are in good agreement with data obtained from chemical diffusion experiments using coulometric titration by Lankhorst and Bouwmeester [12]. Unfortunately, no data are provided by these authors at p_{O_2} values below 10^{-2} bar.

A possible explanation for the decrease of $\tilde{D}$ at low p_{O_2} values observed in this study is the ordering of oxygen vacancies on the oxygen sublattice. By virtue of the high level of oxygen nonstoichiometry exhibited by phases $La_{1-x}Sr_xCoO_{3-\delta}$, the assumption of randomly distributed non-interacting point defects is probably an oversimplified picture. In literature, ample evidence has been provided by XRD, electron diffraction and HRTEM measurements that nonstoichiometry in the oxygen-deficient perovskites is often accommodated by vacancy ordering to a degree which depends both on oxygen partial pressure and temperature [21-23]. Investigations by Adler *et al.* [24] using high temperature ^{17}O-NMR on perovskite oxides $BaInO_{2.5}$, $BaIn_{0.67}Zr_{0.33}O_{3-\delta}$, $BaIn_{0.67}Ce_{0.33}O_{3-\delta}$, and the related compounds $La_{0.6}Sr_{0.4}Co_{0.8}Cu_{0.2}O_{3-\delta}$ and $La_{0.6}Sr_{0.4}Co_{0.8}Cu_{0.2}O_{3-\delta}$ made clear that in all these phases only few oxygen vacancies are mobile below 800ºC. For both cobalt-containing compounds the signal intensity was found to increase steadily with temperature up to the maximum temperature of 950ºC in their study, suggesting a concomitant increase in the density of mobile oxygen anions.

Considerations of the mechanism of oxygen transport in oxygen-deficient perovskite structures indicate that both the migration energy ΔH_m and the enthalpy associated with the formation of mobile oxygen vacancies ΔH_f contribute to the apparent activation energy of $\tilde{D}$. To a first approximation ΔH_m may be taken as constant, *i.e.* independent of the level of oxygen nonstoichiometry. This implies that any variation in the activation energy with p_{O_2} can be ascribed to corresponding changes in ΔH_f. It is seen in table 3.2 that $E_{\tilde{D}}^a$ for phases $La_{1-x}Sr_xCoO_{3-\delta}$ increases with decreasing p_{O_2}. This can be rationalised by the increased energy of formation of mobile oxygen vacancies in the ordered structure.

3.5.2   Oxygen surface transfer

From comparison of the data presented in figure 3.3, it is evident that the surface transfer coefficients K_{tr} for phases $La_{1-x}Sr_xCoO_{3-\delta}$ display the same trend as the chemical diffusion coefficients $\tilde{D}$ with a change of temperature or p_{O_2}. The strong correlation observed between $\tilde{D}$ and K_{tr} suggests that oxygen vacancies play a major role in the surface oxygen transfer of these materials. Noteworthy is that the correlation is even observed in regions of temperature and p_{O_2}, where vacancy ordering is assumed. This may be taken as evidence

that the concentration of mobile oxygen vacancies, rather than the extent of oxygen nonstoichiometry, plays a decisive role in oxygen surface transfer. This strong correlation between $\tilde{D}$ and K_{tr} is also reflected in the weak temperature and p_{O_2} dependencies observed for the parameter L_c in this study.

A correlation between the tracer diffusion coefficient D^* and the surface exchange coefficient k_s for various perovskite- and fluorite-related structures was previously noted by Kilner [25] and De Souza and Kilner [26]. When $\log(k_s)$ is plotted as a function of $\log(D^*)$ a correlation is apparent, albeit that a different correlation is found for the perovskite and fluorite structures. For the perovskites, a slope close to 0.5 is found from linear regression on the logarithmic data [25]. One exception is La$_{1-x}$Sr$_x$CoO$_{3-\delta}$ ($x = 0.2$, 0.5) for which this slope is reported to be 0.69 [26]. It should be noted that all D^* and k_s values in the latter study were obtained from depth-profiling SIMS after isotope exchange at selected temperature at a p_{O_2} of 1 bar.
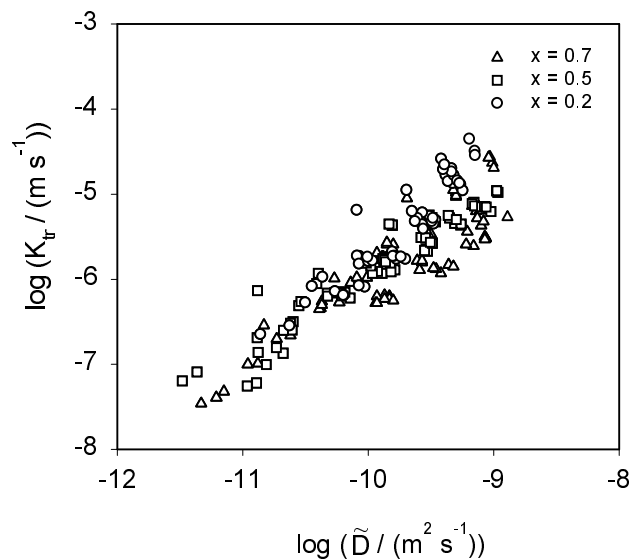
Figure 3.7:   Double logarithmic graph showing the correlation between $\tilde{D}$ and K_{tr} for the La$_{1-x}$Sr$_x$CoO$_{3-\delta}$ compositions investigated.

Figure 3.7 shows $\log(K_{tr})$ versus $\log(\tilde{D})$ for the La$_{1-x}$Sr$_x$CoO$_{3-\delta}$ compositions. All data measured in this study, regardless of temperature and p_{O_2}, have been included. The slope is approximately equal to 1. Although significant scatter is present, the graph clearly indicates that the two parameters are correlated even for the materials with different strontium contents.

In the ranges of temperature and p_{O_2} covered by the present experiments, L_c for La$_{1-x}$Sr$_x$CoO$_{3-\delta}$ varies approximately between 50 and 150 μm, which is close to the value of 100 μm reported by Kilner [25]. For La$_{0.3}$Sr$_{0.7}$CoO$_{3-\delta}$, the value of L_c from conductivity relaxation is found to be an order of magnitude smaller than that from isotope exchange as reported by Van Doorn *et al.* [27]. Further investigation is required to understand this difference.

3.6   Concluding remarks

Data from the present study suggests that the surface transfer coefficients K_{tr} and the chemical diffusion coefficients $\tilde{D}$ for phases La$_{1-x}$Sr$_x$CoO$_{3-\delta}$ are correlated. The general trend displayed is that both parameters decrease strongly with decreasing p_{O_2} below about 10^{-2} bar at all temperatures. This behaviour is unexpected for the diffusivity of oxygen in the oxygen-deficient perovskite structures from the point of view of point defect considerations and indicates that oxygen vacancies at low enough p_{O_2} are less mobile due to ordering phenomena. It is surprising to note that the correlation between K_{tr} and $\tilde{D}$ extends even in those regions where vacancy ordering is assumed to occur. This is tentatively explained by the key role of the concentration of mobile oxygen vacancies, rather than the extent of oxygen nonstoichiometry, in determining the rate of both processes.

3.7   References

1   E.A. Hazbun, "Ceramic Membrane for Hydrocarbon Conversion," US Patent 4,791,079, 1988

2   A.G. Dixon, W.R. Moser and Y.H. Ma, "Waste Reduction and Recovery using O$_2$-permeable Membrane Reactors," *Ind. Eng. Chem. Res.*, 33 3015 (1994)

3   T.J. Mazanec, "Novel solid multi-component membranes, electrochemical reactors and use of membranes and reactor for oxidation reactions," European Patent Application 0,399,833, 1990

4   R.M. Thorogood, R. Srinivasan, T.F. Yee and M.P. Drake, "Composite mixed conductor membranes for producing oxygen," US Patent 5,240,480, 1993

5   M. Liu, A.V. Joshi and Y. Shen "Mixed ionic-electronic conductors for oxygen separation and electrocatalysis," US Patent 5,273,628, 1993

6   A.J.Burggraaf and Y.S. Lin, "Method for manufacturing ultrathin inorganic membranes," US Patent 5,160,618, 1992

7   M.F. Carolan, P.N. Dyer, J.M. LaBar, Sr., and R.M. Thorogood "Process for recovering oxygen from gaseous mixtures containing water or carbon dioxide which process employs ion transport membranes," US Patent 5,261,932, 1993

8   T.J. Mazanec, T.L. Cable and J.G. Frye, "Electrocatalytic cells for chemical reaction," *Solid State Ionics* **53-56** [1] 111-18 (1992)

9   H.J.M. Bouwmeester, H. Kruidhof, A.J. Burggraaf, "Importance of the surface exchange kinetics as rate limiting step in oxygen permeation through mixed-conducting oxides", *Solid State Ionics* **72**, 185 (1994)

10 R.H.E. van Doorn, H. Kruidhof, H.J.M. Bouwmeester, A.J. Burggraaf, *Mater. Res. Soc. Symp. Proc.* 369, Solid State Ionics IV, G. -A. Nazri, J. -M. Taracson, M.S. Schreiber, Eds., Materials Research Society, Pittsburgh, 377 (1995)

11 Y. Teraoka, T. Nobunaga, N. Yamazoe, "Effect of cation substitution on the oxygen semipermeability of perovskite-type oxides", *Chem. Lett.*, 503 (1988)

12 M.H.R. Lankhorst and H.J.M. Bouwmeester, "Determination of oxygen nonstoichiometry and diffusivity in mixed conducting oxides by oxygen coulometric titration. I. chemical diffusion in La$_{0.8}$Sr$_{0.2}$CoO$_{3-\delta}$", *J. Electrochem. Soc.* **144**, 1261 (1997)

13 J. Mizusaki, J. Tabuchi, T. Matsuura, S. Yamauchi, K. Fueki, "Electrical conductivity and seebeck coefficient of nonstoichiometric La$_{1-x}$Sr$_x$CoO$_{3-\delta}$", *J. Electrochem. Soc.* **136**, 2082 (1989)

14 J. Crank, 'The Mathematics of Diffusion', 2nd ed., p. 60, Oxford University Press, Oxford (1979)

15 M.W.den Otter, H.J.M. Bouwmeester, B.A. Boukamp, H. Verweij, "Reactor flushtime correction in relaxation experiments", *J. Electrochem. Soc.*, **148**, J1-J6 (2001)

16 M.W. den Otter, L.M. van der Haar, H.J.M. Bouwmeester, "Numerical evaluation of eigenvalues of the sheet diffusion problem in the surface/diffusion mixed regime", *Solid State Ionics* **13**, 259 (2000)

17 R.H.E. van Doorn, H. Kruidhof, A.N. Nijmeijer, L. Winnubst, A.J. Burggraaf, "Preparation of La$_{0.3}$Sr$_{0.7}$CoO$_{3-\delta}$ perovskite by thermal decomposition of metal-EDTA complexes", *J. Mat. Chem.* **8**, 2109 (1998)

18 Relaxation Analysis software, version 1.2, by B.A. Boukamp, Internet: http://www.ct.utwente.nl/~ims/

19 M.W. den Otter, 'A study of oxygen transport in mixed conducting oxides using isotopic exchange and conductivity relaxation', Ph.D. thesis, University of Twente, the Netherlands, Chapter 7 (2000)

20 J. Mizusaki, Y. Mima, S. Yamauchi, K. Fueki, "Nonstoichiometry of the perovskite-type oxides La$_{1-x}$Sr$_x$CoO$_{3-\delta}$", *J. Solid Sate Chem.* **80**, 102 (1989)

21 C.N.R. Rao, J. Gopalakrishnan, K. Viyasagar, "Superstructures, ordered defects & nonstoichiometry in metal oxides of perovskite & related structures", *Indian J. Chem.*, **23A**, 265 (1984)

22 P. Hagenmuller, M. Pouchard, J.C. Grenier," Nonstoichiometry in the perovskite-type oxides: an evolution from the classical Schottsky-Wagner model to the recent high Tc superconductors", *Solid State Ionics*, **43**, 7 (1990)

23 R.H.E. van Doorn and A.J. Burggraaf, "Structural aspects of the ionic conductivity of La$_{1-x}$Sr$_x$CoO$_{3-\delta}$", *Solid State Ionics*, **128**, 65 (2000)

24 S. Adler, S. Russek, J Reimer, M. Fendorf, A. Stacy, Q. Huang, A. Santoro, J. Lynn, J. Baltisberger, U. Werner, "Local structure and oxide-ion motion in defective perovskites", *Solid State Ionics* **68**, 193 (1994)

25 J.A. Kilner, Isotopic exchange in mixed and ionically conducting oxides, in Proc. 2nd Int. Symp. Ionic and Mixed conducting ceramics, 94-12, T.A. Ramanarayanan, W.L. Worell, H.L. Tuller, Eds., The Electrochem. Soc. Pennington, N.J., 174 (1994)

26 R.A. de Souza, J.A. Kilner, *Solid State Ionics,* "Oxygen transport in La$_{1-x}$Sr$_x$Mn$_{1-y}$Co$_y$O$_{3\pm\delta}$ perovskites, Part II. Oxygen surface exchange", **126**, 153 (2000)

27 R.H.E. van Doorn, I.C. Fullarton, R.A. de Souza, J.A. Kilner, H.J.M. Bouwmeester, A.J. Burggraaf, "Surface oxygen exchange of La$_{0.3}$Sr$_{0.7}$CoO$_{3-\delta}$,", *Solid State Ionics*, **96**, 1 (1997)

4

Preparation of perovskite supports

Abstract

*Porous La$_{1-x}$Sr$_x$CoO$_{3-\delta}$ supports were prepared by using two different techniques. The first technique was based on pressing of pre-sintered powders, made is this laboratory, which were homogenised by sieving and classification through sedimentation. By controlling the pre-sintering temperature of the powder, 30% porous materials with an average pore diameter of 0.8 µm could be obtained after sintering at 1100°C. The gas permeability of these materials is sufficiently high to apply them as support for thin film La$_{1-x}$Sr$_x$CoO$_{3-\delta}$ membranes. A method was proposed to enhance the surface morphology of the supports by applying a perovskite coating. The second preparation technique was based on compact formation by pressure filtration of commercial perovskite powder dispersed in a suitable medium. Applying the minimum allowable sintering temperature of 1020°C resulted in 30% porous materials with an average pore diameter of 0.3 µm. The morphology of these substrates is superior to that of the substrates prepared via pressing. A relatively small amount of defects was caused by inhomogeneities in the powder. Although the number of defects should still be decreased and the gas permeability of these substrates approaches the minimum requirements for application as membrane support, it is concluded that the latter substrates are most suitable for supporting thin film La$_{1-x}$Sr$_x$CoO$_{3-\delta}$ membranes. Furthermore, it was shown that centrifugal casting is a promising technique for the development of high-quality dense and porous La$_{1-x}$Sr$_x$CoO$_{3-\delta}$ membranes and supports with tubular geometry.*

4.1   General introduction

The challenge of developing dense high-flux oxygen separation membranes by preparing micrometer thick membranes includes the development of porous supports in order to give the membrane sufficient mechanical stability. For the preparation of the thin film membrane itself several chemical and physical techniques can be employed, like sol-gel coating, chemical and electrical vapour deposition, sputtering and pulsed laser deposition. However, regardless of which deposition technique is used, the development of a thin dense membrane starts with developing a suitable membrane support since the properties of the deposited layers strongly depend on the membrane support. In general, the support should meet the following requirements:

- A narrow pore size distribution, at least near the surface on/in which the top-layer will be deposited. It is assumed that the pore size should be smaller than the thickness of the top-layer to be applied

- The ability to withstand the membrane operation temperature for an extended period of time without any chemical and structural changes taking place

- Similar thermal and chemical expansion behaviour of the support and the top layer

- The mass transport resistance of the support should not determine the rate of permeation

- Sufficient mechanical strength

A support material that lies readily at hand in view of availability and price is α-Al$_2$O$_3$ [1-3]. Substantial knowledge is available on its processing into homogeneous and highly porous substrates. However, the expansion coefficient of α-Al$_2$O$_3$ differs greatly from that of most mixed-conducting perovskites. This difference has both a physical and a chemical origin. At room temperature the difference in (physical) thermal expansion coefficient is a factor 2-3: 6×10^{-6} K^{-1} for α-Al$_2$O$_3$ against 15×10^{-6} K^{-1} for La$_{0.4}$Sr$_{0.6}$Co$_{0.2}$Fe$_{0.8}$O$_{3-\delta}$[*]. When the material is heated and the pO$_2$ of the surrounding atmosphere is kept constant, oxygen is released from the lattice, starting at temperatures typically around 600°C. In Kröger-Vink notation the accompanying reaction is given by:

$$2O_O^x + 4Fe_{Fe}^x \rightarrow 4Fe_{Fe}^{'} + 2V_O^{\cdot\cdot} + O_2(g)$$ (4.1)

---
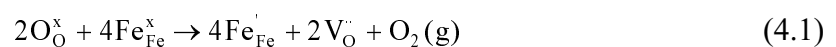
[*] This composition is used as illustration since reliable thermal expansion data are available. The thermal expansion behaviour of La$_{1-x}$Sr$_x$CoO$_{3-\delta}$ is similar although the actual values of the expansion coefficients are still higher.

Simultaneously with the formation of oxygen vacancies, a valence change of the metal cations occurs. Although the oxygen vacancies consume less space in the lattice than the oxygen ions, the increase of the ionic radii of the cations dominates and the net result is an additional lattice expansion adding to the physical expansion. As indicated by the results of Tai *et al.* [4], this effect contributes 14×10^{-6} K^{-1} to the thermal expansion coefficient of $La_{0.4}Sr_{0.6}Co_{0.2}Fe_{0.8}O_{3-\delta}$, yielding a total expansion coefficient of 29×10^{-6} K^{-1} in the temperature range 800-1000°C. Figure 5.1 summarises the results for $La_{1-x}Sr_xCo_{0.2}Fe_{0.8}O_{3-\delta}$. The slopes of the lines in this figure are the expansion coefficients. The increase in expansion coefficient at high temperatures is most outspoken for the compositions with high strontium content, caused by the fact that strontium facilitates the formation of oxygen vacancies. Because of the difference in expansion behaviour between α-Al_2O_3 and virtually all oxygen permeable MIEC perovskite materials, the former is not a suitable support material. Experiments indeed showed that thin dense perovskite layers deposited on top of α-Al_2O_3 substrates, are severely cracked when heated to 600°C [5,6].
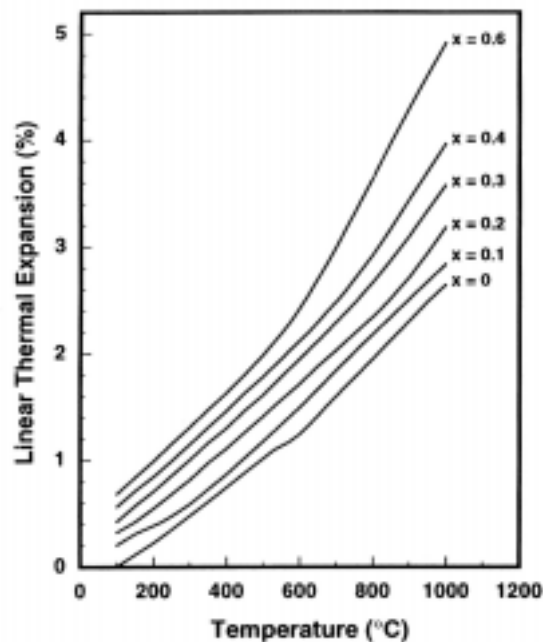
Figure 5.1: Linear thermal expansion of $La_{1-x}Sr_xCo_{0.2}Fe_{0.8}O_{3-\delta}$ as reported by Tai *et al.*[4]. Used with permission of the publishers.

A good alternative might be the use of sintered metal alloy supports. They possess the advantage that their expansion coefficient can be readily tuned by varying the metal compositions of the alloys. On the other hand, such metals do not show a variation in expansion coefficient with temperature that is similar to that of the perovskites mentioned. Mismatch problems will therefore also be likely to occur for combinations of these

materials. Another major drawback of the use of metal alloys is their general tendency towards oxidation at usual membrane operation conditions.

Altogether, the application of supports consisting of the same material as the dense top layer appears to be the best option. However, in literature little knowledge is available about the processing of perovskite materials into suitable supports. Teraoka *et al.* [7] looked in some detail at the preparation of porous perovskite supports, but their approach leads to substrates with large pores of about 30 μm diameter, which is too large for applying a dense μm thick top layer. In addition, Dionysiou *et al.* [8] reported some results on the preparation of porous proton-conducting perovskite oxides. Their results suggest an approach to prepare porous supports with variable porosity and pore size by controlling the calcination and final sintering temperature of respectively the powder and the compact. In the first part of this chapter this approach is further developed and applied to prepare flat disc-shaped porous $La_{1-x}Sr_xCoO_{3-\delta}$ ($x = 0.7$, 0.5, 0.2) samples. In the second part, an alternative approach is employed. This technique, derived from an analogous method to prepare α-Al_2O_3 supports, is based on pressure filtration of a (quasi-) stable powder dispersion in a liquid medium. In the third and final part of this chapter, the preparation of both tubular perovskite supports as well as dense tubular membranes is described. In this part, centrifugal casting is employed as consolidation technique.

Part 1: Flat supports prepared by pressing

The calcination or (pre-) sintering temperature of the powder and the compact are expected to have a strong influence on the final porosity and pore size of the resulting support [7,8]. To obtain membrane supports that comply with the requirements mentioned in the introduction, the influence of these and other relevant processing parameters on the final support properties is investigated. Parameters studied are the sinter temperature of the compact, the isostatic pressure during compaction, the milling time and the calcination or pre-sintering temperature of the powder. The pore size distribution and gas permeability of the perovskite supports are evaluated as functions of the above mentioned processing parameters. In addition the effect of surface modification by applying a coating is investigated.

4.2   Experimental

4.2.1   Preparation

The supports were prepared via a procedure that was derived from the method described by Van Doorn *et al*. [9] to produce dense mixed conducting membranes, which consists of the following steps. Metal nitrates are dissolved and mixed in the appropriate stoichiometric ratio. EDTA is added as a complexing agent and the excess water is evaporated until the solution becomes viscous. The solution is then pyrolysed in a stove at 240°C. The as-obtained powder is calcined at 940°C. Subsequently, the powder is ball-milled in acetone in a plastic container on a roller bench rotating at 55 rpm. ZrO_2 milling balls of 15 and 2 mm are used with a weight ratio of 1:5. The weight ratio of powder and milling balls is 1:12. Acetone is added in a 1:1 volume ratio. Milling is applied until a powder with a fairly sharp particle size distribution around 1 μm is obtained. The required milling time is 6 h. Disc-shaped compacts, obtained after isostatically pressing the powder at 400 MPa, are sintered in ambient atmosphere.

The above processing route was used as a starting point for a number of exploratory experiments. The influence of calcination temperature, milling time, isostatic pressure and sintering temperature on the properties of the final support was investigated. The powder

was characterised by means of particle size analysis by laser scattering[*]. The porosity of the sintered specimens was determined using Archimedes density measurements by immersion in Hg. Scanning Electron Microscopy (SEM) and Hg-intrusion[†] were used to investigate the pore shape and pore size distribution respectively. The samples were polished using Al_2O_3 slurry on a polishing cloth. First a rough polishing step was applied with SiC[‡] paper. After this step, the substrates were polished on a cloth with two Al_2O_3 slurries, containing grains of 0.3 and 0.05 μm, respectively. The gas permeability of the samples at room temperature was determined by dead-end permeation measurements. An absolute pressure difference was applied across the membrane while an atmospheric pressure was kept at the low-pressure side of the support. The gas flow through the porous materials was measured with a mass flow meter. The permeability at high temperature under a partial pressure difference was measured using the set-up described in [10], employing a feed stream of 100 ml/min O_2 and a He permeate sweep of 50 ml/min. For permeation measurements, all samples were cut into discs of 15 mm diameter and 1 mm thickness.

Initial experiments were performed on $La_{0.3}Sr_{0.7}CoO_{3-\delta}$. Based on the results of these experiments, a final preparation procedure was developed which was also used for the preparation of the $La_{0.5}Sr_{0.5}CoO_{3-\delta}$ and $La_{0.8}Sr_{0.2}CoO_{3-\delta}$ substrates.

4.2.2   Surface modification by coating

An obvious approach to improve the surface morphology of the polished samples is the application of a coating, preferably of the same composition as the substrate. In this study dip-coating is employed. For a general description of this coating technique, the reader is referred to appendix A of this thesis.

The substrates prepared via pressing were provided with a 2 μm thick coating layer by dip-coating the support in a fine particle slurry, followed by drying at room temperature and sintering in ambient atmosphere for 10 h with heating and cooling rates of 0.5°C/min. Two sintering temperatures were applied: 850°C and 1100°C. For the preparation of the coating slurry, $La_{0.3}Sr_{0.7}CoO_{3-\delta}$ powder that was calcined at 850°C was used. The powder was dispersed in 3 wt% solution of polyvinyl pyrolydone[§] (PVP) in isopropyl alcohol (IPA). The PVP served as a sterical colloidal stabiliser. The powder loading of the suspension was 10 wt% relative to the total weight of the IPA and perovskite powder. The suspension was

---

[*] Leeds & Northtrup Microtrac X100, USA
[†] Carlo Erba Porosimeter 2000, Italy
[‡] 35 μm grain size, Struers, Denmark
[§] MW 360,000, Janssen Chimica, Belgium

milled for 10 h in a planetary mill at 200 rpm. YSZ milling jars were used, containing 11 YSZ balls with a diameter of 10 mm and one with a diameter of 20 mm. The jar was filled for 80% with 30g suspension. After milling, the slightly viscous suspension was allowed to stand for 6 days, during which a deposit was formed containing all particles larger than 2 μm, as measured by laser scattering. The suspension was decanted and subsequently used to dip the substrates. The particle loading in the dipping suspension was 7wt%.

4.3   Results and discussion

4.3.1   Preparation

Variation of the sintering temperature

Sintering the compact at 1100°C yielded a substrate with a porosity less than 10% and a very low oxygen permeability at room temperature. Decreasing the sintering temperature to 1000°C resulted in 25% porous supports showing a fairly homogeneous porosity, as can be seen in figure 5.2. Nevertheless, at room temperature and under an *absolute* pressure difference of 1 bar, the oxygen flux through these supports was 2×10^{-6} mole·cm^{-2}·s^{-1}, which is still relatively low. For comparison, the oxygen flux through a dense 0.5 mm thick $La_{0.3}Sr_{0.7}CoO_{3-\delta}$ bulk membranes is of the order of 1×10^{-6} mole cm^{-2} s^{-1}, measured under a
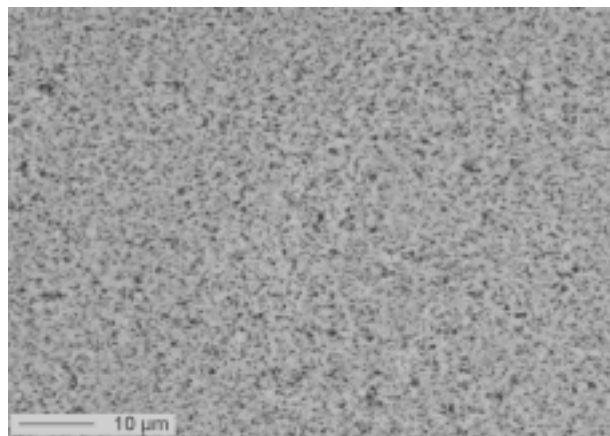
Figure 5.2:   SEM picture of a polished $La_{0.3}Sr_{0.7}CoO_{3-\delta}$ sample sintered at 1000°C

partial pressure difference of 1 bar at 1000°C. Since under a partial pressure difference gas transport due to viscous flow does not contribute, the flux through the support under these conditions is expected to be lower than 2×10^{-6} mole cm^{-2} s^{-1}. Considering this, it is concluded that the permeability of the supports sintered at 1000°C is still too low. When a

dense $La_{0.3}Sr_{0.7}CoO_{3-\delta}$ top layer is applied, the mass transport through the support mainly determines the membrane performance instead of the membrane thickness.

Variation of the applied isostatic pressure

Varying the isostatic pressure did not have a profound effect on the porosity and homogeneity of the resulting sintered substrate. Therefore an isostatic pressure of 400 MPa was maintained.

Variation of the calcination temperature and milling time

The sinter activity of the powder was decreased by raising the calcination temperature of the powder from 940 to 1150°C. Subsequent sintering of the compact for 10 h at 1100°C, with heating and cooling rates of 0.5°C/min, yielded a support with a porosity of 30%. Sintering at 1100°C ensures a stable porosity up to membrane operation temperatures of at least 1000°C. However, the pore size distribution of the resulting support was not optimal. During the high-temperature calcination step large and hard agglomerates were formed with a highly irregular size and shape. A further increase in the powder calcination temperature yielded supports that were very brittle and could not withstand any handling. This was caused by the presence of large pores but also by the very low sinter activity of the agglomerates in the calcined powder. Attempts to homogenise the calcined powder by applying a short wet milling treatment did not yield satisfactory results. The homogeneity of the powder increased but so did the sinter activity. On the other hand, grinding the powder in a mortar followed by sieving[*] improved the powder homogeneity while
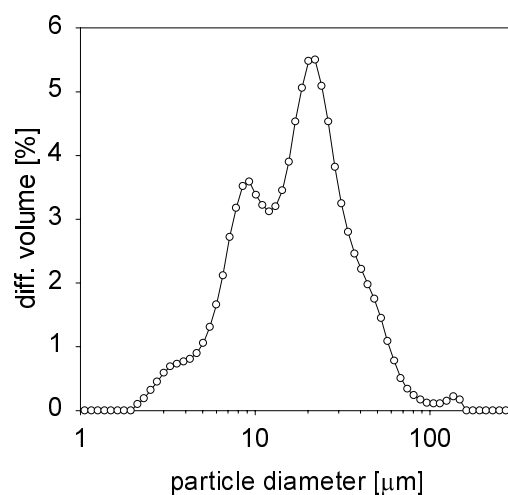

Figure 5.3:   Particle size distribution of the pre-sintered, sieved and classified powder

---

[*] Retsch ASTM, Germany

maintaining a low sinter activity. The best supports were obtained from the sieve fraction with particle sizes smaller than 53 µm. To prevent inhomogeneous sintering of the compact and to increase the gas permeability of the sintered supports, particles smaller than 2 µm were removed by classification through sedimentation. This was achieved by dispersing the powder ultrasonically in 2-propanol during 5 minutes. The powder loading of the resulting suspension was 10wt%. This suspension was allowed to settle for 1 h. The sediment was collected, dried and calcined at 450°C for 2 h and sieved again. The particle size distribution of the resulting powder turned out to be bimodal and rather broad, as shown in figure 5.3.

After compaction followed by sintering at 1100ºC, the supports had a porosity of 30%. Figures 5.4 and 5.5 show SEM and Hg-intrusion data for a $La_{0.3}Sr_{0.7}CoO_{3-\delta}$ support. The average pore diameter determined by Hg-intrusion is 0.9 µm. An explanation for the bimodal pore size distribution is the irregular particle shape and the broad particle size distribution, leading to inhomogeneities in the support. Pores with a diameter larger than around 2 µm contributed approximately 15% to the total pore volume, as determined by Hg-intrusion. The SEM micrograph in figure 5.4 shows a considerably larger amount of these large pores. This discrepancy might be caused by the polishing procedure prior to SEM analysis. Because of the low sinter activity of the powder grains, the cohesion between grains in the sintered support is rather weak. It is assumed that grains at the surface are removed during polishing.
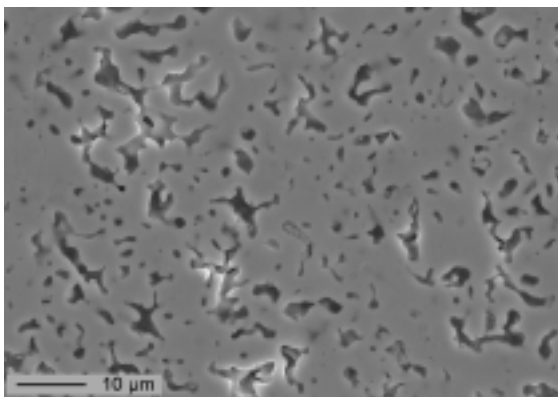
Figure 5.4: SEM picture of a polished $La_{0.3}Sr_{0.7}CoO_{3-\delta}$ support, sintered at 1100°C, prepared from presintered, sieved and classified powder
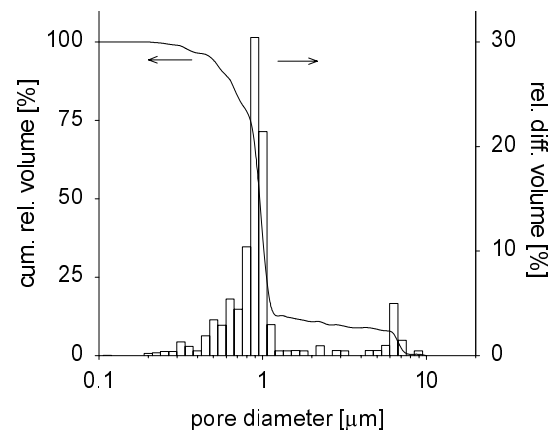
Figure 5.5: Pore size distribution of the support shown in figure 5.4, determined via Hg-intrusion

Figure 5.6 shows the oxygen and nitrogen permeance of the support shown in figure 5.4. From these data, measured at room temperature, the average pore diameter and tortuosity was calculated according to the method outlined by Veldsink *et al.* [11]. From both the nitrogen and oxygen permeance, an average pore diameter of 0.7 µm was calculated, which

corresponds well with the data from Hg-intrusion. The tortuosity in both cases was found to be 2.8.
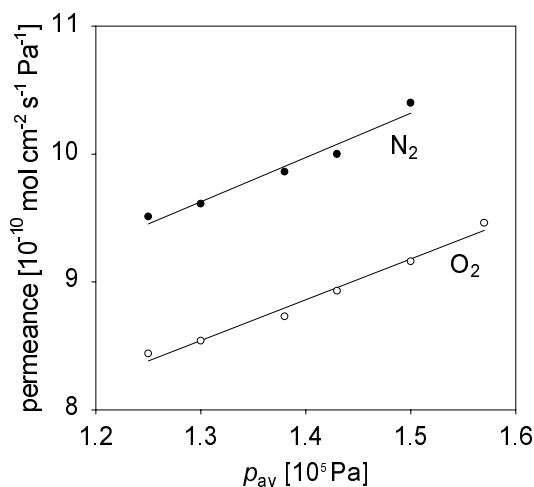
Figure 5.6:   Oxygen and nitrogen permeance of the La$_{0.3}$Sr$_{0.7}$CoO$_{3-\delta}$ support shown in figure 5.4, measured at room temperature

The oxygen flux through the support measured at room temperature and under an absolute pressure difference of 1 bar is 9.0×10^{-5} mole cm^{-2} s^{-1}, as can be inferred from the data shown in figure 5.6. At 1000°C, under a *partial* pressure difference of 1 bar, an oxygen flux of 1×10^{-5} mole cm^{-2} s^{-1} was measured. Comparing these values to the earlier mentioned highest measured flux through dense it can be concluded that the permeability exceeds that through dense La$_{0.3}$Sr$_{0.7}$CoO$_{3-\delta}$ membranes by approximately one order of magnitude.

4.3.2   Surface modification by coating

In figures 5.7 and 5.8, SEM pictures of a coated La$_{0.3}$Sr$_{0.7}$CoO$_{3-\delta}$ support are shown. When these are compared with figure 5.4, the improvement in the surface morphology is obvious. Sintering at 1100°C results in a very open structure as can be judged from figure 5.8. The applied coating is able to bridge pores with a diameter smaller than approximately 5 μm meaning that not all the large pores could be covered. Measurements at room temperature showed that the coating layer does not influence the permeability of the substrate.
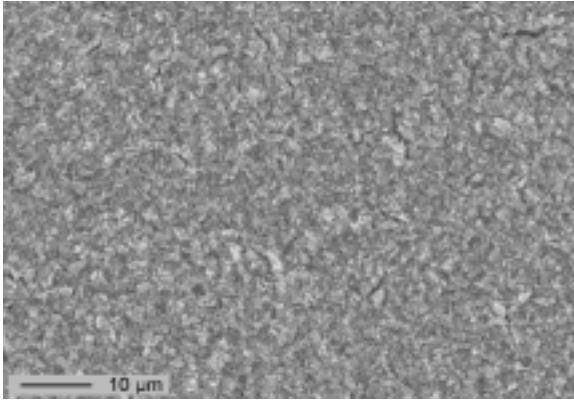
Figure 5.7: SEM picture of a coated $La_{0.3}Sr_{0.7}CoO_{3-\delta}$ substrate. The coating is sintered at 850°C.
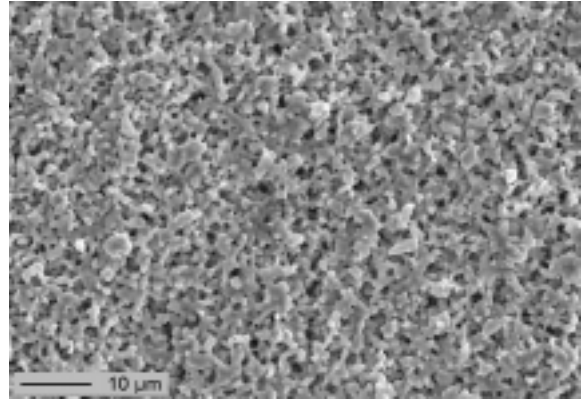
Figure 5.8: SEM picture of a coated $La_{0.3}Sr_{0.7}CoO_{3-\delta}$ substrate. The coating is sintered at 1100°C.

4.4 Final preparation route

The preparation route selected for coated $La_{1-x}Sr_xCoO_{3-\delta}$ substrates, prepared via pressing and sintering of pre-sintered powders, can be summarised as follows:

- Powder preparation via EDTA-complexation route
- Calcination of the pyrolysis product at 1150°C
- Grinding and sieving to obtain a powder with the particle size below 53 μm
- Removal of the fraction smaller than 53 μm via sedimentation
- Uniaxial shaping and isostatic pressing at 400 MPa
- Sintering at 1100°C for 10 h
- Polishing followed by dip coating
- Sintering at 1100°C for 10 h

4.5 Results for *x* = 0.5 and *x* = 0.2

Following the same preparation procedures, the results obtained for $La_{1-x}Sr_xCoO_{3-\delta}$ with x=0.5 were similar to that of the supports of composition with x = 0.7. For x=0.2, the mean pore diameter and the permeation were found to be somewhat lower. Table 5.1 gives porosity, mean pore diameter and oxygen flux measured at room temperature under an absolute pressure difference of 1 bar, for all compositions. The shape of the pore size distribution of both other compositions did not differ from that of the $La_{0.3}Sr_{0.7}CoO_{3-\delta}$ supports.

Table 5.1:   Porosity, average pore diameter (determined by Hg-intrusion) and oxygen flux at room temperature for all three compositions

Composition	Porosity (%)	Average pore diameter (μm)	O_2 flux* (mole cm^{-2} s^{-1})
$x = 0.7$	30	0.89	1.4×10^{-4}
$x = 0.5$	32	1.00	2.0×10^{-4}
$x = 0.2$	34	0.40	8.0×10^{-5}

*Measured at room temperature under an absolute pressure difference of 1 bar. Support thickness: 1 mm.

Part 2: Flat supports prepared by pressure filtration

The demand for powders with a high homogeneity is a universal problem in the field of ceramic processing. In the current tendency to develop more and more sophisticated ceramic structures, the quality of the ceramic starting powder increasingly becomes decisive. The same applies to the development of perovskite supports. Even though several techniques are available for the preparation of perovskite powders with small primary particles [9,13-15], in practice these particles generally form agglomerates, the form and size of which completely determine the properties of the powder, green compact and resulting porous support. As was shown in the first part of this chapter, the formation of agglomerates can be used advantageously in the preparation of porous supports. However, it was also shown that it is difficult to control the agglomeration and to tune the agglomerate size in such a way that a homogeneous porous structure is obtained.

The powder morphology problems mentioned above justify the great need for a robust synthesis technique that produces perovskite powders consisting of non-agglomerated particles of the desired size and with a sharp size distribution. Up till now, only highly dedicated techniques, based on emulsion processing, enable the synthesis of small, non-agglomerated ceramic particles [16]. Although the perspective for these techniques is bright, their application does not exceed the small laboratory scale yet. Therefore, it is still necessary to revert to the more established but less advanced synthesis techniques. Of all these, one of the best options appears to be spray pyrolysis. This technique is based on the atomisation of a suitable precursor solution, followed by drying of the droplets and subsequent calcination and sintering of the resulting particles. The process combines a complexation reaction powder synthesis with the important additional advantage of uniquely controlling the particle formation environment by compartmentalising the precursor solution into droplets. The particle size can be controlled in a relatively easy way by using an appropriate atomiser and by adjusting the precursor concentration. For more details on the spray pyrolysis technique, the reader is referred to an excellent review by Messing *et al.* [17].

Powders prepared by spray pyrolysis generally have a better morphology than powders prepared via bulk pyrolysis methods, like the EDTA synthesis employed in the first part of this chapter. Therefore, in the second approach for developing further optimised perovskite supports, which is described in the current part of this chapter, commercial

$La_{0.5}Sr_{0.5}CoO_{3-\delta}$[*] powder prepared by spray pyrolysis is used. In stead of pressing, pressure filtration is used as consolidation technique. Although pressing is a fast technique, it is generally difficult to obtain a defect-free compact due to inferior flowing properties of the starting powder and high friction during pressing, which both result in inhomogeneous mould filling. Although the flow properties can be improved by powder granulation and additives can diminish friction, a more elegant compaction process is provided by pressure filtration of a (quasi-) stable dispersion of the powder in a liquid medium. This convenient compaction technique does not rely on the flow properties and has proved to be successful in the preparation of homogeneous α-Al_2O_3 supports [12].

4.6   Process characteristics

Consolidation via pressure filtration of a suspension mainly consists of four process steps: suspension preparation, filtration, drying and sintering of the compact. During dispersion of the powder in the liquid medium, all particle aggregates should be destroyed. By choosing the appropriate medium and/or stabilising agent(s), the resulting suspension should be stable to a degree that during filtration no large-scale agglomeration occurs. The shrinkage of the compact during drying facilitates the release of the compact from the mould. After drying, the temperature program for the sintering step should be chosen in such a way that additives are allowed to burn off without damaging the compact. Although specific knowledge on the preparation of stable $La_{1-x}Sr_xCoO_{3-\delta}$ suspensions is very scarce, a comprehensive overview on the general subject of suspension stability has been given by Everett [18].

4.7   Experimental

4.7.1   Medium selection

Sedimentation experiments were performed using 50wt% $La_{0.5}Sr_{0.5}CoO_{3-\delta}$ suspensions based on combinations of various media and stabilising agents. These experiments were carried out as a qualitative screening of the applicability of some common, easily accessible media and stabilisers, and not as an in-depth study on perovskite suspension stability. For all experiments, commercial $La_{0.5}Sr_{0.5}CoO_{3-\delta}$ powder[†] was used. The

---

[*] 99.9%, Praxair Specialty Ceramics, USA
[†] 99.9%, Praxair Specialty Ceramics, USA

stabilisers were dissolved in the medium in which the powder was subsequently dispersed using ultrasound. The suspensions were allowed to settle in identical vessels, containing equal amounts of suspension. The sedimentation rate was measured by recording the time required for the formation of a clearly visible deposit. The following media were tested: water, ethanol, methanol, 1-propanol, 2-propanol, acetone and ethylmethylketone. The influence of the following additives was investigated: polyvinylpyrolydone[*] (PVP), polyvinylalcohol[†] (PVA), ammonium polymethacrylate[‡] (APMA) and polyvinylbutyral[§] (PVB). Depending on their solubility in the various media, they were applied in concentrations of 0.1, 0.5 and 1wt% relative to the powder.

4.7.2   Support preparation

The 50wt% suspensions were prepared by dispersion of the powder in the medium by an ultrasonic treatment in a rosette cell during 15 minutes under water cooling, using a frequency of 20 kHz and a transducer output of 100W. After dispersion, the suspension was sieved through a 0.1mm sieve. The suspension was evacuated for 10 minutes in an exicator to remove air bubbles. Subsequently, the suspension was filtered by vacuum suction through a hydrophobic Durapore[®] filter[**], which was mounted in an especially designed filter cup. Before using the cups they were greased with Vaseline[®] by dipping the rings into a solution of Vaseline[®] in petroleum ether. The filter cups were filled with suspension in such a way that an approximately 3 mm thick cast remained after removal of the medium. The latter usually took around 30 minutes. The green supports were released from the cups and dried overnight at room temperature in air. The green bodies were sintered for 10 h at various temperatures and using various heating rates. The sintering behaviour of the compacts was investigated by means of dilatometry. The porosity of the sintered supports was determined by Archimedes density measurements by immersion in Hg. Scanning Electron Microscopy (SEM) and Hg-intrusion were used to investigate the pore shape and pore size distribution respectively. The gas permeability of the supports at room and high temperature was measured via the same procedures as mentioned in section 4.2.1.

Prior to polishing, the sintered supports were cut into discs with a diameter of 15 mm, with thicknesses ranging from 0.5 to 2 mm. Two pre-grinding steps were performed manually

---

[*] M W 360,000, Janssen Chimica, Belgium
[†] M W 145.000, Merck, Germany
[‡] Darvan[®] C, R.T. Vanderbilt Company Inc., USA
[§] Acros Organics, Belgium
[**] 0.1 µm pores, Ø 32 mm, Millipore, Ireland

on SiC[*] paper and on a glass plate with a water based diamond slurry[†], respectively. The final finishing was performed through an automated mechano-chemical polishing procedure performed on a silk cloth, using a colloidal silica suspension[‡] and water mixed in a volume ratio of 1:1, together with 5vol% of H_2O_2 for 10 minutes.

4.8   Results and discussion

4.8.1   Medium selection

The results of the sedimentation experiments using the suspensions without an additive are listed in table 5.2. According to these data, 2-propanol seems the most suitable suspension medium. The observed suspension stability differs substantially from the suspensions based on other media. For comparison, table 5.2 also shows the theoretical sedimentation velocities, calculated via Stokes' law:

$$v = \frac{2ga^2(d_p - d_m)}{9\eta} \tag{4.2}$$

In this equation, g is the gravitational acceleration, a the radius of the particle, η the viscosity of the medium, while d_p and d_m are the density of the particle and the medium, respectively. The mean particle diameter determined from SEM observations was taken to

Table 5.2:   Comparison between the time τ_s required for formation of a visible deposit and the theoretical sedimentation velocity v_s calculated with equation (4.2)

Medium	τ_s (*min*)	v_s ($\mu m\ s^{-1}$)
Water	5	1.91
Methanol	15	3.32
Ethanol	15	1.65
1-propanol	15	0.88
2-propanol	25	0.79
Acetone	10	6.2
Ethylmethyl ketone	5	4.5

be 0.8 μm, which is in agreement with specifications provided by the manufacturer. Table 5.2 shows that the theoretical sedimentation velocity reaches a minimum for 2-propanol, which suggests that the sedimentation rate is mainly determined by the density and viscosity of the medium and not by the agglomeration of powder particles. In addition,

---

[*] 35 μm grain size, Struers, Denmark
[†] 3 μm grain size, Buehler, USA
[‡] OP-U Suspension, Struers, Denmark

none of the applied stabilisers had a beneficial effect as they generally caused lower suspension stability in the investigated concentration range. The only exception was PVB, the addition of which to 2-propanol showed no influence on suspension stability.

Considering the above, the 2-propanol suspension without additives was selected to be the most suitable and convenient for the filtration experiments. Choosing a non-aqueous medium has the additional advantage to prevent ion leaching, which was observed in the case of water-based $La_{0.6}Sr_{0.4}CoO_{3-\delta}$ suspensions [19]. Besides an uncontrollable influence on the suspension stability, this dissolution of ions can have a negative effect on the phase purity of the material after processing.

4.8.2   Sintering characteristics

The dry green bodies obtained after filtration of a 50wt% $La_{0.5}Sr_{0.5}CoO_{3-\delta}$ suspension in 2-propanol, showed a porosity of 51% and possessed a relatively low mechanical strength. This required careful manual handling. The sintering behaviour of such a compact is presented in figures 5.9 and 5.10.
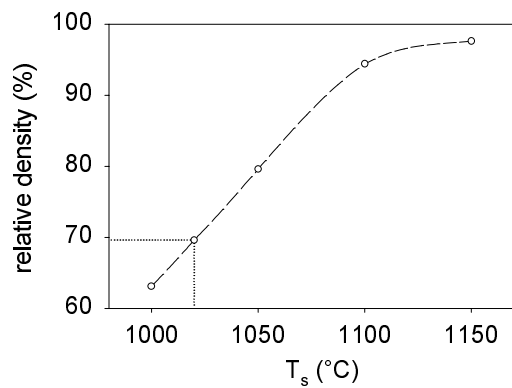
Figure 5.9:   Influence of the sintering temperature T_s on the final support density after sintering for 10 h in air
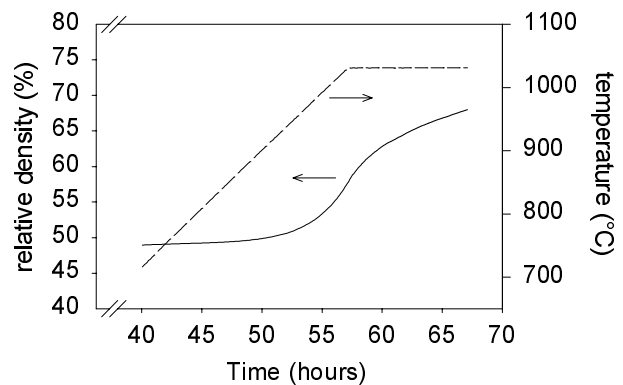
Figure 5.10:   Densification during sintering for 10 h at 1020°C, heating rate: 0.3°C/min

Based on the data presented in figure 5.9, the sintering temperature for the supports was chosen to be 1020°C, which is 20°C above the maximum membrane operation temperature. Sintering for 10 h at this temperature yields a residual porosity of 30%. A lower sintering temperature involves a too high risk of residual sintering during membrane operation. With a sintering temperature of 1020°C, the equilibrium between sinter stability and porosity is already very delicate, as shown in figure 5.10. This figure shows the densification behaviour at 1020°C as a function of time, which after 10 h of sintering is still continuing. However, when the sintered compact was cooled to room temperature and

again heated to 1000°C, additional densification did not occur on a time scale of at least 48 h. Figure 5.9 clearly shows that in the range from 1000 to 1100°C, the sintering temperature strongly influences the support porosity. This necessitates careful control of temperature during sintering, since a temperature increase of 25°C above 1020°C already decreases the porosity with 10%.

During sintering of the supports, a heating rate up to 2°C/min was applied. The sintered supports were slightly bent, most probably caused by modest segregation during the filtration process. Faster sintering of the surface layer of the compact, which due to the sedimentation process has a greater amount of smaller particles, causes a concave curvature.

4.8.3   Support morphology

Figures 5.11 shows the surface morphology of a polished support. The average pore diameter determined via Hg intrusion is 0.32 μm. The corresponding pore size distribution in figure 5.12 shows a small secondary peak around 7 μm. The total volume of these pores contributes approximately 8% to the total pore volume. SEM observations indeed indicated the presence of some, mainly spherical inhomogeneities, of which an example is shown in figure 5.13. This picture suggests that this type of defects is caused by the presence of large spherical particles in the starting powder. The polishing treatment seems to have bisected the hollow particle, revealing its wall thickness. This explanation is confirmed by figure 5.14, which indeed shows the presence of such a spherical particle in the powder. In addition, the particle size distribution as supplied by the manufacturer tails towards particles of 10 μm, as can be seen in figure 5.15. The occurrence of these large (hollow) spheres is a problem typically related to spray pyrolysis and depends strongly on the precipitation conditions and precursor characteristics [64].

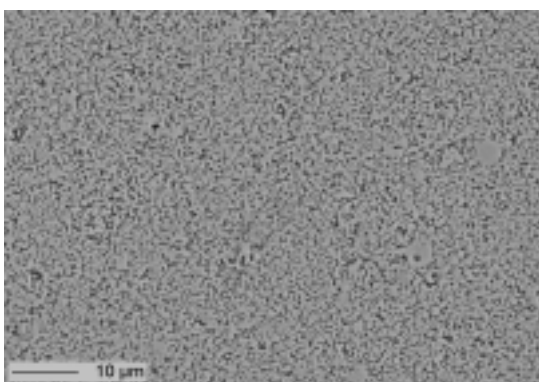Figure 5.11:   SEM picture of a polished $La_{0.5}Sr_{0.5}CoO_{3-\delta}$ support prepared via filtration and sintered in air for 10 h at 1020°C.
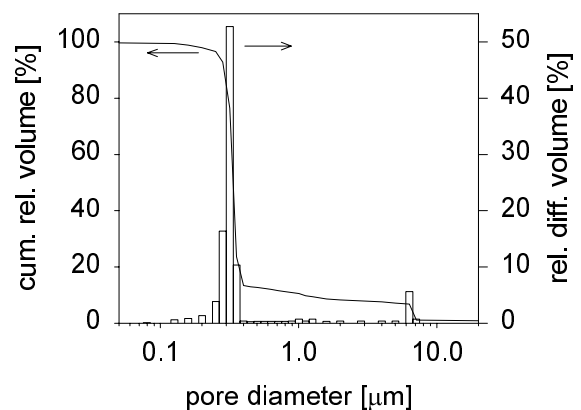
Figure 5.12:   Pore size distribution of the support shown in figure 5.11, determined via Hg-intrusion

Milling of the powder to remove the inhomogeneities was not considered an option since it further increases the sinter activity of the powder. Classification through sedimentation of the suspension might be effective although it should be realised that a large hollow particle does not necessarily settle faster than a smaller massive particle, which makes it questionable whether all inhomogeneities will be removed. Powder classification through the application of micro sieves might be a promising option. This technique however needs further development, which falls beyond the scope of this research.
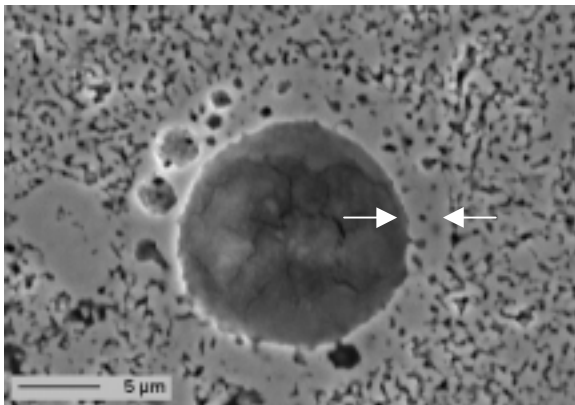
Figure 5.13: SEM picture of a spherical inhomogeneity in the support; the arrows indicate the wall thickness of the hollow particle that supposedly caused the defect.
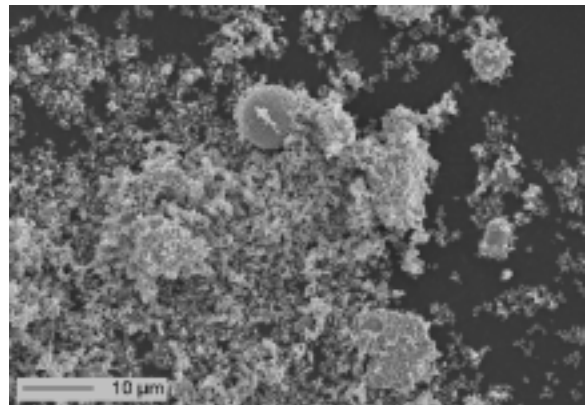
Figure 5.14: SEM picture of the powder used for the support preparation, showing a large spherical particle
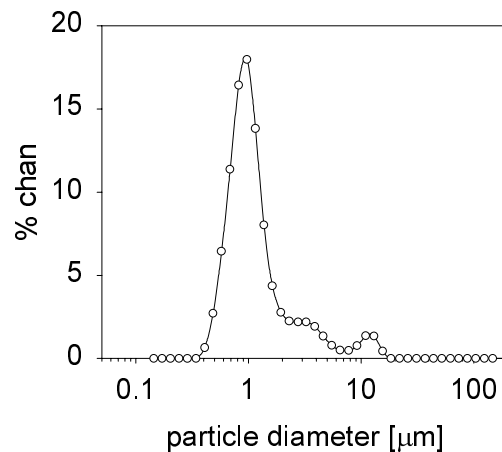
Figure 5.15: Particle size distribution of the commercial $La_{0.5}Sr_{0.5}CoO_{3-\delta}$ powder

4.9   Support permeability

Figure 5.16 shows the oxygen and nitrogen permeance of the support shown in figure 5.11, measured at room temperature. From both the oxygen and nitrogen permeance data, an average pore diameter of 0.40 μm and a tortuosity of 2.6 was calculated. The pore size corresponds well with data from Hg-intrusion. The oxygen flux through the support measured at room temperature under an absolute pressure difference of 1 bar was 4.2×10^{-5} mole cm^{-2} s^{-1}, as can be inferred from the data shown in figure 5.6. At 1000°C, under a partial pressure difference of 1 bar, an oxygen flux of 5×10^{-6} mole cm^{-2} s^{-1} was measured. This value illustrates that the permeability of these supports enters the critical region in which mass transport through the support will start to determine the performance of the thin film membrane.
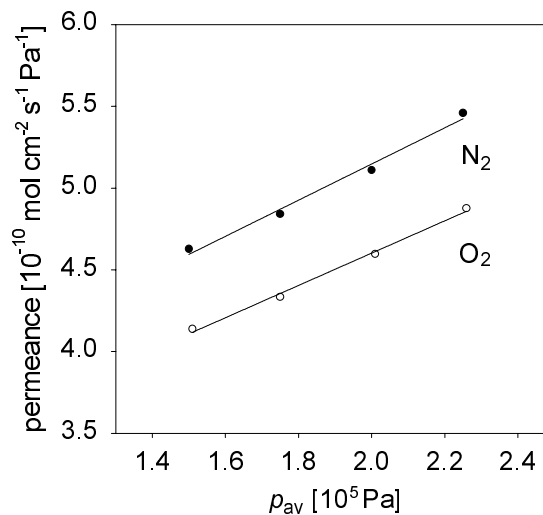
Figure 5.16:   Oxygen and nitrogen permeance of the La$_{0.5}$Sr$_{0.5}$CoO$_{3-\delta}$ support shown in figure 5.11, measured at room temperature

4.10   Final preparation route

The preparation of La$_{1-x}$Sr$_x$CoO$_{3-\delta}$ supports via pressure filtration of a powder suspension can be summarised as follows:

- Ultrasonic dispersion of 50wt% commercial powder in 2-propanol
- Removal of the liquid suspension medium by pressure filtration
- Drying overnight
- Sintering at 1020°C for 10 hours
- Polishing

Part 3:   Tubular substrates prepared by centrifugal casting

In addition to a high permeability, selectivity and stability, membrane geometry is also an important aspect in industrial membrane applications. Although membrane modules consisting of stacked flat-plate membranes have been developed, for industrial applications tubular membranes are often preferred over flat discs due to the relative ease of sealing tubes into modules. Currently, the vast interest in dense membranes for oxygen separation purposes has turned the development of high-quality tubular oxygen separation membranes into a prominent issue.

Tubular membranes are mainly prepared by conventional ceramic processing techniques like pressing and extrusion [20-23]. The disadvantage of these techniques is that the resulting tubes often have a considerable surface roughness and that defects and tube unroundness are difficult to avoid. Recently, centrifugal casting has shown to be a very suitable technique to prepare high quality tubular α-Al_2O_3 membrane supports with superior surface morphology and roundness. The successful application of this technique has opened new perspectives in the development of better and more advanced tubular perovskite supports and membranes. The last part of this chapter describes the results of the first exploratory centrifugal casting experiments performed to prepare porous as well as dense $La_{0.5}Sr_{0.5}CoO_{3-\delta}$ tubes.

4.11   Process characteristics

The centrifugal casting process consists of the following steps: suspension preparation, casting, drying and sintering. The preparation procedure for the casting suspension is analogous to the one outlined in section 4.6. This suspension is transferred into a cylindrical mould, which is then axially rotated in a centrifuge. Since the smaller (lighter) particles will sediment slower than the larger ones, a compact with graded porosity is obtained. The roughness of the inner surface is low due to the final sedimentation of the smallest particles while the mould and the size of the largest particles mainly determine the roughness of the external surface. The classifying nature of the deposition process will prevent the presence of heavier powder inhomogeneities at the inner surface of the tubular compact. For a quantitative description of the centrifugal casting process, the reader is referred to Biesheuvel *et al.* [24,25]

4.12 Experimental

4.12.1 Suspension preparation

Commercial $La_{0.5}Sr_{0.5}CoO_{3-\delta}$ powder[*] was employed to prepare the suspensions. The suspension composition was derived directly from the preparation procedure of tubular α-Al_2O_3 membrane supports as described in [2]. Ammonium polymethacrylate[†] was used as binder in amounts varying from 1.7 to 8.3 wt% relative to the powder. The pH of the suspension was controlled by addition of ammonia and was varied between 4 and 10. In all cases, the powder loading of the suspensions was chosen to be 50wt%. The powder was dispersed in the medium by an ultrasonic treatment in a rosette cell during 15 minutes under water cooling, using a frequency of 20 kHz and a transducer output of 100W.

4.12.2 Cast formation

A commercial centrifuge[‡] was employed, equipped with Delrin moulds[®][§] with a length of 16 cm and an inner diameter of 21.5 mm. Prior to filling, the moulds were greased with Vaseline[®] by dipping them into a solution of Vaseline[®] in petroleum ether. The filled moulds were rotated for 20 minutes at 20.000 rpm. This revolution number was reached within 1 minute. After rotation, the remaining liquid was poured out of the moulds and the cast was dried inside the mould in a climate chamber for two days at 30°C and 60% relative humidity. After drying, the green compacts were removed from the mould and sintered horizontally at 1150°C for the dense tube and 1020°C for the porous tube in stagnant air for 10 h. Heating and cooling rates of 0.3°C/min were employed. The heating trajectory contained two plateaus of one hour each. The first was situated at 230°C, which according to the manufacturer is the disintegration temperature of the binder. The second plateau at 400°C was incorporated to reduce internal stress due to slow equilibration of the oxygen non-stoichiometry throughout the sample. The density of the sintered tubes was determined by Archimedes density measurements by immersion in Hg. The morphology of the surfaces and cross-sections of the tube was investigated by SEM.

---

[*] 99.9%, Praxair Specialty Ceramics, USA
[†] Darvan[®] C, R.T. Vanderbilt Company Inc., USA
[‡] CEPA, GLE, Carl Padberg GmbH, Germany
[§] Du Pont de Nemours, The Netherlands

4.13 Results and discussion

The compacts obtained after drying were all crack-free and easy to remove from the mould, regardless of the employed binder concentration. After sintering at 1150°C, crack-free tubes were obtained from casts prepared from suspensions with a binder concentration of 5 wt% and a pH of 9.5. Although several crack-free tubes were prepared, the reproducibility of the process was low. Figure 17 shows a photograph of a tube, sintered at 1150°C, with a relative density of more than 95%. All tubes showed a bright lustre on the inside due to the surface smoothness. The figures 5.18 and 5.19 show the surface morphology of a (polished) cross section of a tube, which has a total thickness of 1.3 mm and a relative density of 95%. Sintering at 1020°C instead of 1150°C yielded tubes with a porosity of 83%. This density is significantly higher than that of the flat supports, prepared from the same powder via pressure filtration and sintered at the same temperature. A possible reason for this is that the centrifugation process yields a denser packing of particles than the filtration process. A powder with a larger average particle size is required to obtain tubes with a higher porosity, while employing the same sintering temperature.

Figure 5.17: Photograph of a sintered 95% dense $La_{0.5}Sr_{0.5}CoO_{3-\delta}$ tube with a length of 13 cm.
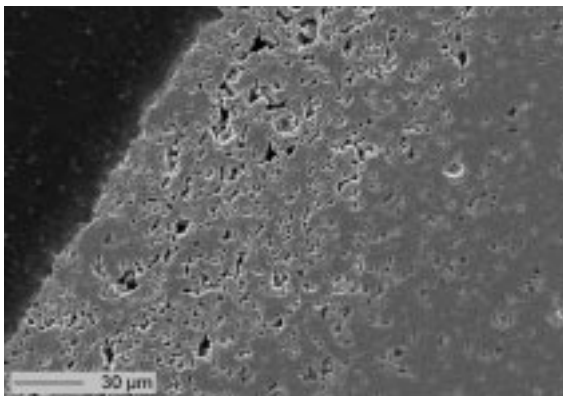

Figure 5.18: Cross section (outer side) of a tube sintered at 1150°C with relative density of 95%
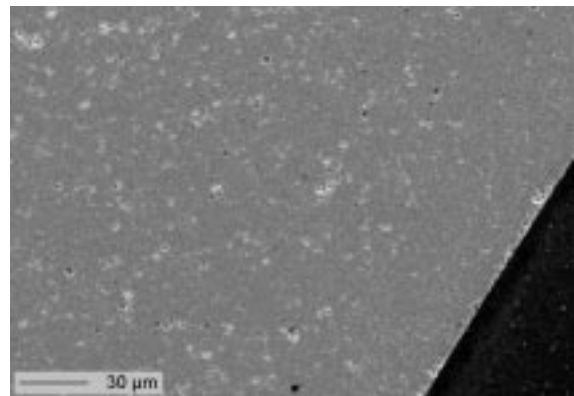
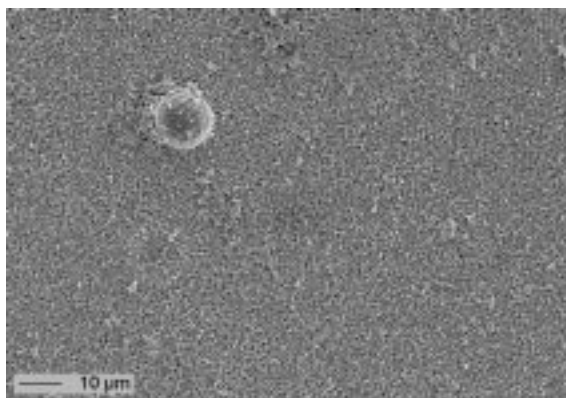Figure 5.19: Cross section (inner side) of the tube of figure 5.18

Figure 5.20: Inner surface of a tube sintered at 1020°C with a relative density of 83%
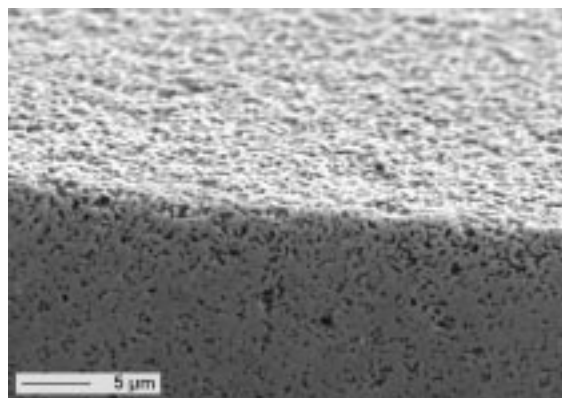

Figure 5.21: Cross section of the inner surface of the tube of figure 5.20

Due to low reproducibility of the results, the relation between the binder concentration and the sinter-cracking of the tubes could not be established unambiguously. The low reproducibility is most probably caused by the relatively low stability of the starting suspensions. Generally, sedimentation was visible within several minutes after the ultrasonic treatment. For pH values higher than 7, the pH of the suspension did not have a measurable influence on the suspension stability. When the suspension was made acidic, it turned into a viscous paste unsuitable for further processing. Employing the more stable 2-propanol based suspensions, derived from the filtration experiments, yielded green supports that were too weak to process. Besides the poor suspension stability, another critical issue is the roundness of the tubes. During horizontal sintering of the tubes a slight elliptical deformation occurs. The variation in diameter amounts to approximately 2% relative to the mean tube diameter of 18 mm. This deformation can probably be avoided by rotation of the tube during sintering or by sintering in a vertical position.

Despite the high relative density of the tube in the figures 5.18 and 5.19, these figures clearly show the gradient in porosity caused by the classification during the casting process. This illustrates that centrifugal casting technique provides an elegant preparation route for highly permeable supports with graded porosity. However, in the further development and optimisation of this approach two important problems still have to be tackled. The first is the homogeneity of the starting powder. The presence of the spherical particle in figure 5.20 clearly illustrates that the classifying nature of the centrifugal casting process does not prevent the presence of these large inhomogeneities at the inner tube surface, most likely because these spheres are hollow and therefore relatively light. Secondly, the sintering procedure for such a graded compact requires careful consideration. In particular for the mixed conducting perovskites materials mentioned in this chapter, all showing high expansion coefficients, the stress that develops during sintering might have a detrimental influence on obtaining crack-free supports.

4.14   General concluding remarks

The above mentioned results and discussion illustrate the complexity of developing suitable $La_{1-x}Sr_xCoO_{3-\delta}$ perovskite materials to be used as supports for µm-thick membranes. The process window is highly narrowed down by homogeneity, sinter stability and permeability requirements in combination with the sintering properties of this type of ceramic material. The supports prepared by pressing pre-sintered classified powder show a high permeability but the surface homogeneity, which can be improved by coating, is critical. Pressure filtration proved to be very suitable for preparing perovskite supports. Supports prepared from the commercial powder using this technique have the highest homogeneity; however this results in a permeability that approaches the borders of what is acceptable. Although the number of support defects should be decreased by refinement or classification of the starting powder, the latter supports can be considered as best suitable for supporting thin film membranes. For the preparation of the industrially more attractive tubular dense $La_{1-x}Sr_xCoO_{3-\delta}$ membranes and porous supports, exploratory experiments have shown centrifugal casting to be a promising technique. It is expected that when the powder homogeneity, suspension stability and sinter conditions are further optimised, high quality dense tubes or tubes with graded porosity can be obtained.

4.15   References

1. R.M. de Vos and H. Verweij, "High-Selectivity, High-Flux Silica Membranes for Gas Separation," *Science* 279 (1998) 1710
2. A. Nijmeijer, C. Huiskes, N.G.M. Sibelt, H. Kruidhof and H. Verweij, "Centrifugal casting of tubular membrane supports," *Am. Ceram. Soc. Bull.* **77** (1998) 95
3. J. Dong, K. Wegner and Y. S. Lin, "Synthesis of Submicron Polycrystalline Silicalite Films on Porous Ceramic Supports", *J. Membr. Sci.* 148 (1998) 233
4. L.W. Tai, M.M. Nasrallah, H.U. Anderson, D.M. Sparlin and S.R. Sehlin, "Structure and electrical properties of $La_{1-x}Sr_xCo_{1-y}Fe_yO_3$. Part 2. The system $La_{1-x}Sr_xCo_{0.2}Fe_{0.8}O_3$", *Solid State Ionics* 76 (1995) 273
5. E.A.F. Span, F.J.G. Roesthuis, D.H.A. Blank, H. Rogalla, "Structural and electrical properties of $La_{0.5}Sr_{0.5}CoO_3$ films on $SrTiO_3$ and porous α-Al_2O_3 substrates", *Applied Physics A*, 69 S783 (1999)
6. Chapter 6 of this thesis
7. Y. Teraoka, T. Fukuda, N. Miura and N. Yamazoe, "Development of oxygen semipermeable membrane using mixed conductive perovskite-type oxides (part1), preparation of porous sintered discs of perovskite type oxide", *J. Ceram. Soc. Jpn. Inter.* Ed. 97 (1989) 458
8. D. Dionysios, X. Qi, Y.S Lin, G. Meng, D. Peng, "Preparation and characterizarion of proton conducting terbium doped strontium cerate membranes" *J. Mebr. Sci.*, **154** (1999) 143
9. R.H.E. van Doorn, H. Kruidhof, A. Nijmeijer, L. Winnubst and A.J. Burggraaf, "Preparation of $La_{0.3}Sr_{0.7}CoO_{3-\delta}$ perovskite by thermal decomposition of metal-EDTA complexes," *J. Mater. Chem.* 8 (1998) 2109
10. J.E. ten Elshof, H.J.M. Bouwmeester and H. Verweij, "Oxygen transport through $La_{1-x}Sr_xFeO_{3-\delta}$ membranes. I. Permeation in air/He gradients", *Solid State Ionics* 81 (1995) 97
11. J.W. Veldsink, G.F. Versteeg, W.P.M. van Swaaij, "An experimental study of diffusion and convection of multicomponent gases through catalytic and non-catalytic membranes", *J. Membr. Sci.* 92 (1994) 275
12. A. Nijmeijer, H. Kruidhof, R. Bredesen and H. Verweij, "Preparation and Properties of Hydrothermally Stable γ-Alumina Membranes", *J. Am. Ceram. Soc.* **84** [1] 136 (2001).

13. T. Matsuura, T. Ishigaki, J. Mizusaki, S. Yamauchi, K. Fueki, "Single crystal growth of perovskite-type $La_{1-x}Sr_xMO_3$ (M=Fe,Co) solid solutions", *Jap, J. Appl. Phys.* **23** (1984) 1172

14. S. Bilger, E. Syskakis, A Naoumidis, H Nickel, "Sol-gel synthesis of strontium-doped lanthanum manganite", *J. Am. Ceram. Soc.*, **75** (1992) 964

15. D.H.A. Blank, H. Kruidhof, J. Flokstra, "Preparation of $Yba_2Cu_3O_{7-\delta}$ by citrate synthesis and pyrolysis", *Appl. Phys.* **21** (1988) 226

16. F.C.M. Woudenberg, W.F.C. Sager, N.G.M. Sibelt, H. Verweij, "Dense nanostructured $t-ZrO_2$ coatings at low temperatures via modified emulsion precipitation", submitted to Adv. Mater.

17. G.L. Messing, S. Zhang and G.V. Jayanthi, "Ceramic powder synthesis by spray pyrolysis," *J. Am. Ceram. Soc.*, **76** (1993) 2707

18. D.H. Everett, "Basic Principles of Colloid Science", 2nd edition, John Wiley & Sons, Inc., New York (1995)

19. S. Kaji and N. Sakamoto, "Effect of strontium ions leached from $La_{0.6}Sr_{0.4}CoO_3$ on flow property in an aqueous system," *J. Mater. Sci.*, **17** (1998) 1719

20. S. Li, H. Qi, N. Xu and J. Shi, "Tubular Dense Perovskite Type membranes. Preparation, Sealing and Oxygen Permeation Properties," *Ind. Eng. Chem. Res.*, **38** (1999) 5028

21. N. Xu, S. Li, W. Jin, J. Shi and Y.S. Lin, "Experimental and Modelling Study on Tubular Dense membranes for Oxygen Permeation," *AIChE Journal*, **45** (1999) 2519

22. W. Jin, S. Li, P. Huang, N. Xu, J. Shi and Y.S. Lin, "Tubular Lanthanum Cobaltite Perovskite Type Membrane Reactors for Partial Oxidation of Methane to Syngas," *J. Membr. Sci.*, **166** (2000) 13

23. S. Li, W. Jin, P. Huang, N. Xu, J. Shi and Y.S. Lin, "Tubular Lanthanum Cobaltite Perovskite-type Membrane for Oxygen Permeation," *J. Membr. Sci.*, **166** (2000) 51

24. P.M. Biesheuvel, A. Nijmeijer and H. Verweij, "Theory of batchwise centrifugal casting," *AIChE J.*, **44** (1988) 1914

25. P.M. Biesheuvel and H. Verweij, "Calculation of the composition profile of a functionally graded material produced by centrifugal casting", *J. Am. Ceram. Soc.*, **83** (2000) 743

5

Preparation of dense $La_{0.5}Sr_{0.5}CoO_{3-\delta}$ thin-film membranes on porous supports by pulsed laser deposition

Abstract

Dense, homogeneous and crack free thin films (5-30 μm in thickness) of $La_{0.5}Sr_{0.5}CoO_{3-\delta}$ were deposited on porous $La_{0.5}Sr_{0.5}CoO_{3-\delta}$ substrates at 650°C, using pulsed laser deposition. The structural evolution and microstucture of the deposited films were investigated using X-ray diffraction (XRD), atomic force microscopy (AFM) and scanning electron microscopy (SEM). Initial deposition experiments on porous α-Al_2O_3 supports were unsuccessful as crack formation occurred during cooling after the deposition process due to thermal mismatch. The deposited $La_{0.5}Sr_{0.5}CoO_{3-\delta}$ films are considered as promising candidates for application as oxygen separation membrane.

5.1   Introduction

Various techniques are available for the deposition of thin oxide films. Among the most prominent ones are chemical vapour deposition (CVD), electrochemical vapour deposition (EVD), wet chemical sol-gel and suspension techniques, sputtering and pulsed laser deposition (PLD). Since in 1988 the first high temperature superconducting layers of $YBa_2Cu_3O_7$ with correct stoichiometry and phase were deposited using PLD [1], this technique has received a lot of attention. Using PLD, high quality layers can be fabricated with excellent texture and various crystallographic orientations [2-7]. PLD can be employed to deposit layers of high-Tc superconductors, ferrites, ferroelectrics, opto-

electronics, tribological coatings, metals, insulators, and biomaterials. The process is simple, fast and can be employed at relatively high (oxygen) background pressures, which renders it particularly suitable for the growth of multi-component oxides.

Although thin film growth and epitaxy of oxidic materials is an issue that currently receives scientific and technological interest, PLD has been used mainly for the deposition of thin films onto non-porous, i.e. dense, substrates. The possibility of using PLD for the deposition of dense oxide films onto porous substrates offers perspectives to develop membranes for oxygen separation. Typically, these mixed-conducting membranes operate at temperatures ranging from 800 to 1000°C. For reduced operating temperatures or higher oxygen fluxes either thinner or more conductive membranes are needed. The objective of this work is the fabrication of thin continuous layers of perovskite $La_{0.5}Sr_{0.5}CoO_{3-\delta}$ on porous supports.

As the thermal expansion of $La_{0.5}Sr_{0.5}CoO_{3-\delta}$ is significant, deposition requires a support which is preferably made from the same material, in order to avoid crack formation related with thermal mismatch. When wet chemical deposition techniques are employed, an additional sintering step is always required to densify the deposited thin layer. Besides high deposition rates and process simplicity, the further advantage of PLD is that deposition can be carried out at elevated temperature, avoiding a post-deposition sintering step. A dense and crystalline film is formed, provided that a substrate is used with a surface roughness which is lower than the thickness of the film to be deposited.

The acceptor-doped $La_{1-x}Sr_xCoO_{3-\delta}$ perovskites-type materials have been extensively studied for application as oxygen separation membrane. Several studies on epitaxial films of these materials have been performed [8,9,10] and it has been demonstrated that for the material with x=0.5 crystalline layers can be grown on single-crystalline $SrTiO_3$ substrates using PLD [11]. However, so far no attempts have been made to grow these materials on macroporous substrates. In this chapter, the use of PLD to deposit dense continuous films of $La_{0.5}Sr_{0.5}CoO_{3-\delta}$ on macroporous supports of α-Al_2O_3 and $La_{0.5}Sr_{0.5}CoO_{3-\delta}$ is considered. The developed microstructure of the films is presented. Results of oxygen permeation experiments are presented in Chapter 6 of this thesis. The growth kinetics of the $La_{0.5}Sr_{0.5}CoO_{3-\delta}$ thin films on both porous and dense substrates has been reported elsewhere [11-13].

5.2 Pulsed laser deposition

During a PLD experiment, a pulsed laser beam is focussed onto a source of the material to be deposited, also denoted as the target. Due to the high energy density of the laser pulse the target material vaporises at the spot where the laser beam hits the target. Consequently, the vapour absorbs most of the energy of the laser pulse and transforms into an energetic pulse. Typical time scales for plasma formation are in the order of 20 ns. The plasma expands into the surrounding ambient in a plume-shaped form. When a substrate is placed into this plume, the evaporated material will partly deposit onto the substrate. Both the target and substrate are mounted in a vacuum chamber.

Important parameters during the deposition process are the absorption coefficient and the reflectivity of the target material, the pulse duration, wavelength and energy of the laser beam, the laser repetition frequency and the target-to-substrate distance. Moreover, the substrate temperature and the ambient oxygen pressure are important. The latter has a substantial influence on the properties of the deposited film and determines the plasma size. Since PLD allows background pressures that are significantly higher than those used in regular vapour deposition techniques, it is especially suitable for *in-situ* preparation of complex oxides or compounds that are unstable at low oxygen pressures.
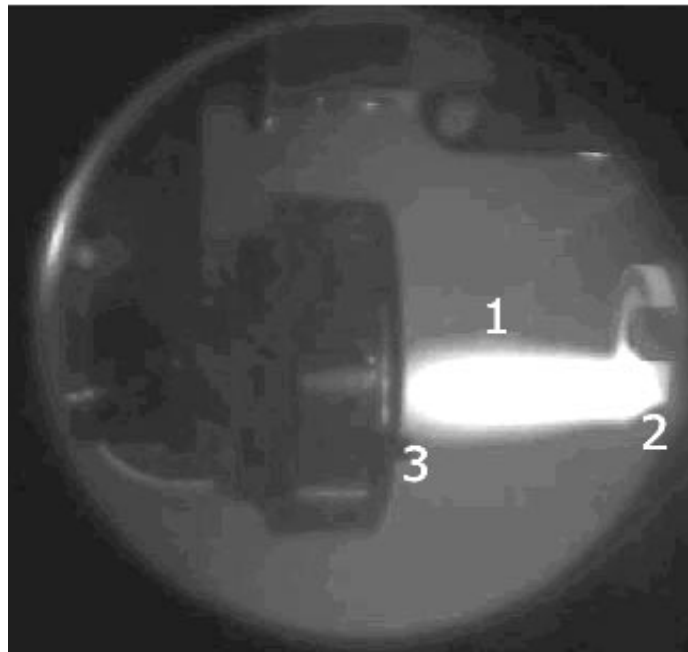
Figure 5.1:   The development of a plasma (1) due to laser interaction with the target (2). The plasma extends to the substrate (3) where deposition takes place.

5.3   Experimental

The deposition experiments were carried out in a vacuum chamber, which was equipped with a turbo pump, gas inlet, target holder with a rotation mechanism and a substrate holder including a heater. The substrate was clamped to the heater under spring load. The substrate heater enabled variation of the substrate temperature in the range from room temperature to 800°C. During deposition, the target was rotated to enable uniform erosion of the target. A pulsed KrF excimer laser was used with a wavelength of 248 nm and a pulse duration of 30 ns. For all experiments a laser repetition frequency of 20 Hz was employed. The energy density of the laser beam was 1.5 J/cm^2. According to results obtained during a preliminary study on PLD of $La_{0.5}Sr_{0.5}CoO_{3-\delta}$ [12], this fluency is well above the threshold value for stoichiometric ablation. Using these settings, a deposition rate was achieved of approximately 10 μm/h. Figure 5.2 gives a schematic representation of the PLD set-up. After deposition, the films grown at high temperature were annealed in 1 bar oxygen for 1 h at the deposition temperature.

Figure 5.2:   Schematic representation of the pulsed laser deposition set-up [13]

Initial deposition experiments were performed on 30% porous 2 mm thick α-Al$_2$O$_3$ supports with a mean pore diameter of 80 nm [14]. Although problems were expected related with the large difference in thermal expansion coefficient (TEC) between α-Al$_2$O$_3$

and La$_{0.5}$Sr$_{0.5}$CoO$_{3-\delta}$, high-quality supports were available in our laboratory. These were used in scouting experiments to investigate the influence of various deposition parameters. Subsequently, deposition experiments were performed on home-made 30% porous 0.5 mm thick La$_{0.5}$Sr$_{0.5}$CoO$_{3-\delta}$ supports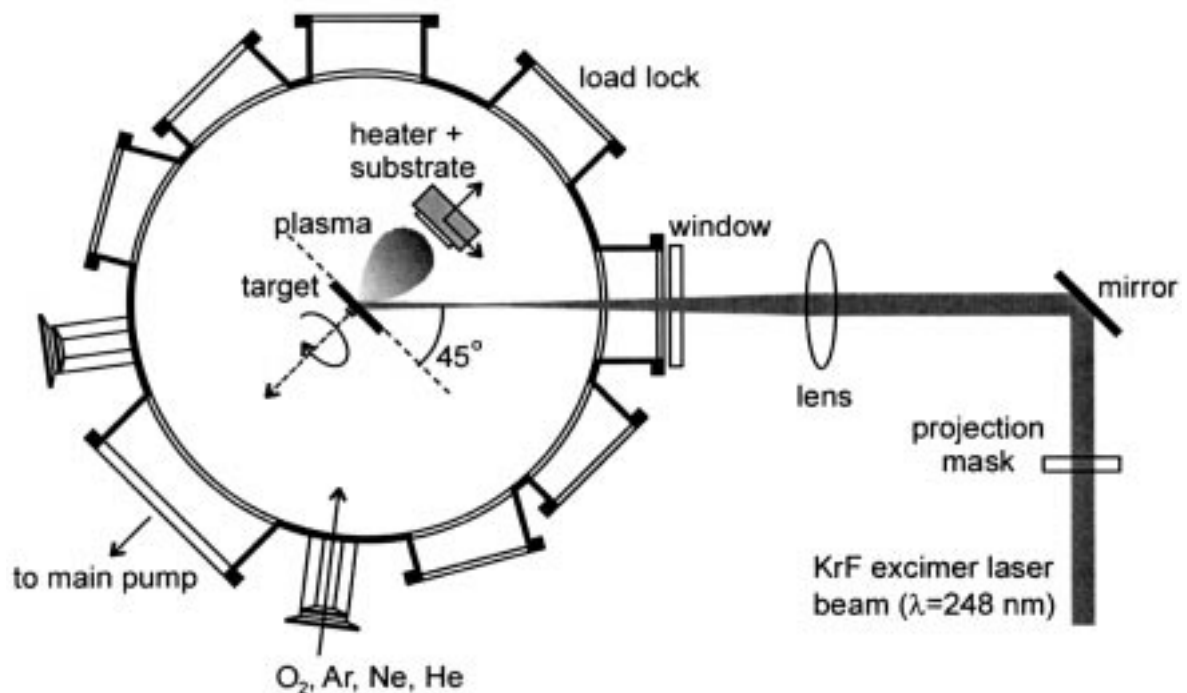 with a mean pore diameter of 0.3 μm. These supports were prepared via pressure filtration of a suspension made from commercial powder as described in chapter 4 of this thesis. After deposition, the resulting thin film membranes were characterised by SEM, AFM, EDX and XRD using Cu-K$_\alpha$ radiation. The gas tightness of the films deposited on the α-Al$_2$O$_3$ membranes was checked by nitrogen permeation measurements, using a dead-end permeation cell. An absolute pressure difference up to 3 bar was applied across the membrane while the low-pressure side of the membrane was kept at atmospheric pressure.

5.4 Results and discussion

5.4.1 Deposition on porous α-Al$_2$O$_3$ substrates

EDX and SEM demonstrated that stoichiometric, 1 μm thick polycrystalline films were obtained at a substrate temperature of 650°C. The corresponding XRD pattern is shown in Figure 5.3. All peaks not belonging to the support could be indexed on the basis of a perovskite lattice. The oxygen pressure and the target-to-substrate distance proved to have a decisive influence of the morphology of the film. In general, dense and uniform films were obtained at an ambient oxygen pressure of 1.0 Pa and a target-to-substrate distance of 43 mm. Atomic force microscopy (AFM) was used to resolve the grain structure. Figure 5.4 shows an AFM micrograph of such a film. In general, the rms-surface roughness was found to be below 10 nm. Higher background oxygen pressures and/or target-to-substrate distance led to films with an increased roughness and porosity [11,13]. When the deposited films were cooled to room temperature, crack formation occurred, regardless of the applied cooling rate. This crack formation is attributed to the different thermal expansion of the α-Al$_2$O$_3$ support compared with the La$_{0.5}$Sr$_{0.5}$CoO$_{3-\delta}$ film.
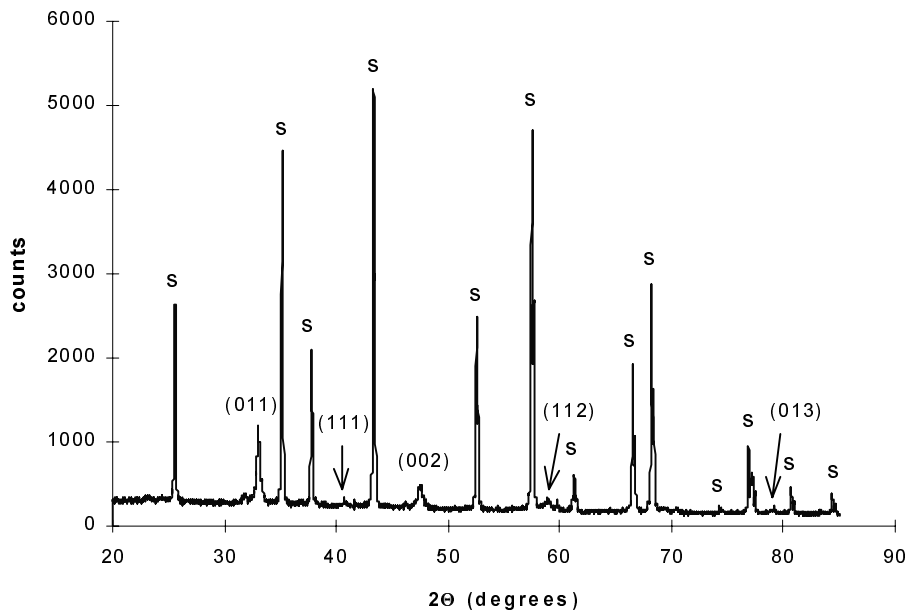
Figure 5.3: X-ray diffractogram of an α-Al$_2$O$_3$ supported La$_{0.5}$Sr$_{0.5}$CoO$_{3-\delta}$ film. The peaks caused by the perovskite phase are indexed, the support peaks are marked with an 's'.
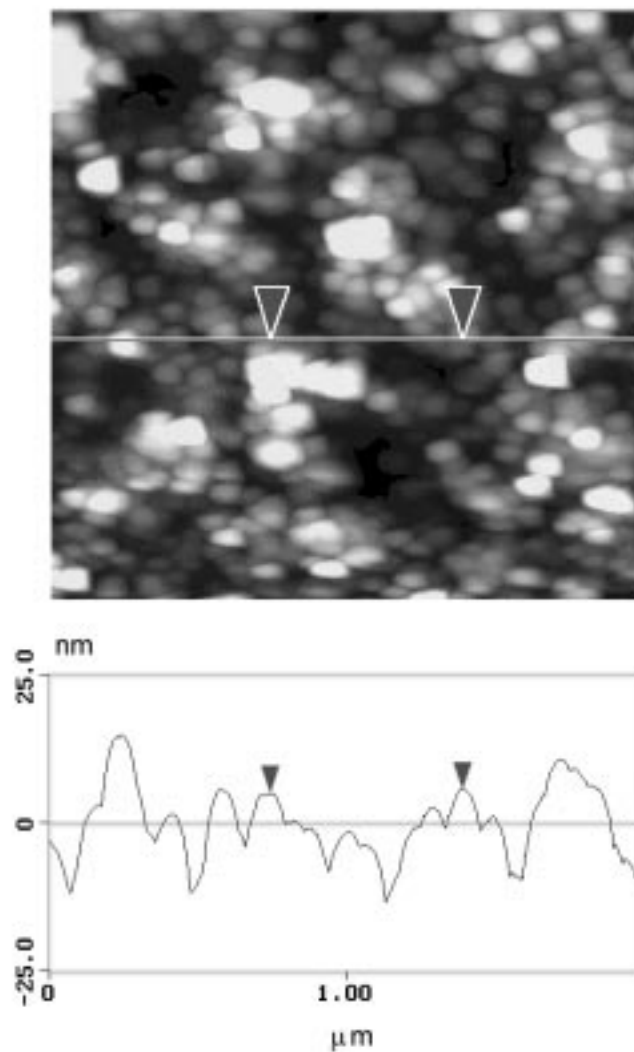
Figure 5.4: AFM height image with cross-section of a 1 μm thick α-Al$_2$O$_3$ supported La$_{0.5}$Sr$_{0.5}$CoO$_{3-\delta}$ film

Deposition at room temperature yielded amorphous films. These films, obtained at the same ambient oxygen pressure and target-to-substrate distance as the films grown at 650°C, were dense and crack free. Nitrogen permeation could not be detected. Annealing of these films at 650°C in air for 10 h resulted in the formation of crystalline films, but also introduced cracks. Figure 5.5b and c shows SEM micrographs of the films grown at room temperature and 650°C, at an oxygen pressure of 1.0 Pa and with a target-to-substrate distance of 43 mm.
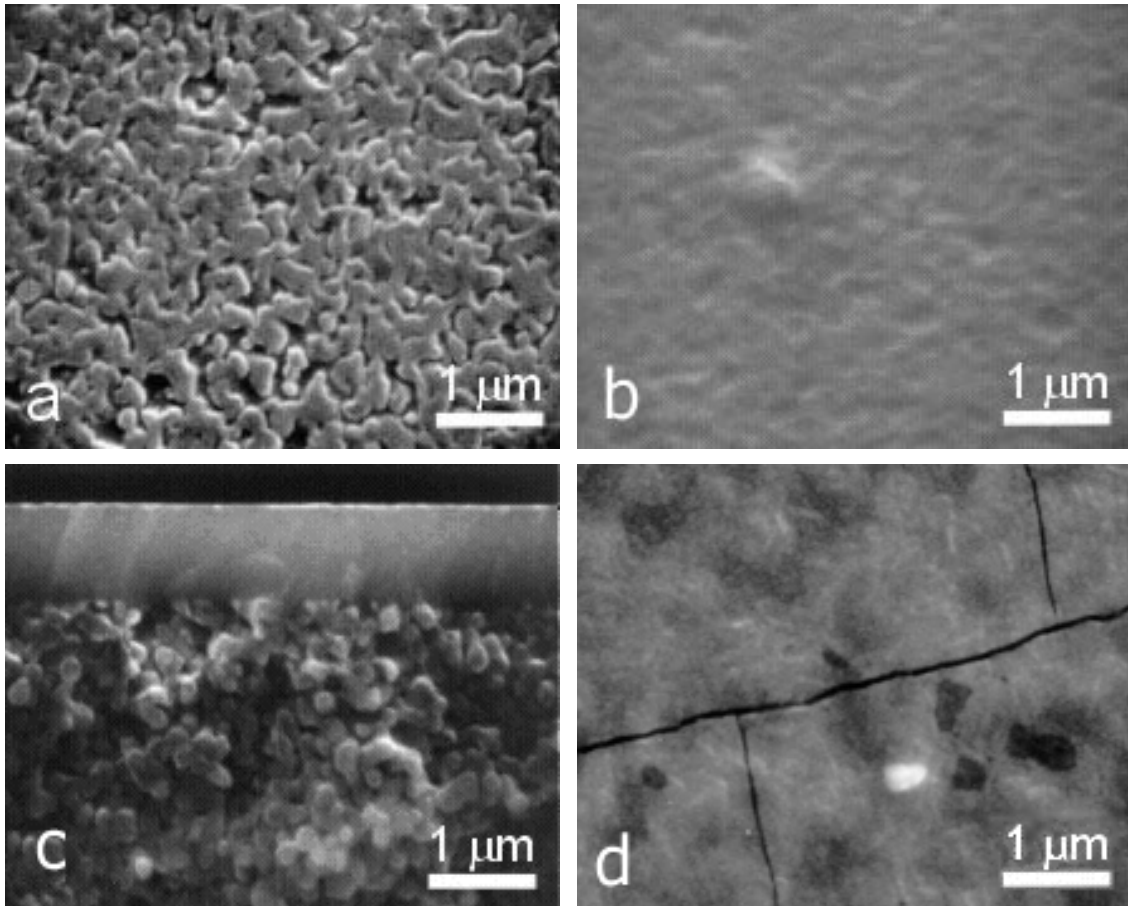
Figure 5.5: SEM pictures of: the typical surface morphology of a polished α-Al$_2$O$_3$ support (a), a 1 µm thick La$_{0.5}$Sr$_{0.5}$CoO$_{3-\delta}$ film deposited on top of such a support at room temperature (b) and a cross section of the deposited film (c). Picture (d) shows a film grown at 650°C, clearly featuring the cracks resulting from cooling after deposition.

5.4.2 Deposition on porous La$_{0.5}$Sr$_{0.5}$CoO$_{3-\delta}$ substrates

The deposition parameters used for the fabrication of the α-Al$_2$O$_3$ supported films served as a starting point for the deposition experiments on porous La$_{0.5}$Sr$_{0.5}$CoO$_{3-\delta}$ supports. As shown in the figures 5.6a and b, these supports exhibit a much coarser surface morphology than the α-Al$_2$O$_3$ supports, which requires deposition of thicker films. Since the perovskite supports are more prone to crack formation, due to stoichiometric equilibration problems,

they were slowly heated at a rate of 1°C/min to 650°C in 1 bar of oxygen. Subsequently, the oxygen pressure was lowered to 1 Pa at which the deposition was performed. Layers were grown with a thickness varying from 2 to 30 μm. After deposition, the oxygen pressure was slowly increased in 4 h form 1 Pa to 1 bar, in which the membrane was annealed at the deposition temperature for 1h. Subsequently the membrane was cooled to room temperature.
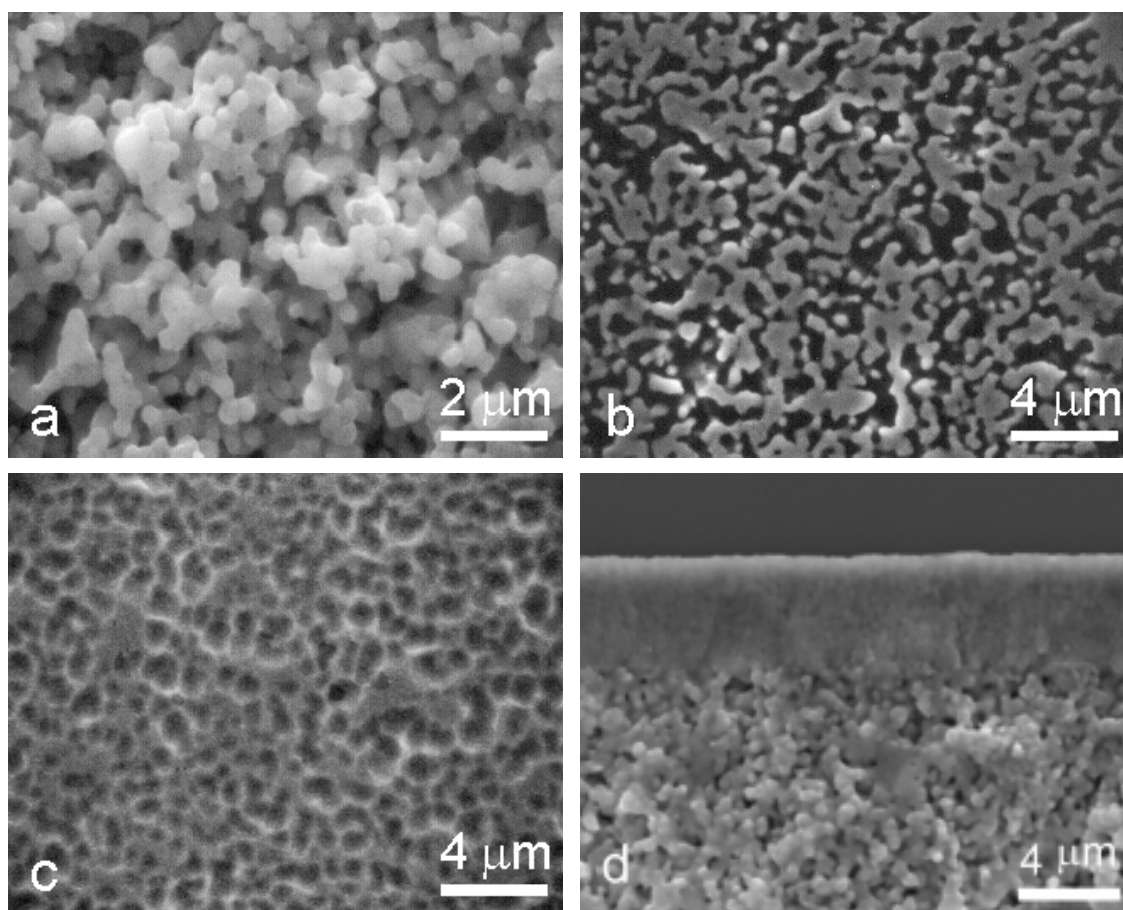
Figure 5.6: SEM pictures of: the typical surface morphology of a $La_{0.5}Sr_{0.5}CoO_{3-\delta}$ support as prepared via filtration (a), the same support after polishing (b), a 5 μm thick $La_{0.5}Sr_{0.5}CoO_{3-\delta}$ film deposited on top of such a support (c). Picture (d) shows a cross section of the all-perovskite system.

Figure 5.6b shows the surface morphology of a film 5 μm in thickness. Cracking of the films was not observed, provided that cooling rates below 0.5°C/min were applied after the annealing step. The imprint of the support causes the surface texture of the film shown in Fig. 5.6b. Despite this structure, the deposited layer bridges all support pores and appears to be dense as was confirmed by high temperature oxygen permeation measurements [15]. AFM indicated all films to exhibit a rms-surface roughness of 60 to 100 nm. Figure 5.8 shows a typical AFM micrograph.
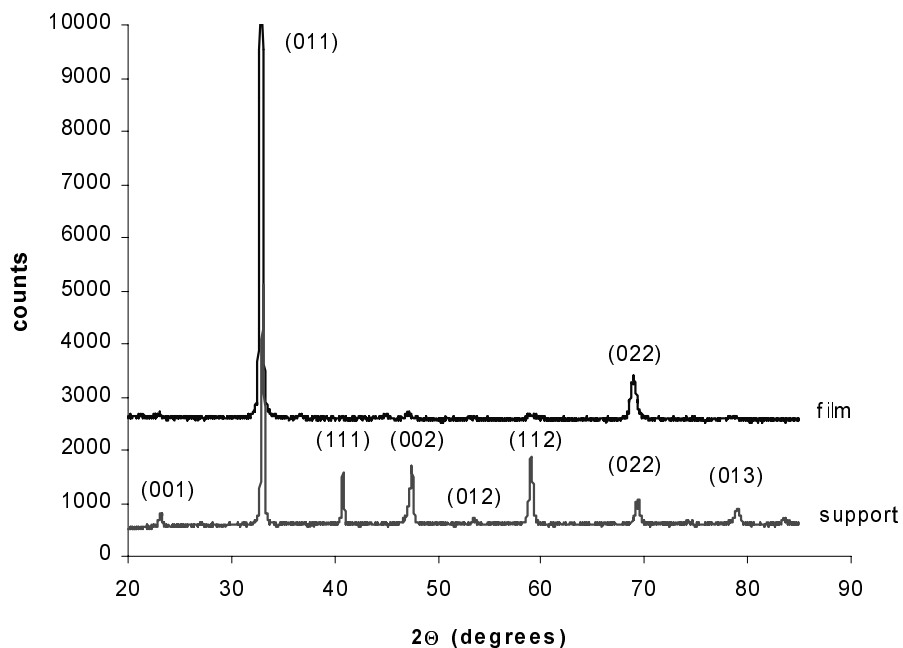
Figure 5.7: XRD pattern of a La$_{0.5}$Sr$_{0.5}$CoO$_{3-\delta}$ support and a deposited La$_{0.5}$Sr$_{0.5}$CoO$_{3-\delta}$ film. The film shows a strong preferential (011) growth.
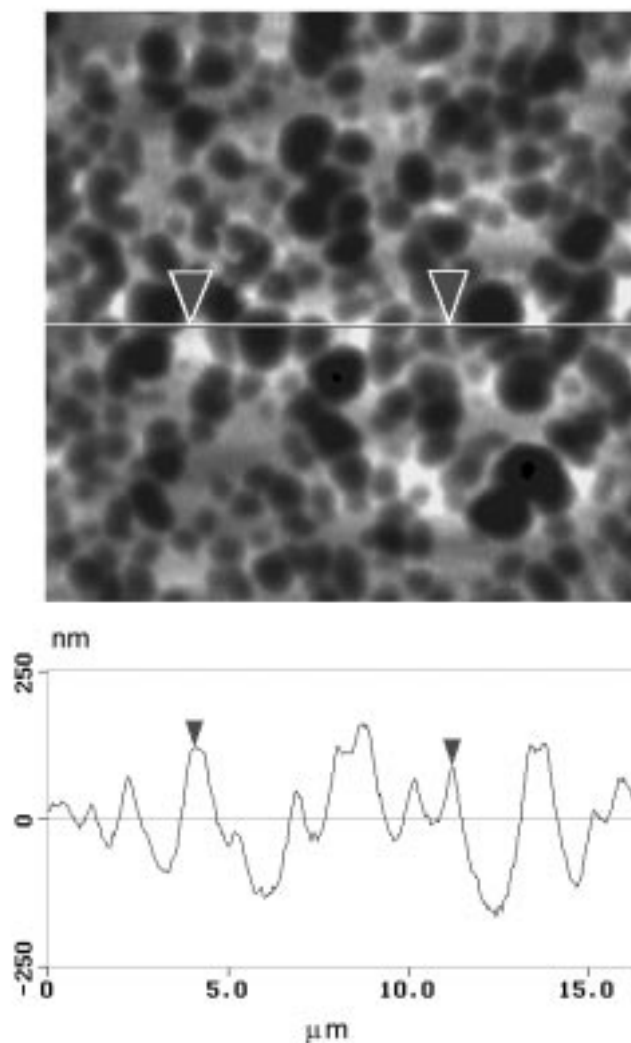
Figure 5.8: AFM height image with cross-section of a 5 μm thick La$_{0.5}$Sr$_{0.5}$CoO$_{3-\delta}$ supported La$_{0.5}$Sr$_{0.5}$CoO$_{3-\delta}$ film

It is interesting to note that in contrast to the polycrystalline α-Al_2O_3 supported films, the layers grown on the $La_{0.5}Sr_{0.5}CoO_{3-\delta}$ have a preferential orientation. Figure 5.7 shows the XRD pattern of the supported film. Only the (011) and (022) reflections are observed.

5.5   Conclusions

Dense films (10 - 30 μm) of $La_{0.5}Sr_{0.5}CoO_{3-\delta}$ were successfully deposited on porous substrates of similar composition using pulsed laser deposition. Fine grain and crack free films of the cubic perovskite were obtained at a temperature of 650°C, which films show strong preferential orientation. These films are considered as promising candidates for application as oxygen separation membrane.

5.6   References

1. B. Roas, L. Schultz, G. Endres, "Epitaxial-Growth Of $YBa_2Cu_3O_{7-X}$ Thin-Films By A Laser Evaporation Process", *Appl. Phys. Lett.*, **53** (16) 1557 (1988)
2. J.T. Cheung, H. Sankur, CRC critical reviews in solid state and materials science, **15** 63 (1988)
3. R.P.J. IJsselsteijn, D.H.A. Blank, P.G. Out, F.J.G. Roesthuis, J. Flokstra, H. Rogalla, "Droplets and outgrowths on high-Tc laser ablated thin films"; pp. 251-56 in: *High Tc Superconductor Thin Films,* Edited by L. Correra, 1992
4. D.H.A. Blank, R.P.J. IJsselsteijn, P.G. Out, H.J.H. Kuiper, J. Flokstra and H. Rogalla, "High Tc-thin prepared by laser ablation: Material distribution and droplet problem", *Mat. Science & Eng. B*, **B13** [1] 67 (1992)
5. D.B. Chrisey, G.K. Hubler, Pulsed laser deposition of thin films, Wiley, New York 1994
6. G. Koster, G.J.H.M. Rijnders, D.H.A. Blank, H. Rogalla, "Imposed layer by layer growth by pulsed laser interval deposition", *Appl. Phys. Lett.*, **74** 3729 (1999)
7. G. Koster, K. Verbist, G.J.H.M. Rijnders, H. Rogalla, G. van Tendeloo, D.H.A. Blank, "Structure and properties of $(Sr,Ca)CuO_2$-$BaCuO_2$ superlattices grown by pulsed laser interval deposition", Physica C **353** 167 167 (2001)
8. J.T. Cheung, P.E.D. Morgan, D.H. Lowndes, X.Y. Zheng, J. Breen, "Structural and electrical properties of $La_{0.5}Sr_{0.5}CoO_3$ epitaxial films", *Appl. Phys. Lett.*, **62** 2045 (1993)
9. C.S. Hou, C.C. Chou, H.F. Cheng, "Effect of processing parameters on structure of pulsed laser deposited $La_{0.5}Sr_{0.5}CoO_3$ thin films", *Appl. Surf. Sci.*, **114** 207 (1997)
10. M.Y. Li, Z.L. Wang, S.S. Fan, Q.T. Zhao G.C. Xiong, "Influences of substrates and substrate temperatures on characteristics of epitaxial $La_{0.5}Sr_{0.5}CoO_3$ thin films", *Thin Solid Films*, **323** 304 (1998)
11. E.A.F. Span, F.J.G. Roesthuis, D.H.A. Blank, H. Rogalla, "Structural and electrical properties of $La_{0.5}Sr_{0.5}CoO_3$ films on SrTiO3 and porous α-Al_2O_3 substrates", *Appl. Phys. A*, **69** 783 (1999)
12. E.A.F. Span, F.J.G. Roesthuis, D.H.A. Blank, H. Rogalla, "Pulsed laser ablation of $La_{0.5}Sr_{0.5}CoO_3$", *Appl. Surf. Sci.*, **150** 171 (1999)
13. E.A.F. Span, L.M. van der Haar, D.H.A. Blank, H.J.M. Bouwmeester, H. Rogalla, H. Verweij, "Supported perovskite gas separation membranes by pulsed laser deposition", *Advances in Science and Technology,* **29** 1055 (2000)
14. A. Nijmeijer, H. Kruidhof, R. Bredesen, H. Verweij, "Preparation and properties of hydrothermally stable gamma-alumina membranes", *J. Am. Ceram. Soc.* **84** [1] 136 (2001)
15. Chapter 6 of this thesis

6

Oxygen permeation through supported thin-film $La_{0.5}Sr_{0.5}CoO_{3-\delta}$ membranes

Abstract

Oriented thin films of $La_{0.5}Sr_{0.5}CoO_{3-\delta}$ were deposited on porous support layers with the same composition by pulsed laser deposition. Permeation measurements in the range 700-1000°C showed that the oxygen fluxes through the supported thin film membranes are significantly higher than those measured for pressed disc membranes. Minor leakage, amounting up to 5% of the total oxygen flux, was caused by the presence of inhomogeneities in the porous support layer, which could not be covered by the laser deposition process. In the experimental range of thickness 7.5-20 μm, the oxygen flux is found to be independent of membrane thickness. Using data of supported thin-film membranes together with that observed for pressed disc membranes a characteristic membrane thickness was calculated of about 50 μm. This value nicely agrees with that extracted from data of conductivity relaxation experiments if it is assumed that the porous support structure removes surface exchange limitations at the interface between porous support and thin film membrane. Analysis shows that mass transport through the porous support structure contributes to the overall permeation resistance at 1000°C and becomes negligible at temperatures around 700°C.

6.1   Introduction

The concept of a thin-film supported membrane is frequently documented in literature as a promising approach in order to maximise oxygen fluxes through mixed-conducting oxides [1-6]. So far only a few studies have been reported, which showed a limited degree of success. This is mainly due to the technological difficulties associated with fabrication of a dense and crack-free thin film, which must be contiguous with the porous support layer. Not only a suitable deposition technique is required that allows formation of a dense thin film with the correct stoichiometry and phase, the formed thin films are vulnerable and prone to defect formation.

In the previous chapter, it was described how pulsed laser deposition (PLD) was successfully employed to deposit crystalline and stoichiometric $La_{0.5}Sr_{0.5}CoO_{3-\delta}$ thin films onto porous supports. To avoid chemical interactions and to minimise differential thermal expansion effects the porous support material had the same composition as the thin film membrane. In this chapter, the oxygen permeation properties of these supported thin-film membranes are presented. The oxygen fluxes are compared with those measured through pressed disc membranes, measured in an earlier study [7].

6.2   Theoretical considerations

Oxygen transport permeation through a thin film supported membrane consists of several rate determining steps. Figure 6.1 gives a schematic representation of relevant transport processes.

6.2.1   Pore diffusion

Molecular oxygen has to diffuse into the pores of the macroporous support. Diffusion inside the pores can take place according to several mechanisms, amongst which Knudsen diffusion, molecular diffusion and viscous flow (Darcy flow) are considered to be the most important ones. As a combination rule, gas phase transport in the porous layer is conceived such that Knudsen and molecular diffusion are in series, whereas viscous flow is in parallel with diffusion. Since the membranes are measured under a *partial* pressure gradient and the pores of the support layer are smaller than an average value of about $10\mu m$, the contribution of viscous flow can safely be ignored. The Knudsen number indicates which of the two diffusion mechanisms prevails:

$$K_{\mathrm{n}} = \frac{\lambda}{d_{\mathrm{p}}} \tag{6.1}$$

in which λ is the mean free path of the gas molecule and d_{p} the average pore diameter of the support. From kinetic gas theory the mean free path is calculated via:

$$\lambda = \frac{kT}{\sqrt{2}\pi d^2 p} \tag{6.2}$$

in which d is the kinetic molecular diameter of the permeating gas and p the absolute pressure. Knudsen numbers below 1 indicate that molecular diffusion dominates, while values above 1 indicate a Knudsen diffusion regime. Molecular diffusion is non-selective, while Knudsen diffusion is proportional to the inverse square root of the molecular mass M according to [8]:

$$J_{\mathrm{K}} = -\frac{d_p \varepsilon}{3\tau} \sqrt{\frac{8}{\pi RTM}} \frac{\mathrm{d}p}{\mathrm{d}z} \tag{6.4}$$

in which ε and τ are the porosity and the tortuosity of the porous support, respectively. The ideal Knudsen separation factor equals the ratio of the inverse square root of their molar mass. For nitrogen and oxygen this factor amounts to $N_2/O_2 = 1.07$.

6.2.2   Surface transfer and ionic bulk transport

Once arrived at the surface of the dense thin film, molecular oxygen is dissociated, ionised and incorporated into the perovskite lattice. The oxygen ions are transported driven by the gradient in oxygen chemical potential to the oxygen-lean side of the thin film membrane, where they are recombined again to form oxygen molecules. Both the surface transfer and bulk transport process may limit the rate of oxygen permeation. The oxygen flux can be increased by ionic conduction through the walls of the pores, as shown in figure 6.1

Bulk diffusion of oxygen can be described using the Wagner equation [9]. Assuming linear transport kinetics for surface exchange, the classical Wagner equation for one-dimensional oxygen transport can be modified into [5,10]:

$$j_{\mathrm{O}_2} = -\frac{1}{1 + (2L_{\mathrm{c}}/L)} \frac{t_{\mathrm{el}}\sigma_{\mathrm{ion}}}{16F^2} \frac{\Delta\mu_{\mathrm{O}_2}^{\mathrm{total}}}{L} \tag{6.5}$$

in which σ_{ion} is the average value of the ionic conductivity of the membrane with thickness L brought into an oxygen chemical potential gradient $\Delta\mu_{O_2}^{total}$. For $La_{1-x}Sr_xCoO_{3-\delta}$, the electronic transference number t_{el} can be taken to be unity. L_c is the characteristic membrane thickness, below which the oxygen flux is predominantly controlled by surface exchange. When $L >> L_c$, the term $(1+2L_c/L)^{-1}$ approaches unity and equation (6.5) reduces to the classical Wagner expression for bulk oxygen transport.
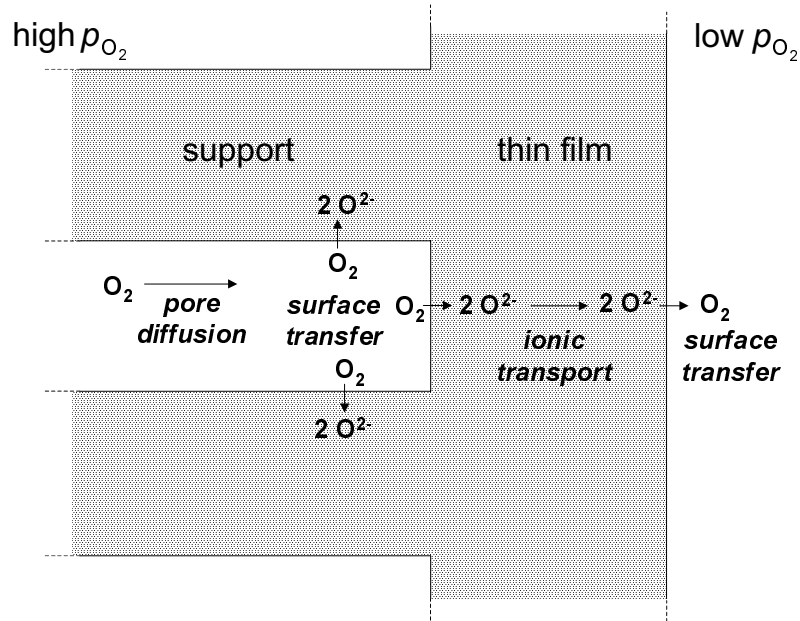
Figure 6.1: The various transport mechanisms that occur during oxygen permeation through a thin supported dense membrane. The high oxygen pressure side is assumed to be the support side.

Experimental measurements of the oxygen permeation can often be described using:

$$j_{O_2} = \frac{\sigma_{ion}^0 RT}{4^2 nF^2 L}\left[p'^{n}_{O_2} - p''^{n}_{O_2}\right] \tag{6.6}$$

which equation can be derived from the classical Wagner equation assuming a power law dependence between the oxygen ionic conductivity and p_{O_2} [5]. Accordingly, σ_{ion}^0 is the ionic conductivity at standard state, whereas the prime and double prime notation denote the high and low oxygen partial pressure side of the membrane, respectively. When all oxygen vacancies contribute to transport, the power index n can be directly correlated to the functional dependence of the oxygen non-stoichiometry with p_{O_2}.

6.3   Experimental

6.3.1   Membrane preparation

The 7.5 to 20 μm thick La$_{0.5}$Sr$_{0.5}$CoO$_{3-\delta}$ films that were investigated in this study, were grown on 30% porous, 0.5 mm thick La$_{0.5}$Sr$_{0.5}$CoO$_{3-\delta}$ supports, using PLD as deposition technique. The supports with an average pore diameter of 0.36 μm were prepared via pressure filtration of a suspension. The compacts were dried and sintered in air at 1020°C for 10 h. Prior to the deposition, the supports were mechano-chemically polished. Details of the support preparation and polishing procedure are given in chapter 4 of this thesis. The deposition of the thin film membranes using PLD was performed at 650°C using an oxygen background pressure of 1.0 Pa. After deposition the oxygen pressure was increased to 1 bar after which the membrane was cooled to room temperature at rates below 0.5°C min^{-1}. Details of the PLD deposition process can be found in chapter 5 of this thesis.

6.3.2   Permeation measurements

Oxygen permeation experiments were performed in the range from 750 to 1000°C. The membranes were sealed into a quartz reactor at 1000°C using glass rings[*]. Sealing was performed on the thin-film side of the membrane. After the sealing temperature was reached, the measurement was started after 45 min. Heating and cooling rates were 0.5°C/min. One side of the sample disc was exposed to air (100 ml/min). The oxygen partial pressure at the other side was controlled by regulating the helium gas flow rate (0-56 ml/min), assuming ideal gas mixing conditions in that part of the reactor. The oxygen concentrations in both feed and permeate streams were monitored through YSZ based oxygen sensors, made in this laboratory. Quantitative analysis of the oxygen concentration was performed with a gas chromatograph, which also measured the N$_2$ concentration in the sweep gas to check for inadequate sealing or membrane leakage.

To minimise the effect of mass transfer limitations imposed by the porous support layer, measurements were performed with the high oxygen partial pressure applied on the support side of the membrane. A schematic representation of the experimental set-up is given in figure 6.2

---

[*] 8252, Schott Netherlands B.V.
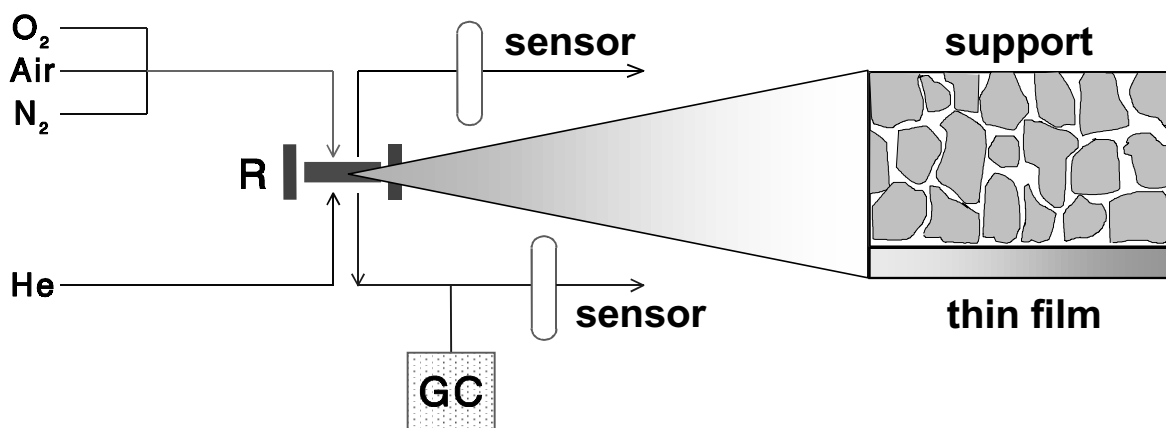
Figure 6.2   Schematic representation of the permeation reactor and set-up; R = reactor, GC = gas chromatograph

6.4   Results and discussion

6.4.1   Membrane preparation

Figure 6.3 shows SEM micrographs of the top-surface and cross section of a typical membrane. The imprint visible in the top view is caused by the structure of the porous support layer. X-ray confirmed formation of an (011) oriented thin film perovskite phase [11].
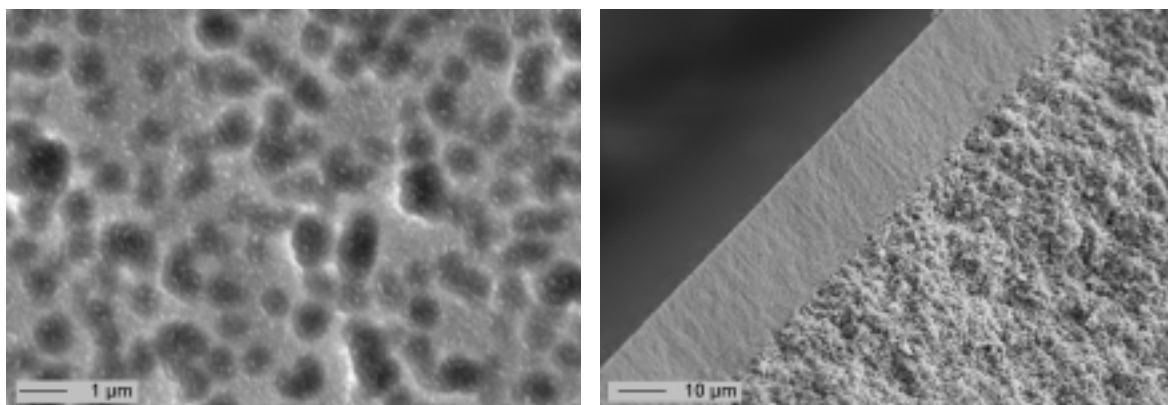
Figure 6.3: Top view (left) and cross section (right) of a 20 μm thick $La_{0.5}Sr_{0.5}CoO_{3-\delta}$ film on a 30% porous support of the same composition.

6.4.2   Permeation

Figure 6.4 shows the oxygen permeation of supported 7.5 and 20 μm thin-film membranes, measured under a constant He sweep rate of 56 ml/min. For comparison, data of oxygen permeation through unsupported 0.44 and 2.08 mm thick disc membranes measured under

the same conditions [7] is shown. Compared with the 0.44 mm thick membrane, the 20 μm thick membrane shows a permeation which is about a factor 4 higher at 1000°C. At 750°C, this factor has increased to about 11. Compared with the oxygen flux measured through the 2.08 mm thick disc membrane, extrapolated to a temperature of 750°C, the increase in oxygen flux is almost a factor of 25.
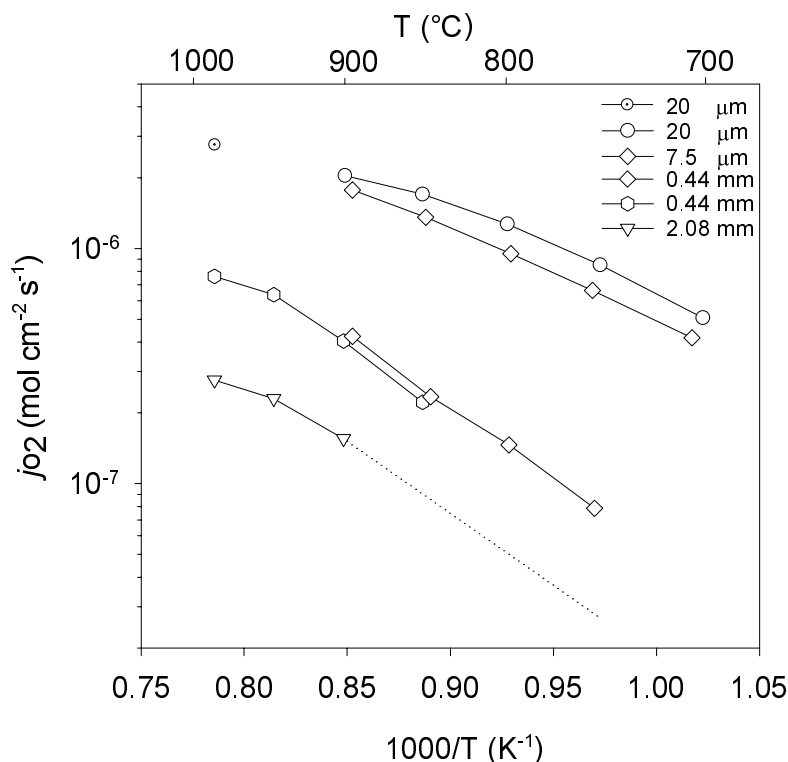
Figure 6.4: Arrhenius plots of oxygen permeation through supported 7.5 and 20 μm thick La$_{0.5}$Sr$_{0.5}$CoO$_{3-\delta}$ membranes. For comparison, the oxygen permeation through unsupported 0.44 mm thick and 2.08 mm thick membranes is also given. The data are collected using a fixed He-sweep rate of 56 ml/min.

At 900°C and lower temperatures, the permeation of the thin film membranes remained stable during the time span of the measurements (5 h). However, in exploratory measurements carried out at 1000°C the oxygen flux was found to show a sharp decrease with time, reducing to approximately 60% of its initial value in the first 5 h. In figure 6.4, the initial flux of a 20 μm thick membrane at 1000°C is plotted, measured immediately after connection of the gas lines. Sintering effects can possibly explain the observed decrease of the oxygen flux, since the temperature of 1000°C is close to the sinter temperature of the porous support.

For the thin film membranes a nitrogen flux of 1×10^{-7} mole cm^{-2} s^{-1} was measured, which was found to be independent of temperature. At 900°C under a He-sweep rate of

56 ml/min, this corresponds to a nitrogen leakage rate of approx. 5% of the total flux. This leakage is caused by the presence of a minor amount of support defects, which could not be covered by the thin film. These defects resulted from the presence of spherical inhomogeneities in the powder obtained form spray pyrolysis from which the supports were prepared. In figure 6.5, a SEM micrograph of a support defect and a defect in the thin film are shown. The micrograph of the film was taken after permeation measurements at 1000°C. Note that the film has developed a grain structure, which differs substantially from that exhibited by the film immediately after deposition, as shown in the left micrograph of figure 6.3. For the membranes measured at 900°C, this grain structure was not observed. This confirms the occurrence of a sintering effect at 1000°C, which influence the properties of the thin film. Although the degree of preferential (011) orientation of the films was slightly diminished after the permeation experiments, no secondary phases were observed according to X-ray diffraction.
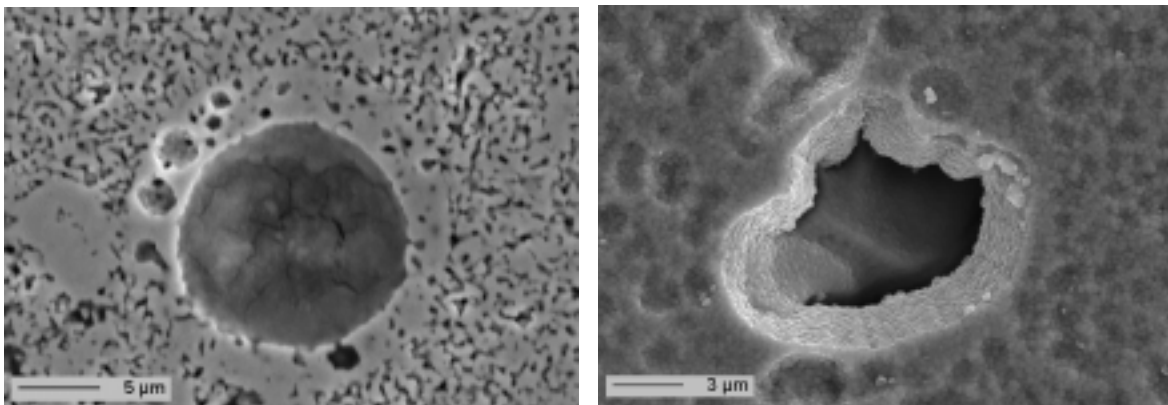
Figure 6.5: A spherical support defect (left) and a defect in a 10 μm thick film (right), deposited on a support containing such defects. The left micrograph was taken after the permeation of the membrane was measured at 1000°C.

A possible explanation for the weaker temperature dependence of the oxygen flux through the supported thin-film membranes than that through unsupported disc membranes is the occurrence of mass transfer limitations imposed by the porous support. When a worst-case scenario is considered, in which mass transport through the porous support is solely determined by Knudsen diffusion, the flux through the support is described by equation (6.4). This equation can be used to calculate the driving force required to sustain the experimental oxygen flux. Taking a value of 2.5 for the tortuosity of the support, which is obtained from room temperature permeation measurements [12], calculation indicates that, at 1000°C, the Knudsen diffusion process consumes 30% of the available partial pressure gradient. At 700°C, this value drops off to 5%. The Knudsen number for oxygen

transport, calculated from equations (6.1) and (6.2), using a molecular diameter for oxygen of 0.34 nm [13], varies from 0.95 and 0.73 in the temperature range from 1000 to 700°C. Since the values for K_n are close to 1, Knudsen diffusion and molecular diffusion contribute about equally to the transport resistance in the porous support. Nonetheless, the above calculations indicate that mass transfer limitations are of some importance at 1000°C, while they become negligibly small at 700°C.
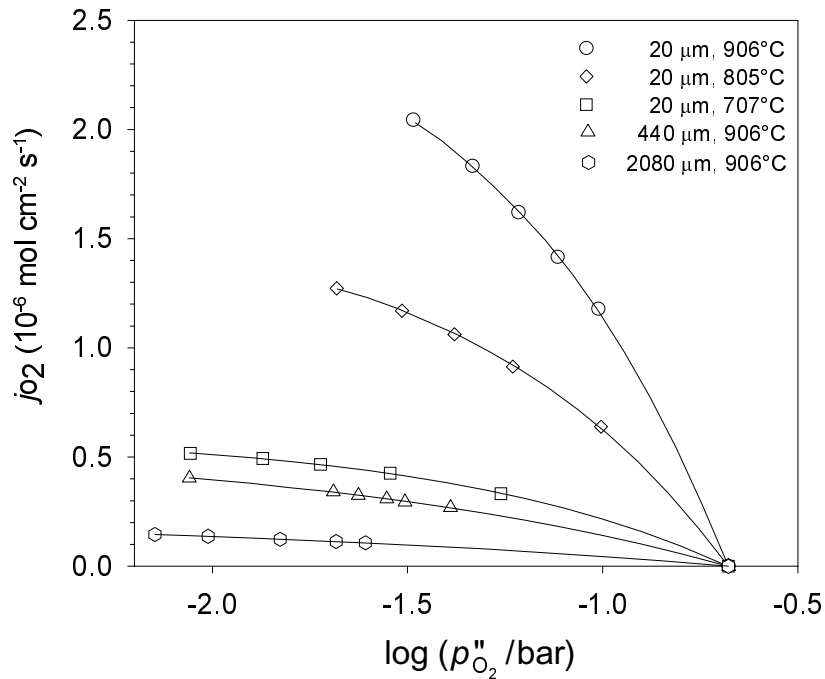
Figure 6.6: Dependence of j_{O_2} on $\log(p''_{O_2})$ at various temperatures for a supported 20 μm thick film. Results for non-supported pressed disc membranes [7] are also shown for comparison. The drawn lines represent the fit of the data to equation (6.6)

The dependence of the flux on the oxygen partial pressure maintained at the oxygen-lean side of the membrane is presented in figure 6.6. Results are shown for both supported and unsupported membranes. From figure 6.6 it follows that at 906°C, under an identical oxygen partial pressure gradient, the flux for a supported 20 μm thick membrane is more than a factor 20 higher compared to the unsupported 2 mm thick pressed disc membrane.

The solid lines indicate the fit of the experimental data to equation (6.6). The fitting procedure yields values for the power index n and for an apparent ionic conductivity at standard state. These are listed in table 6.1 together with corresponding values found for the unsupported membranes. The power index n for the supported thin-film membranes is significantly higher than that obtained for the unsupported disc membranes. As discussed above, at 900°C, gas phase diffusion through the porous support layer may still exert a

partial control of the oxygen fluxes. The observed power indexes can therefore not be used for distinguishing between surface exchange and gas phase diffusion.

Table 6.1:   Values of the power index n and the ionic conductivity σ_{ion}^0 obtained from fitting the j_{O_2} - $\log(p_{O_2}'')$ curves to Eq. (6.6). An asterisk refers to an unsupported membrane.

L (μm)	T (°C)	n	σ_{ion}^0 (mS cm^{-1})
20	707	0.59 ± 0.02	33 ± 2
20	805	0.66 ± 0.02	99 ± 5
20	906	0.71 ± 0.02	185 ± 10
440*	906	0.38 ± 0.02	267 ± 11
740*	906	0.40 ± 0.02	387 ± 23
2080*	906	0.29 ± 0.01	333 ± 7

In figure 6.4 it is seen that the oxygen flux through the thin film membrane of thickness 7.5 μm is approximately equal to that observed for the 20 μm thick membrane. Mass transfer limitations cannot account for this observation, since the agreement is found for all temperatures covered by the flux measurements. A plausible explanation is that in this thickness range the oxygen flux is dominantly controlled by surface exchange. In figure 6.7, the flux at 900°C is plotted as a function of membrane thickness in a double logarithmic graph. This plot contains flux data of unsupported as well as of supported membranes. The drawn line indicates the fit of the experimental data to equation (6.5), which yielded a characteristic thickness of 50 μm and an apparent ionic conductivity of 160 mS cm^{-1}. The value found for L_c is a factor two smaller than that from data of electrical conductivity relaxation [14,15]. However, it cannot be excluded that the porous support, which is made from the same material as the thin film membrane, contributes to a smaller L_c value [3,16-18]. Calculations using the dusty gas model by Thorogood *et al*. [3], showed that porous mixed conducting layers having an average pore radius ranging from 0.1 to 10 μm, situated contiguous to the thin mixed conducting film membrane, provide increased interfacial area to counteract kinetic surface limitations, but do not cause any significant pressure drop or resistance to mass transfer.
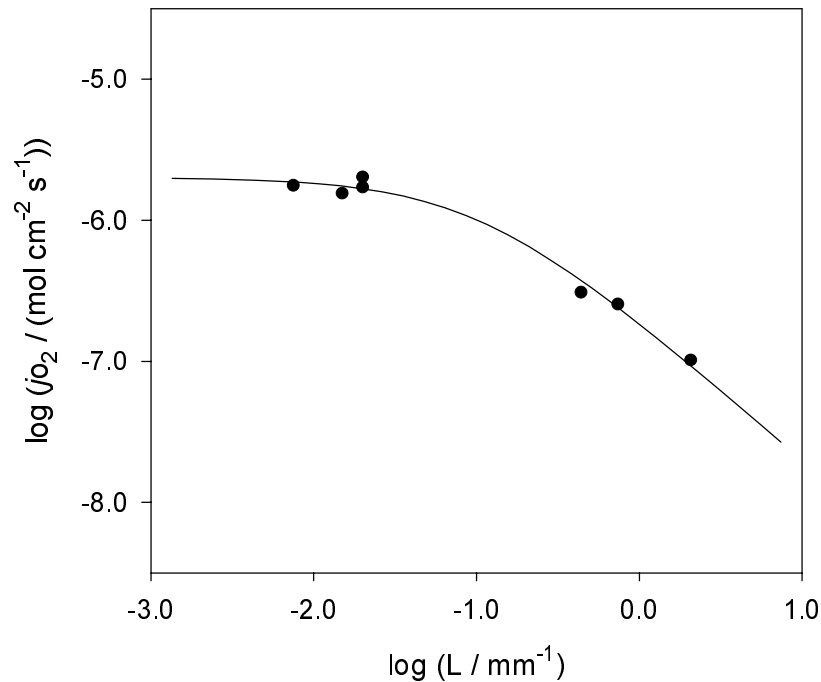
Figure 6.7: Membrane thickness dependence of the oxygen flux at 900°C and p''_{O_2} = 0.03 bar. The drawn line indicates the fit of the data to equation (6.5)

6.5   Summary and conclusions

It was shown that the oxygen flux through dense membranes is significantly increased by reducing the membrane thickness to the μm-range. At 906°C, the oxygen flux through the supported thin film membranes is increased with a factor of 20 relative to that measured through unsupported 2 mm thick disc membranes. Corrections were applied for oxygen leakage, amounting up to 5% of the total oxygen flux. This leakage was caused by the presence of inhomogeneities in the porous support layer, which could not be covered by the laser deposition process. In the experimental range of thickness 7.5-20 μm the oxygen flux is found to be independent of membrane thickness. Using data of supported thin-film membranes together with data observed for pressed disc membranes a characteristic membrane thickness was calculated of about 50 μm. This value nicely agrees with that extracted from data of conductivity relaxation experiments if it is assumed that the porous layer structure removes surface exchange limitations at the interface between porous support and thin film membrane. Analysis shows that mass transport through the porous support structure contributes to the overall permeation resistance at 1000°C. At lower temperatures, its influence becomes significantly smaller.

6.6   References

1. Y. Teraoka, T. Fukuda, N. Miura and N. Yamazoe, "Development of oxygen semipermeable membrane using mixed conductive perovskite-type oxides (part 1), preparation of porous sintered discs of perovskite type oxide", *J. Ceram. Soc. Jpn. Inter.* Ed. 97 458 (1989)
2. Y. Teraoka, T. Fukuda, N. Miura and N. Yamazoe, "Development of oxygen semipermeable membrane using mixed conductive perovskite-type oxides (part 2), preparation of dense film of perovskite type oxide on porous substrate", *J. Ceram. Soc. Jpn. Inter.* Ed. 97 523 (1989)
3. R.M. Thorogood, R. Srinivasan, T.F. Yee and M.P. Drake, "Composite mixed conductor membranes for producing oxygen," US Patent 5,240,480, 1993
4. H.J.M. Bouwmeester, H. Kruidhof, A.J. Burggraaf, "Importance of the surface exchange kinetics as rate limiting step in oxygen permeation through mixed-conducting oxides", *Solid State Ionics* 72, 185 (1994)
5. H.J.M. Bouwmeester, A.J. Burggraaf, "Dense ceramic membranes for oxygen separation", in: CRC Handbook of Solid State Electrochemistry, ed. P.J. Gellings and H.J.M. Bouwmeester, CRC Press, Boca Raton 1997
6. P.N. Dyer, R.E. Richards, S.L. Russek, D.M. Taylor, "Ion Transport Membrane Technology For Oxygen Separation And Syngas Production", *Solid Sate Ionics* 134, 21 (2000)
7. Chapter 2 of this thesis
8. M. Knudsen, "Die Gesetze der Molekularströmung und der innern Reibungsströmung der Gase durch Röhren", *Ann. Phys.* 28 75 (1909)
9. C. Wagner, W. Schottky, "Beitrag zur Theorie des Anlaufvorganges", *Z. Phys. Chem*, B11 25 (1930)
10. H.J.M. Bouwmeester, H. Kruidhof and A.J. Burggraaf, "Importance of the surface exchange kinetics as rate limiting step in oxygen permeation through mixed-conducting oxides", *Solid State Ionics*, 72 185 (1994)
11. Chapter 5 of this thesis
12. Chapter 4 of this thesis
13. D.W. Breck, "Zeolite Molecular Sieves", Wiley- Interscience, New York, 1974.
14. L.M. van der Haar, M.W. den Otter, M. Morskate, H.J.M. Bouwmeester, H. Verweij, "Chemical diffusion and oxygen surface transfer of $La_{1-x}Sr_xCoO_{3-\delta}$ studied with electrical conductivity relaxation", *submitted*
15. Chapter 3 of this thesis
16. H. Deng, M. Zhou, B. Abeles, "Diffusion reaction in mixed ionic-electronic solid oxide membranes with porous electrodes", *Solid State Ionics* 74 75 (1994)
17. H. Deng, M. Zhou, B. Abeles, "Transport in solid oxide porous electrodes: Effects of gas diffusion", *Solid State Ionics* 80 213 (1995)
18. M. Zhou, H. Deng,, B. Abeles, "Transport in mixed ionic electronic conducting solid oxide membranes with porous electrodes: Large pressure gradient", *Solid State Ionics* 93 133 (1997)

7

Permeation and transport properties of nickel and copper substituted La$_{0.5}$Sr$_{0.5}$CoO$_{3-\delta}$

Abstract

The influence of substitution of cobalt in La$_{0.5}$Sr$_{0.5}$CoO$_{3-\delta}$ with 1 to 8 mole % of either copper or nickel on the oxygen permeation rate and transport parameters was investigated. Oxygen permeation data at 900-1000°C indicate that nickel and copper doping results in a significant increase in the permeation rate. The largest increase in flux was measured for the lowest dopant concentration, amounting to a factor 1.4 for the nickel-doped and 1.7 for the copper-doped sample. Conductivity relaxation data obtained at 650-750°C for the samples showing the highest oxygen permeation rate, indicate that doping increases both the surface transfer and the bulk diffusion rates.

7.1   Introduction

The rate of oxygen permeation through mixed-conducting perovskite membranes can be increased by reducing the membrane thickness provided that bulk diffusion rate limits overall oxygen transport. The previous chapter described how this approach was applied successfully to increase the oxygen flux through dense $La_{0.5}Sr_{0.5}CoO_{3-\delta}$ membranes. Reducing the membrane thickness from 500 to 20 μm enlarged the flux with a factor 20 at 900°C. The thickness of the thin-film membrane is less than the characteristic thickness L_c, below which oxygen transport is the rate-determining by the surface transfer reaction. In chapters 2 and 3 it was shown that the value of L_c for $La_{1-x}Sr_xCoO_{3-\delta}$ membranes is approximately 100 μm. The enhancement of the surface reaction is therefore of importance to further increase the oxygen flux through these membranes.

The rate of oxygen transfer can be improved by surface modification. A successful approach appeared to be coating of the membrane surface with a porous layer having the same composition as the membrane [1,2]. This procedure effectively enlarges the surface area available for oxygen transfer. Another possibility is the dispersion of exchange active foreign phases on the membrane surface.

An alternative approach is intrinsically doping the membrane material with exchange active constituents. These dopants, which are incorporated as hetero-atoms in the perovskite lattice of the membrane, should enhance the surface transfer rate and should not have a negative influence on the bulk diffusion of oxygen. Studies of Inoue *et al.* [3,4] showed that B-site doping of $La_{1-x}Sr_xCoO_{3-\delta}$ oxygen sensor electrodes with 2 mole % of nickel leads to a significant increase in the exchange current density. This observation suggests that the presence of nickel at the perovskite surface has a beneficial effect on the rate of surface transfer. A similar effect was observed by Inoue *et al.* when $La_{1-x}Sr_xCoO_{3-\delta}$ was slightly doped with copper.

This chapter focuses on the influence of B-site doping on oxygen fluxes through $La_{0.5}Sr_{0.5}CoO_{3-\delta}$ membranes in which the cobalt is substituted with 1 to 8 mole % of either copper or nickel. In addition to oxygen permeation measurements, the electrical conductivity relaxation technique is used to study the relevant transport parameters.

7.2   Theory

7.2.1   Oxygen permeation

Bulk diffusion of oxygen through a dense membrane with thickness *L,* placed in an oxygen partial pressure gradient, can be described by the Wagner equation [5]:

$$j_{O_2} = -\frac{RT}{4^2 F^2 L} \int_{\ln p'_{O_2}}^{\ln p''_{O_2}} t_{el} \sigma_{ion} d \ln p_{O_2} \qquad (7.1)$$

where $p'_{O_2} > p''_{O_2}$. For the acceptor-doped cobaltites investigated in the present study, the electronic transference number t_{el} can be assumed to be unity. The ionic conductivity σ_{ion} may vary with temperature and oxygen partial pressure.

To estimate the influence of surface exchange processes on the permeation the following modification of equation (7.1) can be derived [6,7], which is valid only in the limit of small oxygen partial pressure gradients:

$$j_{O_2} = -\frac{1}{1 + (2 L_c / L)} \frac{t_{el} \sigma_{ion}}{16 F^2} \frac{\Delta \mu_{O_2}^{total}}{L} \qquad (7.2)$$

In this equation, L_c is the characteristic membrane thickness at which surface transfer and bulk diffusion consume an equal share of the total gradient in oxygen chemical potential, $\Delta \mu_{O_2}^{total}$.

7.2.2   Electrical conductivity relaxation

In electrical conductivity relaxation experiments, the time dependent response of the apparent conductivity $\sigma(t)$ of a solid oxide sample is monitored after application of a step-wise change in ambient oxygen partial pressure. The change in conductivity is caused by the adaptation of the sample's oxygen stoichiometry to the new oxygen partial pressure. When small steps in oxygen partial pressure are applied, the relative change in conductivity $\bar{\sigma}$ can be equated to the relative change of the mass *m* of the sample:

$$\bar{\sigma} = \frac{\sigma(t) - \sigma_0}{\sigma_\infty - \sigma_0} = \frac{m(t) - m_0}{m_\infty - m_0} \qquad (7.4)$$

In the current study, flat rectangular samples are used with a thickness 2*b*, which is much smaller than the surface area. Using Fick's second law under the assumption of linear

interface kinetics, the following expression for the mass change of the sample can be derived [8]:

$$\overline{\sigma} = \frac{\sigma(t) - \sigma_0}{\sigma_\infty - \sigma_0} = 1 - \sum_{n=1}^{\infty} \frac{2L_\beta^2}{\beta_n^2\left(\beta_n^2 + L_\beta^2 + L_\beta\right)} \exp\left(-\frac{t}{\tau_n}\right) \qquad (7.5)$$

In this expression the time constants τ_n are given by

$$\tau_n = \frac{b^2}{\widetilde{D} \cdot \beta_n^2} \qquad (7.6)$$

and the eigenvalues β_n are obtained from

$$\beta_n \tan \beta_n = \frac{bK_{tr}}{\widetilde{D}} = L_\beta \ . \qquad (7.7)$$

In the regime in which the equilibration rate is limited both by diffusion and surface transfer of oxygen, equation (7.5) makes it possible to obtain the parameters $\widetilde{D}$ and K_{tr} from the experimental relaxation data. In the regime of diffusion or transfer-limited equilibration only $\widetilde{D}$ or K_{tr}, respectively, can be determined. The ratio of $\widetilde{D}$ and K_{tr} determines the value of the characteristic thickness L_c. For more details including a quantitative description of the regimes of mixed, diffusion and transfer controlled kinetics, the reader is referred to den Otter *et al*. [9,10].

7.3   Experimental

7.3.1   Sample preparation

$La_{0.5}Sr_{0.5}Co_{1-x}Ni_xO_{3-\delta}$ and $La_{0.5}Sr_{0.5}Co_{1-x}Cu_xO_{3-\delta}$ (x=0, 0.01, 0.02, 0.04 and 0.08) powders were prepared via thermal decomposition of EDTA precursor complexes derived from a stoichiometric mixture of the metal nitrate solutions [11]. After calcination in air at 940°C and subsequent ball milling, the powders were isostatically pressed at 4000 bar. After sintering at 1150°C in air for 10 h the samples showed a relative density in excess of 96%. X-ray fluorescence[*] was employed to verify the stoichiometry of the obtained materials. Structural characterication was performed by means of X-ray powder diffraction with CuK_α radiation[†], using LaB_6 as internal standard. The powder diffraction patterns were indexed using the TREOR90 program [12]. For permeation measurements, disks were used

---

[*] Philips PW1480
[†] Philips PW3710 based X'pert 1

with a diameter of 15 mm and a thickness between 0.44 and 2.00 mm. For conductivity relaxation experiments thin rectangular samples were used with dimension 0.5×5×20 mm^3. Prior to both permeation and relaxation experiments, the surface of the samples were polished with 1000 MESH SiC, cleaned ultrasonically in ethanol and annealed for 3 h at 900°C.

7.3.2   Permeation measurements

The permeation of the samples was measured under air/helium gradients[*]. The samples were sealed in a quartz reactor tube at 1000°C using glass rings[†]. Measurements were performed at 900 and 1000°C. The oxygen partial pressure at the permeate side was controlled by adjusting the helium flow rate. The oxygen concentration in the gas streams was monitored by means of YSZ-based oxygen sensors and analysed using gas chromatography. A correction was applied to account for non-axial contributions to the measured flux. Further details of the measuring procedure can be found elsewhere [13].

7.3.3   Electrical conductivity relaxation experiments

The electronic conductivity was measured using a four-point AC technique, employing gold wires as electrodes. The sample was mounted in a quartz tube through which two nitrogen diluted oxygen streams[‡] could be passed. Stepwise changes in the oxygen partial pressure were applied, in reducing direction, by switching between the two gas streams. Measurements were performed over a p_{O_2} range of 10^{-4}-1 bar and temperature range of 650-750°C. The relative change in apparent conductivity was recorded and fitted to equation (7.5) [14]. Further details on the experimental set-up, measuring procedure and the criteria followed during data interpretation are given elsewhere [9,15].

7.4   Results

7.4.1   Materials characterisation

X-ray fluorescence results indicated that all synthesised materials exhibited the desired stoichiometry. X-ray diffraction confirmed formation of a single-phase perovskite structure in all cases. All peaks of the X-ray powder diffraction patterns could be indexed on the

---

[*] Air: 100 ml/min, He: 5-50 ml/min
[†] Schott 8252.
[‡] 300 ml/min

basis of a rhombohedral unit cell, except for the copper-doped material with x=0.08, which was found to be cubic. The cell parameters for the various compositions are listed in table 7.1. Apart from the formation of the cubic structure for the copper-doped material, no clear influence of copper and nickel doping on the cell parameters can be observed. Those for the sample with x=0 show close agreement with values reported in literature [16-18].

Table 7.1: Diffraction data for the various compositions. Unless stated otherwise, the cell parameters are based on a hexagonal setting.

$La_{0.5}Sr_{0.5}Co_{1-x}Ni_xO_{3-\delta}$	x=0	x=0.01	x=0.02	x=0.04	x=0.08
a [Å]	5.428(4)	5.429(3)	5.429(7)	5.429(4)	5.429(2)
c [Å]	13.231(4)	13.233(9)	13.233(3)	13.235(1)	13.236(4)
$La_{0.5}Sr_{0.5}Co_{1-x}Cu_xO_{3-\delta}$	x=0	x=0.01	x=0.02	x=0.04	x=0.08[*]
a [Å]	5.428(4)	5.429(2)	5.428(8)	5.429(4)	3.835(6)
c [Å]	13.231(4)	13.241(8)	13.241(4)	13.246(5)	

[*] cubic setting

7.4.2 Permeation

Figure 7.1 shows the permeation of the doped and undoped $La_{0.5}Sr_{0.5}CoO_{3-\delta}$ membranes as a function of oxygen partial pressure. A clear relation is observed between the level of B-site doping and the magnitude of the oxygen flux. Substitution of 1 or 2 mole percent of cobalt with nickel results in a distinct increase of the oxygen flux. Further increasing the nickel concentration leads to lower oxygen fluxes. At a doping concentration of 8 mole %, the flux has dropped below that observed for the undoped material. Copper doping has an
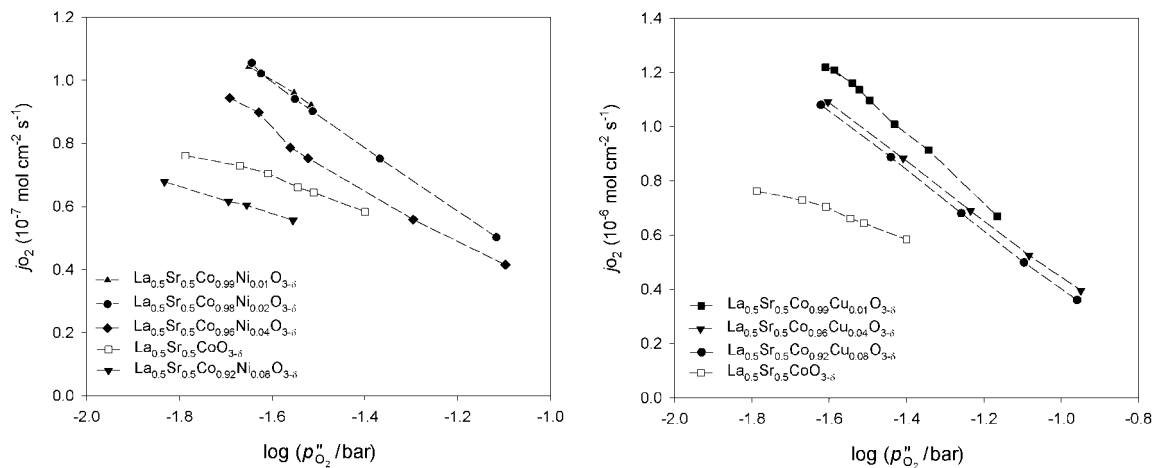

Figure 7.1: Oxygen permeation at 1000°C through 0.5 mm thick nickel-doped (left) and copper-doped (right) $La_{0.5}Sr_{0.5}CoO_{3-\delta}$ membranes. The dashed lines are a guide for the eye and have no theoretical significance

even larger influence on the oxygen flux. Again the composition with the lowest doping concentration shows the highest increase in the oxygen flux. Although not shown here, similar trends were observed at 1000°C.

7.4.3   Electrical conductivity relaxation

The previous section showed that the highest oxygen fluxes are found for nickel and copper dopant concentrations of 1 mole %. These samples were subjected to electrical conductivity experiments for further investigation of their transport properties. In figure 7.2, the chemical diffusion coefficient and surface transfer coefficient are plotted as a function of oxygen partial pressure at 750°C. In agreement with results obtained in earlier work on undoped La$_{0.5}$Sr$_{0.5}$CoO$_{3-\delta}$ [13,19], the equilibration is governed both by diffusion and surface transfer, which implies that both $\tilde{D}$ and K_{tr} can be extracted from the experimental data.

Figure 7.2: $\tilde{D}$ and K_{tr} plotted as a function of oxygen partial pressure at various temperatures for the materials with 1 mole % Ni (left) and Cu (right) doping. The transport parameters for undoped La$_{0.5}$Sr$_{0.5}$CoO$_{3-\delta}$ are also given for comparison. The dashed lines are a guide for the eye.

Figure 7.2 shows that the observed trends of $\tilde{D}$ and K_{tr} for both doped specimens are similar to those measured for the undoped material. However, both transport parameters have increased relative to those of the undoped material. For the nickel-doped material, the increase in the magnitude of $\tilde{D}$ resembles that of K_{tr}. For the copper-doped sample a pronounced increase in the magnitude of K_{tr} is observed, relative to that of the undoped La$_{1-x}$Sr$_x$CoO$_{3-\delta}$. For this material K_{tr} is approximately one order of magnitude higher at

650°C than the value for the undoped material, while only a minor increase in $\tilde{D}$ is observed. The above observations are reflected in the calculated values for L_c, which are given in figure 7.3. No significant change in L_c can be observed for the nickel-doped material. However, for the copper-doped material values for L_c are significantly smaller than those found for the undoped material.

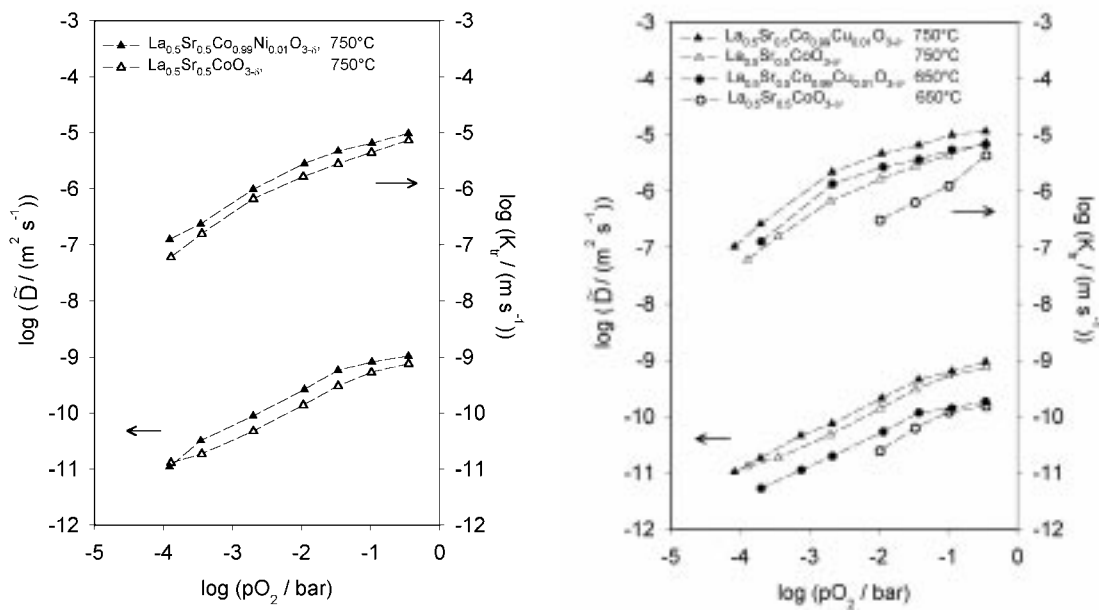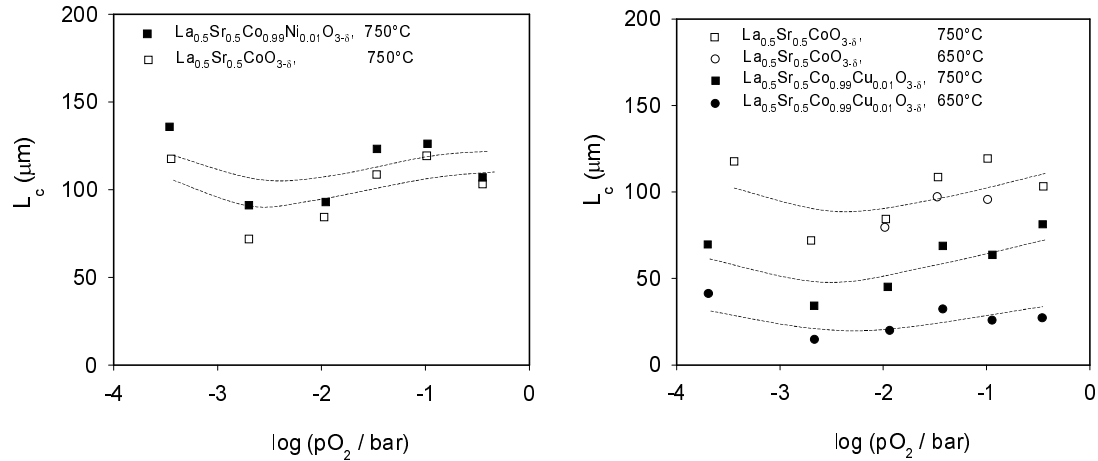Figure 7.3:   Characteristic membrane thickness plotted as a function of oxygen partial pressure at various temperatures for the materials with 1 mole % Ni (left) and Cu (right) doping. The dashed lines are a guide for the eye. The corresponding values for the undoped material are also shown for comparison.

7.5   Discussion

Equation 7.3 can be used to estimate the influence of surface exchange on oxygen permeation, provided that the flux measurements are performed close to equilibrium conditions. In the present study data were collected using oxygen partial pressure gradients not exceeding $\log(p'_{O_2} / p''_{O_2})$=1.3. This equation shows that the oxygen permeation rate is reduced due to surface transfer limitations with a factor $(1+2L_c/L)^{-1}$ relative to that expected from the Wagner equation. Taking the experimental value for L_c of 100 μm, as observed for undoped $La_{0.5}Sr_{0.5}CoO_{3-\delta}$, it is readily calculated that the oxygen flux through a 0.5 mm thick membrane can be increased with a factor 1.4 upon suppressing surface exchange imitations.

For the compositions with 1 and 2 mole % of nickel doping, it is found that the oxygen flux has increased with a factor of 1.4 compared with that of the undoped $La_{0.5}Sr_{0.5}CoO_{3-\delta}$. Doping with 1 mole % of copper results in an enhancement of a factor 1.7. The latter value is beyond the maximum increase expected when oxygen transport is entirely relieved from surface exchange limitations. Although the relaxation and permeation were performed in

different temperature regimes, the former experiments indeed demonstrate an increase in the surface transfer coefficient K_{tr} upon doping with either 1 mole % of copper or nickel. However, the relaxation data also indicate an increased bulk diffusion rate. It thus seems that the observed increase in oxygen flux is due to an increase in both the rate of surface transfer and bulk diffusion. Nickel doping increases the rate of both processes to the same extent, while copper doping preferably increases the surface transfer rate.

According to figure 7.2, the observed trends of $\tilde{D}$ and K_{tr} as a function of the oxygen partial pressure show close agreement. Similar trends were observed for La$_{1-x}$Sr$_x$CoO$_{3-\delta}$ samples with x=0.2 and 0.7 [15,19]. The profound decrease in the diffusivity of oxygen with decreasing p_{O_2} is unexpected from point defect considerations and indicates that oxygen vacancies at lower p_{O_2} values are less mobile due to trapping phenomena, as discussed in detail in chapter 3 of this thesis. Due to the formation of extended defects or vacancy ordering the concentration of 'free' oxygen vacancies available for ionic transport is lowered. It can be argued that doping of the material with of a small amount of a foreign component, in this case copper or nickel, has a disturbing effect on these phenomena and effectively leads to an increased concentration of mobile oxygen vacancies. This can then account for the observed increase in the value of $\tilde{D}$. Another tentative explanation is the presence of fast diffusion paths along grain boundaries. Results of Kharton *et al*. [20] suggest a significant influence of the grain boundary resistance on the permeation behaviour of LaCoO$_{3-\delta}$. The enrichment of the grain boundaries with the applied dopants possibly lowers the grain boundary resistance. Further research is required to provide more evidence for this.

7.6   Summary and conclusions

Substitution of cobalt in La$_{0.5}$Sr$_{0.5}$CoO$_{3-\delta}$ membranes with copper or nickel results in a significant increase in the rate of oxygen permeation. The increase in permeation rate is correlated with the doping level. In the investigated concentration range from 1 to 8 mole %, the lowest dopant concentration corresponds with the largest increase in the permeation. This suggests that doping increases the surface transfer of oxygen. However, conductivity relaxation data of samples with either 1 mole % of copper or nickel indicate that doping increases both the surface transfer and the bulk diffusion rate. The increase in the surface transfer rate is most pronounced for the copper-doped sample. Explanations for the enhancing effect of doping on the bulk transport remain tentative and require a more elaborate investigation.

7.7 References

1. R.M. Thorogood, R. Srinivasan, T.F. Yee and M.P. Drake, "Composite mixed conductor membranes for producing oxygen," US Patent 5,240,480, 1993
2. H. Deng, M. Zhou, B. Abeles, "Diffusion-reaction in porous mixed ionic-electronic conducting solid oxide membranes", *Solid State Ionics*, **74** 75 (1994)
3. T. Inoue, N. Seki, K. Eguchi, H. Arai, "Low-Temperature Operation of Solid Electrolyte Oxygen Sensors Using Perovskite-type Oxide electrodes and Cathodic Reaction Kinetics", *J. Electrochem. Soc.* **137** 2523 (1990)
4. T. Inoue, K. Eguchi, H. Arai, "Low Temperature Operation of Ceria-based Oxygen Sensors Using Perovskite-type Oxide Electrodes", *Chemistry Letters,* 1939 (1988)
5. C. Wagner, W. Schottky, "Beitrag zur Theorie des Anlaufvorganges", *Z. Phys. Chem*, **B11** 25 (1930)
6. H.J.M. Bouwmeester, H. Kruidhof and A.J. Burggraaf, "Importance of the surface exchange kinetics as rate limiting step in oxygen permeation through mixed-conducting oxides", *Solid State Ionics*, **72** 185 (1994)
7. H.J.M. Bouwmeester, A.J. Burggraaf, "Dense ceramic membranes for oxygen separation", in: CRC Handbook of Solid State Electrochemistry, ed. P.J. Gellings and H.J.M. Bouwmeester, CRC Press, Boca Raton 1997
8. J. Crank, 'The Mathematics of Diffusion', 2nd ed., p. 60, Oxford University Press, Oxford (1979)
9. M.W.den Otter, H.J.M. Bouwmeester, B.A. Boukamp, H. Verweij, "Reactor flushtime correction in relaxation experiments", *J. Electrochem. Soc.*, **148**, J1-J6 (2001)
10. M.W. den Otter, L.M. van der Haar, H.J.M. Bouwmeester, "Numerical evaluation of eigenvalues of the sheet diffusion problem in the surface/diffusion mixed regime", *Solid State Ionics* **13**, 259 (2000)
11. R.H.E. van Doorn, H. Kruidhof, A. Nijmeijer, L. Winnubst and A.J. Burggraaf, "Preparation of $La_{0.3}Sr_{0.7}CoO_{3-\delta}$ perovskite by thermal decomposition of metal-EDTA complexes," *J. Mater. Chem.*, **8** [9] 2109 (1998)
12. P.E. Werner, L. Eriksson, M. Westdahl, "TREOR, a semi-exhaustive trial-and-error powder indexing program for all symmetries", *J. Appl. Crystallogr.*, **18** 367 (1985)
13. Chapter 2 of this thesis
14. Relaxation Analysis software, version 1.2, by B.A. Boukamp, Internet: http://www.ct.utwente.nl/~ims/
15. Chapter 3 of this thesis
16. V.V. Kharton, E.N. Naumovich, A.A. Vecher, A.V. Nikolaev, "Oxide ion conduction in solid solutions $Ln_{1-x}Sr_xCoO_{3-\delta}$ (Ln = La, Pr, Nd)", *J. Solid State Chem.*, **120** 128 (1995)
17. A.N. Petrov, O.F. Kononchuk, A.V. Andreev, V.A. Cherepanov, P. Kofstad, "Crystal structure, electrical and magnetic properties of $La_{1-x}Sr_xCoO_{3-y}$", *Solid Sate Ionics*, **80** 189 (1995)
18. N.M.L.P. Closset, R.H.E. van Doorn, H. Kruidhof, J. Boeijsma, "About the crystal structure of $La_{1-x}Sr_xCoO_{3-\delta}$ (0≤x≤0.6)", *Powder Diffraction* **11** 31 (1996)
19. L.M. van der Haar, M.W. den Otter, M. Morskate, H.J.M. Bouwmeester, H. Verweij, "Chemical diffusion and oxygen surface transfer of $La_{1-x}Sr_xCoO_{3-\delta}$ studied with electrical conductivity relaxation", *submitted*
20. V.V. Kharton, E.N. Naumovich, A.V. Kovalevsky, A.P. Viskup, F.M. Figueiredo, I.A. Bashmakov, F.M.B. Marques, "Mixed electronic and ionic conductivity of LaCo(M)O$_3$ (M=Ga, Cr, Fe or Ni), IV. Effect of preparation method on oxygen transport in $LaCoO_{3-\delta}$", *Solid State Ionics* **138** 135 (2000)

8

Conclusions and outlook

8.1 Introduction

The principal goals of the work described in this thesis were the development, fabrication and testing of supported thin-film (5-30 μm) membranes prepared via PLD. The material under consideration was perovskite $La_{1-x}Sr_xCoO_{3-\delta}$ (LSC), the same material as that used to fabricate the porous support. Although the thin-film approach has been advocated frequently in literature, only a few studies have been reported with limited degree of success [1-3]. The results from this study show for the first time that oxygen fluxes can be obtained that are more than one order of magnitude higher than those through pressed-disc membranes (0.44 mm) measured under identical conditions.

A number of other research accomplishments include the following: Analysis showed that mass transport through the porous support contributes to the overall permeation resistance at 1000°C, but becomes negligible at temperatures around 700°C. Data of oxygen permeation and conductivity relaxation showed that for membranes thinner than about 100 μm, the rate of oxygen permeation is predominantly governed by oxygen surface transfer. The results further demonstrated that in the temperature range 600-850°C trapping effects, associated with the ordering of oxygen vacancies, reduce the number of mobile oxygen vacancies in phases $La_xSr_{1-x}CoO_{3-\delta}$ at oxygen partial pressures below 10^{-2} bar. As a consequence, the chemical diffusion coefficient and associated ionic conductivity decrease with decreasing oxygen partial pressures below about 10^{-2} bar.

Although it is rigorously demonstrated in this work that the concept of a supported thin-film membrane is a most promising one, a number of issues still need to be addressed

before large-scale industrial application might become feasible. In this chapter, a number of ideas for further research are presented.

8.2   Membrane stability

The membrane support is of vital importance for the membrane in providing the required mechanical stability. For industrial application, the asymmetric membrane should be able to withstand considerable absolute pressure differences. Mechanical tests of the porous perovskite supports developed in this work revealed that these could endure an absolute pressure difference of about 30 bar. However, thin ceramic films are extremely fragile. Whether these can withstand such a pressure difference still needs further investigation.

Another important issue relates with the stability of the porosity. In this study supports were used that were sintered at the relatively low temperature of 1020°C. This temperature was mainly chosen to ensure enough remnant porosity after sintering. This restricts the membrane operation temperature to about 900°C and lower. Hence, application of the supports at temperatures close to 1000°C will reduce its porosity due to a non-negligible sinter activity at these temperatures. The use of alternative materials with a lower intrinsic sinter activity may offer a solution to this problem.

Another problem relates with the imposed pressure gradient across the ceramic membrane causing lattice expansion mismatch of opposite sides of the dense ceramic membrane. In addition, phenomena like kinetic demixing and/or decomposition can occur. The available theories predict that, if the mobilities of the cations are different and non-negligible at high temperatures, concentration gradients may appear in the oxide in such a way that the high oxygen partial pressure side of the membrane tends to be enriched with the faster moving cation species. Depending of the phase diagram the initially homogeneous oxide may eventually decompose. For a short review on this subject, the reader is referred to appendix B of this thesis. Although this phenomenon has been observed for mixed conducting perovskites [4,5], little is known of its impact on the membrane performance and mechanical properties.

8.3   Mechanism of oxygen transport

Three main transport processes govern the oxygen flux through an asymmetric mixed conducting membrane: mass transfer through the porous support, surface transfer and ionic

diffusion of oxygen through the dense oxide thin film. The impact of these transport processes on the performance of the membrane deserves more attention. Modelling can be used to predict the oxygen flux, to calculate the actual distribution of the oxygen chemical potential across the ceramic membrane and therefore shed led on preferred conditions and design of the asymmetric membrane. However, modelling requires detailed input of relevant transport parameters. Although the physical significance of porosity and tortuosity for diffusion of a gas through a porous medium is reasonably clear, less understood is the behaviour of ionic diffusion of oxygen and surface exchange especially at reduced oxygen partial pressures. In literature, experimental data at low oxygen partial pressures are still scarce. Impedance spectroscopy using electrochemical cells of the type as described in ref. [6] could be useful in separation of contributions from ionic diffusion and surface exchange.

8.4   Membrane design

Knowledge on the influence of the various transport processes on oxygen permeation can help to design an improved membrane or membrane reactor layout. Together with the results obtained from mechanical and ceramic processing studies an appropriate choice can be made regarding the most suitable membrane material. The development of a support with a graded porosity can offer a solution for mass transfer limitations imposed by the support. In this respect, as was illustrated in chapter 4 of this thesis, centrifugal casting is a most promising technique for the development of tubular membrane supports. On top of the smooth inner surface of the asymmetric tubes produced with centrifugal casting, a dense thin-film membrane can be deposited. Although PLD can be used for deposition, other deposition methods like, for example, dip-coating or centrifugal injection casting [7] may be more attractive.

8.5   References

1. Y. Teraoka, T. Fukuda, N. Miura and N. Yamazoe, "Development of oxygen semipermeable membrane using mixed conductive perovskite-type oxides (part 1), preparation of porous sintered discs of perovskite type oxide", *J. Ceram. Soc. Jpn. Inter.* Ed. 97 458 (1989)
2. Y. Teraoka, T. Fukuda, N. Miura and N. Yamazoe, "Development of oxygen semipermeable membrane using mixed conductive perovskite-type oxides (part 2), preparation of dense film of perovskite type oxide on porous substrate", *J. Ceram. Soc. Jpn. Inter.* Ed. 97 523 (1989)
3. W. Jin, S. Li, P. Huang, N. Xu, J. Shi, "Preparation of an asymmetric perovskite-type membrane and its oxygen permeability", *J. Membr. Sci.* **185** 237 (2001)
4. H. Yokokawa, T. Horita, N. Sakai, M. Dokiya, H. Nishiyama, M. Aizawa, T. Kawada, "Stability of lanthanum calcium chromite-lanthanum strontium manganite interfaces in solid oxide fuel cells", *J. Electrochem. Soc.*, **143** 2332 (1996)

5.   R.H.E. van Doorn, H.J.M. Bouwmeester and A.J. Burggraaf, "Kinetic decomposition of $La_{0.3}Sr_{0.7}CoO_{3-\delta}$ perovskite membranes during oxygen permeation," Solid State Ionics, **111** 263 (1998)

6.   S. Diethelm, A. Closset, J. van Herle, A.J. McEvoy, K. Nisancioglu, "Study of oxygen exchange and transport in mixed conducting cobaltates by electrochemical impedance spectroscopy", *Solid State Ionics*, **135** 613 (2000)

7.   P.M. Biesheuvel, A. Nijmeijer, B. Kerkwijk and H. Verweij, "Rapid Manufacturing of microlaminates by centrifucal injection casting," Adv. Eng. Mater., **2** [8] 507 (2000)

Appendix A

Dip-coating of porous substrates

A.1   General description

Dip coating is the term applied to describe all deposition techniques in which a dense or porous substrate is dipped into a (ceramic) precursor solution or suspension. Its simplicity and speed make it highly suitable for deposition of ceramic films onto all kinds of substrates. The procedure requires no specialised apparatus. The object to be coated is simply lowered in the suspension or precursor solution and withdrawn at a suitable speed. It is widely used in the sol-gel processing of ceramic films, amongst others in the preparation of asymmetric porous and dense membranes [1-4]. The dip coating technique allows deposition of coatings with a thickness of typically 0.1 to 100 μm. When a dense layer is required, the surface roughness and the pore size distribution at the support surface determine the minimum required layer thickness. In the following, a description is given of surface modification of a porous ceramic substrate by dip-coating the latter, using a suspension of (sub-)micrometer powders.

A.2   Process characteristics

After the substrate is removed from the suspension in a well-defined manner, a wet and more or less dense dispersion layer of well-defined thickness can be obtained. Two possible compaction modes occur during withdrawal of the substrate from the suspension:

- Capillary filtration
- Film-coating

In figure A.1 both compaction modes are depicted schematically. The suspension and support properties and process parameters most relevant for the process are listed in the inset. Both compaction modes contribute to the film growth, while the role of the capillary filtration process decreases with decreasing substrate porosity.
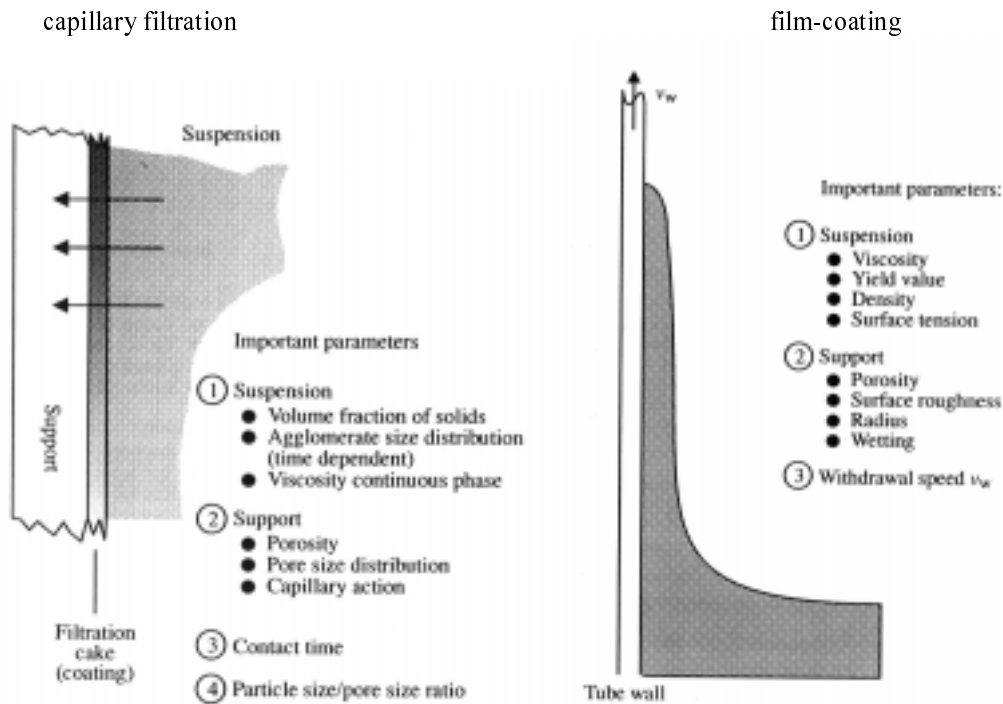
Figure A.1: Schematic representation of the two compaction modes that occur during dip-coating of a porous substrate, in this case a tubular membrane support [8].

A.2.1   Capillary filtration

Capillary filtration occurs when the dry porous substrate comes into contact with the suspension and the pore surface is wetted by the suspension medium. Capillary suction occurs, which effectively drives the particles in the dipping suspension towards the support surface, as in the slip-casting process [5-7]. These particles, which form the building blocks of the ceramic coating, start to clog the pores of the support, until the size of the pores becomes so small that cake formation starts. The pore clogging stage always precedes the cake formation stage and the period in which this process occurs increases with decreasing suspension solids concentration. Therefore, cake formation can be even absent when a suspension with a very low solids concentration is employed which causes saturation of the support to occur already in the pore clogging stage. When capillary filtration is the prevailing compaction mode, the thickness of the layer increases with the contact time until the substrate is saturated with the liquid suspension medium. In this case the film thickness is independent of the withdrawal speed. The capillary action is determined by the porosity and pore size distribution of the support. A higher volume fraction of solids in the suspensions causes a faster growth of the layer. During the filtration process, packing of the particles in the layer takes place.

The formation of a film on a porous substrate via capillary filtration has been investigated by several authors [9-12]. The following general expression can be derived for the growth of the layer:

$$L_c^2 = \frac{2\Delta P t}{\eta \left(\dfrac{\varphi_c}{\varphi_0} - 1 \right) \left(\dfrac{1}{K_c} + \left(\dfrac{\varphi_c}{\varphi_0} - 1 \right) / \varepsilon_1 K_1 \right)} = C\frac{t}{\eta} \qquad (A.1)$$

With:

L_c = compact thickness
ΔP = capillary suction pressure
t = contact time
η = suspension viscosity
φ_c = solids volume fraction in the cake
φ_0 = solids volume fraction in the suspension
K_c = permeability of the compact
K_1 = permeability of the substrate
ε_1 = porosity of the substrate

From equation A.1 it follows that the thickness of the compact is proportional to the square root of the contact time of the substrate with the suspension, while it is inversely proportional to the suspension viscosity. All the support- and compact-related parameters can be incorporated in a constant *C*, which, in turn, is a function of porosity, permeability, capillary pressure, suspension solids volume fraction and compact solids volume fraction. Equation A.1 can be used to predict the growth of the layer when these parameters are known. Usually, the pore properties of the substrate and can be determined rather easily. In addition, the capillary pressure drop can be calculated, taking into account the pore radius of both the compact and the support and the surface tension of the suspension [12]. The permeability of both the substrate and the thin layer can be obtained from the Carman-Kozeny equation [8]. For a more in-depth theoretical treatment of the capillary filtration process, the reader is referred to the references mentioned above.

A.2.2   Film coating

Film coating is the process in which an adhering dispersion layer is formed as a result of the drag force exerted by the substrate during withdrawal from the suspension. The film thickness is independent of the dipping time. However, it increases with increasing withdrawal speed and suspension viscosity. The latter increases with increasing volume fraction of solids in the suspension. The particle packing takes place during the drying of the entrained wet coating.

Assuming Newtonian suspension behaviour, Levich and Landau derived the following expression for the thickness *h* of the layer formed by film coating [13,14]:

$$h = 0.944 \left(\frac{\eta v_w}{\gamma} \right)^{1/6} \left(\frac{\eta v_w}{\rho g} \right)^{1/2} \qquad\qquad (A.2)$$

In this expression v_w represents the withdrawal velocity, γ the surface tension, ρ the density and *g* the gravitational constant. From equation (A.2) it follows that the thickness of the film is proportional to $v_w^{2/3}$ and $\eta^{2/3}$. Although this equation does not include terms for solids concentration, effect of evaporation or angle of inclination, it illustrates that the thickness will increase with withdrawal speed. The surface tension has only a minor influence on the coating thickness. Although many attempts have been made to obtain expressions for non-Newtonian suspension flows, these approximations are usually cumbersome and tend to overestimate the coating thickness considerably.

A.2.3   Drying and sintering

The drying and sintering step, during which consolidation of the wet coating layer takes place, should be performed in such a way that defect formation in the form of cracks and voids is avoided. Usually, the drying step starts simultaneously with the dip-coating step. The withdrawn part of the substrate starts to dry if the vapour pressure of the suspension medium in the ambient is lower than 100%. The microstructure of the green compact obtained after drying is mainly determined by the properties of the coating dispersion. A general treatment on the drying of ceramic bodies can be found in Scherer [15] and Brinker and Scherer [16]. An investigation of drying of coatings consisting of (sub-)micrometer particles has recently been given by Chiu *et al.* [17,18]. The structural changes induced by drying of the particulate coating are minor compared to those induced by sintering. Sintering of dried macroporous coatings for the purpose of support preparation is in general not problematic. However, when a dense layer is required, the tensile stress which occurs during the constrained sintering of the top-layer often gives rise to defects, especially at inhomogeneities at the support surface where non-uniform contraction of the top-layer occurs.

References

1.   N. Miura, Y. Okamoto, J. Tamaki, K. Morinaga, N. Yamazoe, "Oxygen semipermeability of mixed-conductive oxide thick-film prepared by slip casting", Solid State Ionics **79** (1995) 195
2.   J. Luyten, J. Cooyamns, C. Smolders, S. Vercauteren, E.F. Vansant, R. Leysen, "Shaping of multilayer ceramic membranes by dip coating", J. Eur. Ceram. Soc. **17** (1997) 273

3. M. Naito, K. Nakahira, Y. Fukuda, H. Mori, J. Tsubaki, "Process conditions on the preparation of supported microporous SiO_2 membranes by sol-gel modification techniques", *J. Membr. Sci.* **129** 263 (1997)

4. A. Nijmeijer, H. Kruidhof, R. Bredesen and H. Verweij, "Preparation and properties of hydrothermally stable gamma-alumina membranes", *J. Am. Ceram. Soc.* **84** [1] 136 (2001)

5. D.S. Adocock, I.C. McDowall, "The mechanism of filter processing and slip casting", *J. Am. Ceram. Soc.* **40** (1957) 355

6. F.M. Tiller, C.D. Tsai, "Theory of filtration of ceramics I, Slip casting", *J. Am. Ceram. Soc.* **69** (1986) 882

7. J.H.D. Hampton, S.B. Savage, R.A.L. Drew, "Experimental analysis and modelling of slip casting", *J. Am. Ceram. Soc.* **71** (1988) 1040

8. B.C. Bonekamp, "Chapter 6 – Preparation of asymmetric ceramic membrane supports by dip-coating"; pp. 141-225 in: Fundamentals of Inorganic Membrane Science and Technology. Edited by A.J. Burggraaf and L. Cot. Elsevier, Amsterdam, 1996

9. A.F.M. Leenaars, A.J. Burggraaf, "The preparation and characterisation of alumina membranes with ultrafine pores, Part 2: the formation of supported membranes", *J. Colloid Interface Sci.* **105** 27 (1985)

10. F.M. Tiller, C.D. Tsai, "Theory of filtration of ceramics: I: slib casting", *J. Am. Ceram. Soc.*, **69** 882 (1986)

11. F.M. Tiller, N.B. Hsyung, "Theory of filtration of ceramics: II: slib casting on radial surfaces", *J. Am. Ceram. Soc.*, **74** 210 (1991)

12. Y. Gu, G. Meng, "A model for ceramic membrane formation by dip-coating", *J. Eur. Ceram. Soc.* **19** 1961 (1999)

13. V.G. Levich, *Physicochemical Hydrodynamics*, Prentice Hall Englewood Cliffs, NJ, 1962

14. L.E. Scriven, Physics and applications of dip-coating and spin coating, in: *Better ceramics through chemistry III*, MRS, 1988 717

15. G.W. Scherer, "Theory of drying", *J. Am. Ceram. Soc.* **73** 3 (1990)

16. C.J. Brinker, G.W. Scherer, *"Sol-gel science, the physics and chemistry of sol-gel processing"*, Academic Press, Boston, 1990

17. R.C. Chiu, T.J. Garino, M.J. Chima, "Drying of granular films,: I. Effect of processing variables on processing behaviour", *J. Am. Ceram. Soc.* **76** 2257 (1993)

18. R.C. Chiu, T.J. Garino, M.J. Chima, "Drying of granular films,: II. Drying stress and saturation uniformity", *J. Am. Ceram. Soc.* **76** 2769 (1993)

Appendix B

Kinetic demixing and decomposition of multi-component oxides

B.1 General description

The general driving force for diffusion is a gradient in chemical potential. It can be established by a gradient in activity, temperature, stress or an electric field. Diffusion in materials has been investigated for all of these driving forces [1-4]. When the components of the material have different non-zero self diffusion coefficients, they will diffuse at different rates when a gradient in chemical potential is applied. Consequently, the local composition changes. This phenomenon is called kinetic demixing. It can severely alter (electro)chemical and physical properties of the material involved. When the material does not allow a too large stoichiometric variation of the constituents, demixing can lead to the precipitation of a new phase or phases. This process is known as kinetic decomposition and obviously has an even more drastic effect on chemical and physical properties. These phenomena take place even though the material is *thermodynamically stable* at all the chemical potentials in the range of the gradient. This is why these processes are referred to as *kinetic* demixing and decomposition.

B.2 The process of demixing

Taken into consideration is a semi-conducting oxide solid solution (A,B)O in which the oxygen ions are assumed to be immobile and hence form a rigid lattice. The non-stoichiometry exists in the form of cation vacancies via which the cations can move. The degree of non-stoichiometry is a function of temperature and oxygen partial pressure. A difference in oxygen partial pressure at opposite sides of the material gives rise to a gradient in oxygen chemical potential in the material. According to the Gibbs-Duhem relation, the chemical potential of the components in a mixture cannot change independently:

$$N_A d\mu_A + N_B d\mu_B = -N_O d\mu_O \qquad (B.1)$$

In this equation N_i represents the mole fraction and $d\mu_i$ the change in chemical potential. As a result, the change in chemical potential of oxygen is accompanied by an opposite change in chemical potential of A and B. Figure B.1 gives a schematic representation of the resulting gradients in chemical potential.

The gradient in the chemical potential of A and B causes these constituents to diffuse towards the high oxygen partial pressure side, with velocities proportional to their self diffusion coefficient. At this side the lattice is built up and oxygen is incorporated from the gas phase. Vacancies for A and B diffuse to the low oxygen partial pressure side where the lattice is broken down and oxygen is released. The flux of vacancies is charge compensated by a simultaneous flux of electron holes in the same direction. The various diffusion processes are illustrated in figure B.2 [5].
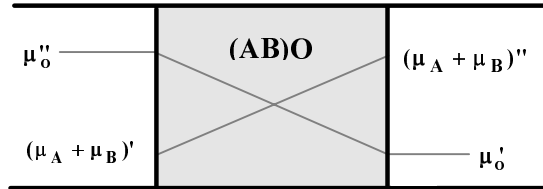

Figure B.1:   Schematic representation of the gradients in chemical potentials developed when different oxygen partial pressures are applied.
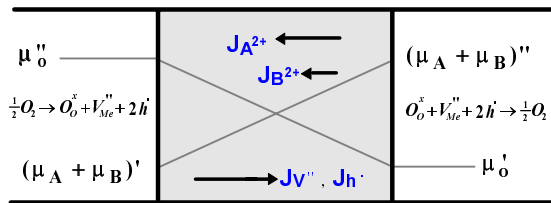
Figure B.2:   Non-steady state diffusion and phase boundary reactions for the (AB)O system.

When the self diffusion coefficient of A exceeds that of B, enrichment with component A occurs at the high oxygen partial pressure side. Due to this increasing concentration gradient, the rate of diffusion decreases. Steady state is reached when the difference in self diffusion coefficients of A and B is balanced by the difference in their concentration profiles. Both constituents now diffuse at the same rate. Equation (B.2) formulates the general steady state condition defined by Schmalzried et al. [1].

Figure B.3:   Steady   state   demixing concentration profiles for the solid solution (A,B)O. Dashed lines represent the initial concentration profiles, solid lines the steady state profiles.

$$\frac{J_A}{c_A} = \frac{J_B}{c_B} = v_{st} \qquad\qquad (B.2)$$

In this equation J_i represents the constituent flux at a fixed point in the immobile laboratory frame and c_i is the constituent concentration at this point. When steady state is established, the concentration profiles of A and B do not change anymore. The whole oxide system

moves with a constant velocity v_{st} towards the high oxygen partial pressure side. This situation is illustrated in figure B.3 [6].

B.3 Modelling of demixing

Quite some effort has been put in the modelling of demixing phenomena in solid solutions. In particular the system (Co,Mg)O has been well investigated. In the modelling of kinetic demixing, the problem to be addressed is the determination of the concentration profiles of the constituents. Two important issues have to be considered. The first is the calculation of the initial time evolution of these profiles, the second is the calculation of the time independent steady state concentration profiles. Historically, two different approaches have been used. Schmalzried and co-workers addressed the steady state problem first [1,7,8,9]. Their approach is a phenomenological one in which macroscopic thermodynamics is used. As a result, the atomistic features of the process are not identified. Vedula extended this procedure and developed a numerical method for the calculation of the time evolution of the demixing profiles [10].

Another approach that has attracted considerable attention is the application of the Path Probability Method (PPM). Sato *et al.* [11] used this statistical mechanical method to treat demixing of solid solutions. It was extended by Ishikawa *et al.* [12] to calculate the time evolution of the demixing profiles. Using the PPM, atomistic features of the diffusion process can be clarified. Both modelling approaches yield reasonably good results for (Co,Mg)O solid solutions. However, an important problem in accounting for the experimentally observed demixing phenomena in other systems is the lack in data on the self diffusion coefficients of the constituents.

B.4 Demixing of mixed conducting perovskites

Schmalzried [5] concluded that, in principle, kinetic demixing or decomposition occurs in all semi-conducting compounds for which the mobilities of the cations differ from each other. A gradient in oxygen chemical potential in the material always gives rise to a gradient in the chemical potentials of the other constituents through the Gibbs-Duhem equation (B.1). Therefore, kinetic demixing is independent of the mobility of the anions. However, in mixed conducting perovskites the main defects are oxygen vacancies which render it possible for oxygen anions to be transported through the material. The concentration of cation vacancies is often negligible in these materials.

Until now, very little knowledge is available about the demixing behaviour in these systems. Yokokawa *et al.* [13-16] have observed demixing of lanthanum manganites for solid oxide fuel cell applications. They ascribed it to the gradient in oxygen potential to which the material was exposed during operation. Van Doorn observed strontium enrichment at the low oxygen partial pressure side of $La_{0.3}Sr_{0.7}CoO_{3-\delta}$ membranes during oxygen permeation [17], which observation was interpreted in terms of demixing phenomena. However, additional experimental and theoretical evidence is required in order to improve the understanding of the demixing-caused degradation of these materials. A complete description of demixing of these materials must also include demixing caused by stress gradients, which is likely to occur in these systems.

References

1   H. Schmalzried, W. Laqua, P.L. Lin, "Crystalline oxide solid solutions in oxygen potential gradients", *Z. Naturforsch.*, **34a** 192 (1979)

2   D. Monceau, G. Petot-Ervas, C. Petot, M.J. Graham, G.I. Sproule, J. Le Duigou, "Kinetic demixing in ceramics under a temperature gradient or during cooling", *Metall. Foundry Eng.*, **20(1)** 277 (1994)

3   D. B. Dimos, "Kinetic demixing and high-temperature creep of solid solution oxides: cobalt-magnesium oxide and zirconium-yttrium oxide", Thesis, Cornell University, USA, 1986

4   M. Filal, M. Tedtoub, D. Monceau, G. Petot-Ervas, C. Petot, "Kinetic demixing of (Co,Mg)O and ZrO_2, Y_2O_3 solid solutions in an electrical field", *Journal de Physique IV*, **3** 1467 (1993)

5   H. Schmalzried, "Chemical kinetics of solids", VCH Verlagsgesellschaft, Weinheim, 1995

6   C.C. Wang, "Degradation of multicomponent oxides under oxygen potential gradients", Thesis, Ohio State University, USA, 1993

7   H. Schmalzried, W. Laqua, "Multicomponent oxides in oxygen potential gradients", *Oxid. Met.*, **15(3-4)** 339 (1981)

8   W. Laqua, H. Schmalzried, "Multicomponent oxides in oxygen potential gradients", *Int. Corros. Conf. Ser.*, Volume Date 1981, NACE-6 (High Temp.Corros.) 115 (1983)

9   H. Schmalzried, "Review: Behavior of (semiconducting) oxide crystals in oxygen potential gradients", *Reactivity of Solids*, **1** 117 (1986)

10   K. Vedula, "Modelling of transient and steady-state demixing of oxide solid solutions in an oxygen chemical potential gradient", *Oxid. Metals*, **28** 99 (1987)

11   T. Ishikawa, H. Sato, R. Kikuchi, S.A. Akbar, "Demixing of materials under chemical potential gradients", *J. Am. Cer. Soc.*, **68** 1 (1985)

12   T. Ishikawa, S.A. Akbar, W. Zhu, H. Sato, "Time evolution of demixing in oxides under an oxygen potential gradient", *J. Am. Cer. Soc.*, **71** 513 (1988)

13   H. Yokokawa, T. Horita, N. Sakai, M. Dokiya, T. Kawada, "Thermodynamic considerations on interfaces in electrochemical devices", International Workshop on Ceramic Interfaces: Properties and Applications III, 1996

14   H. Yokokawa, N. Sakai, T. Horita, M. Dokiya, "Thermodynamic considerations on mass transfer along/across the interfaces", *Proc. Int. Symp. Mat. Chem. Nucl. Env.*, Material Chemistry '96, 401-10

15   H. Yokokawa, T. Horita, N. Sakai, T. Kawada, M. Dokiya, "Role of oxygen at perovskite interfaces", *Proc. - Electrochem. Soc.* **95**-1 975 (1995), (SOFC-IV), -84

16   H. Yokokawa, T. Horita, N. Sakai, M. Dokiya, H. Nishiyama, M. Aizawa, T. Kawada, "Stability of lanthanum calcium chromite-lanthanum strontium manganite interfaces in solid oxide fuel cells", *J. Electrochem. Soc.*, **143** 2332 (1996)

17   R.H.E. van Doorn, H.J.M. Bouwmeester and A.J. Burggraaf, "Kinetic decomposition of $La_{0.3}Sr_{0.7}CoO_{3-\delta}$ perovskite membranes during oxygen permeation," Solid State Ionics, **111** 263 (1998)

Summary

Cobalt based perovskite-type oxygen separation membranes are currently receiving extensive scientific and technological interest due to their wide variety of possible applications in oxygen production, power generation processes and selective hydrocarbon oxidation. A major challenge for large-scale technical applications is to increase the oxygen flux through these membranes and/or to reduce operating temperatures. A logical approach to increase the oxygen flux at a given temperature is the reduction of the membrane thickness to micrometer dimensions by depositing a dense thin-film membrane on a porous support. This approach requires extensive knowledge on oxygen transport properties and ceramic processing of the membrane materials. In this study, the oxygen permeation and transport parameters of dense $La_{1-x}Sr_xCoO_{3-\delta}$ membranes are investigated. The thickness of the membranes under investigation varies from millimeter to micrometer dimensions. In addition, the preparation of the thin-film membrane is studied, which includes the development of a suitable membrane support and the deposition of a dense, micrometer thick film on top of these supports.

In chapter 2, oxygen transport through dense, $La_{1-x}Sr_xCoO_{3-\delta}$ membranes ($x = 0.2$, 0.5 and 0.7) in the thickness range of 0.5-2mm, is investigated using oxygen permeation measurements. The results indicate a clear influence of surface exchange on the oxygen permeation rate. However, the oxygen fluxes remain predominantly controlled by bulk oxygen diffusion through the membrane. The calculated characteristic membrane thickness L_c, below which oxygen transport is predominantly rate limited by surface exchange, varies approximately between 70 and 230 μm. From the oxygen pressure dependence of oxygen permeation it follows that the ionic conductivity of the different compositions $La_{1-x}Sr_xCoO_{3-\delta}$ is unfavourably affected with lowering oxygen partial pressure and temperature, which is attributed to vacancy trapping effects associated with the ordering of oxygen vacancies.

The results of the permeation study are in excellent agreement with observations from conductivity relaxation experiments, which are described in chapter 3. Here, the chemical diffusion coefficient and oxygen transfer coefficients of the same compositions in the series $La_{1-x}Sr_xCoO_{3-\delta}$ are studied using the conductivity relaxation technique. The chemical diffusivity and oxygen surface exchange in the perovskites under study appears to be highly correlated. The general trend displayed is that both parameters decrease with decreasing p_{O_2} below about 10^{-2} bar at all temperatures. This is attributed to ordering of

induced vacancies at low enough oxygen partial pressures. The observation that the correlation between both parameters extends even to the lowest p_{O_2} values in this study, suggests a key role of the concentration of mobile oxygen vacancies, rather than of the extent of oxygen nonstoichiometry, in determining the rate of both processes. The characteristic thickness L_c shows only a weak dependence on oxygen partial pressure temperature and composition and is found to vary between 50 and 150 μm.

Chapters 4 and 5 focus on the development of a supported thin film membrane. In chapter 4, the processing of $La_{1-x}Sr_xCoO_{3-\delta}$ powders into porous supports is described. Two approaches are followed. The first employs pressing of pre-sintered powders, homogenised by sieving and classified through sedimentation. Tuning of the pre-sintering temperature of the powder yields 30% porous materials with an average pore diameter of 0.8 μm. The surface roughness of these supports is rather high but the surface morphology can be improved by applying a perovskite coating. The second approach is based on compact formation by pressure filtration of commercial powder dispersed in isopropanol. Sintering of the substrates at 1020°C resulted in 30% porous materials with an average pore diameter of 0.3 μm. Although a minor amount of defects is present due to inhomogeneities in the powder, the morphology of these substrates is considered to be superior to that of the substrates prepared via pressing. Therefore, it is concluded that the substrates prepared via pressure filtration are most suitable for supporting thin film $La_{1-x}Sr_xCoO_{3-\delta}$ membranes. In the final section of this chapter, the application of centrifugal casting in the development of tubular perovskite substrates is studied. Results of exploratory experiments indicate a great potential of this technique in the preparation of high-quality dense and porous $La_{1-x}Sr_xCoO_{3-\delta}$ tubes. The deposition of $La_{0.5}Sr_{0.5}CoO_{3-\delta}$ films with a thickness of 5-30 μm onto porous substrates using pulsed laser deposition is described in chapter 5. Initial deposition experiments on porous α-Al_2O_3 supports are unsuccessful as crack formation occurs during cooling after the deposition process due to thermal mismatch. When $La_{0.5}Sr_{0.5}CoO_{3-\delta}$ supports are used, dense and crack-free films are obtained.

The permeation measurements of the supported thin-film membranes of $La_{0.5}Sr_{0.5}CoO_{3-\delta}$ are presented in chapter 6. The data show that the oxygen fluxes are significantly higher than those measured for pressed disc membranes. Minor leakage is observed, amounting up to 5% of the total oxygen flux, which is caused by support inhomogeneities, which could not be covered by the laser deposition process. In the experimental range of thickness 7.5-20 μm, the oxygen flux is found to be independent of membrane thickness. A characteristic membrane thickness is calculated of about 50 μm, which value nicely agrees with that extracted from data of conductivity relaxation experiments if it is assumed that

the porous support structure removes surface exchange limitations at the interface between porous support and thin film membrane. Mass transport through the porous support structure contributes significantly to the overall permeation resistance at 1000°C, but its influence becomes negligible at temperatures around 700°C.

In chapter 7, the influence of substitution of cobalt in $La_{0.5}Sr_{0.5}CoO_{3-\delta}$ with 1 to 8 mole % of either copper or nickel on the oxygen permeation rate and transport parameters is studied. Oxygen permeation data indicate that nickel and copper doping results in a significant increase in the permeation rate. The largest increase in flux is measured for the lowest dopant concentration, amounting to a factor 1.4 for the nickel doped and 1.7 for the copper-doped sample. Conductivity relaxation data indicate that doping increases both the surface transfer and the bulk diffusion rates.

The main results achieved in this work are summarised in chapter 8, which also includes recommendations for future research.

Samenvatting

Er bestaat momenteel grote technologische en wetenschappelijk belangstelling voor dichte, kobalt-houdende perovskiet membranen vanwege het brede scala aan toepassingen waarvoor deze membranen geschikt zijn. Mogelijke toepassingen liggen bijvoorbeeld op het gebied van de zuurstofproductie, de energievoorziening en in de selectieve (partiële) oxidatie van koolwaterstoffen. Echter, de zuurstofpermeabiliteit van deze membranen is nog te laag voor grootschalige industriële toepassing. Een logische en tegelijkertijd uitdagende benadering voor het verhogen van de zuurstofflux door deze membranen is het terugbrengen van de membraandikte tot een waarde van enkele micrometers. Om deze membranen voldoende mechanische sterkte te geven dienen ze te worden aangebracht op een poreuze drager. Deze benadering vereist uitgebreide kennis van zowel de zuurstoftransporteigenschappen als de keramische processing van de betreffende membraanmaterialen. In dit onderzoek staan de zuurstofpermeatie-eigenschappen en transportparameters van $La_{1-x}Sr_xCoO_{3-\delta}$ membranen centraal. De dikte van de bestudeerde membranen varieert van millimeters tot enkele micrometers. Bovendien wordt aandacht besteed aan de bereiding van gedragen dunne-film membranen. Hieronder vallen de bereiding van een geschikte poreuze drager en de depositie van een dicht, micrometer dun membraan op deze drager.

In hoofdstuk 2 wordt zuurstoftransport door dichte $La_{1-x}Sr_xCoO_{3-\delta}$ ($x = 0.2$, 0.5 en 0.7) membranen met een dikte variërend van 0.5 tot 2 mm onderzocht door middel van zuurstofpermeatiemetingen. De resultaten laten een duidelijke invloed zien van oppervlakte-uitwisselingsprocessen op de snelheid van zuurstoftransport door deze membranen. De grootte van de zuurstofflux wordt echter voornamelijk bepaald door bulkdiffusie van zuurstof. Om te bepalen in welke mate de oppervlakteprocessen en bulkdiffusie bepalend zijn voor de snelheid van zuurstofpermeatie, is in de literatuur een zogenaamde karakteristieke dikte L_c gedefinieerd. Bij verlaging van de membraandikte beneden deze waarde zal de snelheid van zuurstofpermeatie voornamelijk bepaald worden door oppervlakte-uitwisselingsprocessen, hetgeen uiteindelijk leidt tot een zuurstofflux die onafhankelijk is van de membraandikte. Uit de permeatiemetingen aan de $La_{1-x}Sr_xCoO_{3-\delta}$ membranen volgt een L_c die varieert van 70 tot 230 μm. Uit de variatie van de permeatie met de zuurstofpartiaaldruk blijkt dat de ionogene geleiding voor zuurstof nadelig wordt beïnvloed bij lage zuurstofdrukken en temperaturen. Dit effect wordt toegeschreven aan ordening van zuurstofvacatures.

De resultaten van het permeatieonderzoek komen zeer goed overeen met waarnemingen gedaan aan de hand van geleidingsrelaxatiemetingen. Deze staan beschreven in hoofdstuk 3. In dit hoofdstuk worden de chemische diffusiecoëfficiënt en de zuurstofuitwisselingscoëfficiënt van de zelfde materialen bestudeerd als functie van zuurstofpartiaalspanning en temperatuur. De resultaten tonen aan dat er voor de onderzochte perovskieten een uitgesproken correlatie tussen deze twee transportparameters bestaat. De algemene trend is dat beide parameters bij alle temperaturen sterk afnemen met afnemende zuurstofpartiaaldruk, indien deze lager wordt dan ongeveer 10^{-2} bar. Dit gedrag wordt toegeschreven aan ordening van zuurstofvacatures bij lage zuurstofdrukken. De waarneming dat de correlatie tussen beide parameters zelfs bij de laagste zuurstofdrukken welke onderzocht zijn blijft bestaan, suggereert dat zowel de snelheid van oppervlakte-uitwisseling als die van bulkdiffusie in grote mate afhangt van de concentratie van vrije vacatures, en niet van de totale mate van zuurstof non-stoïchïometrie. De resultaten tonen aan dat de karakteristieke dikte niet sterk afhangt van de zuurstofpartiaaldruk, temperatuur en samenstelling en varieert tussen 50 en 150 μm.

In de hoofdstukken 4 en 5 staat de ontwikkeling van een gedragen dunne film membraan centraal. Hoofdstuk 4 beschrijft de bereiding van poreuze $La_{1-x}Sr_xCoO_{3-\delta}$ dragers. Twee methoden worden gevolgd. Bij de eerste wordt gebruik gemaakt van voorgesinterde poeders, gehomogeniseerd door zeven en geclassificeerd door sedimentatie. Compactering vindt plaats door middel van persen. Afstemming van de sintertemperatuur levert 30% poreuze materialen met een gemiddeld poriediameter van 0.8 μm. De oppervlakteruwheid van deze dragers is vrij hoog maar deze kan verlaagd worden door het toepassen van een perovskiet coating. Bij de tweede methode wordt gebruikt gemaakt van filtratie onder druk van een suspensie van commercieel perovskietpoeder in isopropanol. De resulterende groene compacten worden vervolgens gesinterd bij 1020°C, waarbij 30% poreuze materialen met een gemiddelde poriediameter van 0.3 μm worden verkregen. Ondanks een gering aantal defecten is de oppervlaktemorfologie van deze substraten superieur vergeleken met die van substraten bereid via persen van voorgesinterde poeders. Deze substraten worden dan ook het meest geschikt geacht voor toepassing als drager van dunne film $La_{1-x}Sr_xCoO_{3-\delta}$ membranen. In de laatste sectie van dit hoofdstuk wordt de toepassing van centrifugaal depositie in de bereiding van buisvormige perovskiet substraten onderzocht. De resultaten van het exploratieve onderzoek laten zien dat deze techniek veelbelovend is voor de ontwikkeling van kwalitatief hoogstaande, zowel dichte als poreuze, $La_{1-x}Sr_xCoO_{3-\delta}$ buizen. In hoofdstuk 5 wordt de depositie van 5 tot 30μm dikke $La_{0.5}Sr_{0.5}CoO_{3-\delta}$ films op poreuze substraten met behulp van pulsed laser deposition beschreven. Depositie op poreuze α-Al_2O_3 dragers levert defecte films op doordat deze

scheuren tijdens het afkoelen na depositie. Dit wordt veroorzaakt door het grote verschil in uitzettingscoëfficiënt tussen $La_{0.5}Sr_{0.5}CoO_{3-\delta}$ en α-Al_2O_3. Echter, wanneer depositie plaatsvindt op poreuze $La_{0.5}Sr_{0.5}CoO_{3-\delta}$ substraten, treedt deze scheurvorming niet op en is het resultaat een dichte film.

De permeatiemetingen aan de gedragen dunne film membranen met samenstelling $La_{0.5}Sr_{0.5}CoO_{3-\delta}$ worden beschreven in hoofdstuk 6. De resultaten laten zien dat de zuurstofflux door deze membranen meer dan een orde van grootte hoger is dan die gemeten voor conventionele ongedragen membranen met dezelfde samenstelling, gemeten onder indentieke omstandigheden. De gedragen membranen vertonen een gering lek, in de orde van 5% van de totale zuurstof stroom. Dit lek wordt veroorzaakt door inhomogeniteiten in de drager, welke niet bedekt worden tijdens het depositieproces. Voor de onderzochte dunne film membranen, met een dikte van 7.5 tot 20 μm, is de zuurstofflux onafhankelijk van de filmdikte. De uit deze metingen bepaalde karakteristieke membraandikte is bij benadering 50 μm. Deze waarde komt goed overeen met die bepaald uit geleidingsrelaxatiemetingen, als aangenomen wordt dat de poreuze dragerstructuur de invloed van oppervlakteuitwisselingsprocessen aan het grensvlak tussen de drager en de dunne film, op de totale snelheid van zuurstoftransport, opheft. Het blijkt dat bij 1000°C, het massatransport door de poreuze drager een aanzienlijke bijdrage levert aan de totale weerstand voor zuurstoftransport door het membraan. Echter, deze bijdrage neemt af met temperatuur en is verwaarloosbaar bij temperaturen rond 700°C.

In hoofdstuk 7 wordt de invloed onderzocht van substitutie van kobalt in $La_{0.5}Sr_{0.5}CoO_{3-\delta}$ met 1 tot 8 mol% koper of nikkel op de snelheid van zuurstofpermeatie en de zuurstoftransportparameters. Zuurstofpermeatiemetingen laten zien dat de dotering een duidelijke verhoging van de zuurstofflux tot gevolg heeft. De grootste toename wordt gevonden voor de laagste doteringsconcentratie en bedraagt een factor 1.4 en 1.7 voor respectievelijk het nikkel- en kopergedoteerde materiaal. Geleidingsrelaxatiemetingen laten zien dat de dotering zowel de chemische diffusie als de zuurstofuitwisseling versnelt.

In hoofdstuk 8 worden de belangrijkste resultaten die volgen uit dit onderzoek samengevat en worden aanbevelingen gedaan voor verder onderzoek.

Dankwoord

Mijn promotietijd is voor mij in vele opzichten een hele bijzondere en leerzame periode geweest. Dat er nu uiteindelijk een proefschrift tot stand is gekomen, heb ik grotendeels te danken aan de hulp en steun van de mensen om mij heen. Hier wil ik alle mensen bedanken die, op welke manier dan ook, hebben bijgedragen aan mijn promotieonderzoek.

Als eerste Henny, voor de prettige begeleiding en motivatie in de brede zin van het woord. Dat de hoofdstukken nu zo "lekker lopen en lezen", heb ik voor een groot deel aan jouw inzet te danken. Ik heb de samenwerking als bijzonder plezierig ervaren en heb bewondering voor het enthousiasme wat jij uitdraagt voor de wetenschap. Henk Verweij bedank ik voor de mogelijkheid die hij mij geboden heeft om als OIO onderzoek te verrichten binnen de groep Anorganische Materiaalkunde.

Het team bij EL-TN: Edward, Frank en Dave, bedank ik voor de onmisbare samenwerking en het nauwe overleg, waardoor dit project succesvol afgesloten kon worden. Het technische cluster bij AMK, onder aanvoering van Henk Kruidhof, wil ik bedanken voor alle experimentele en computergerelateerde ondersteuning. In het bijzonder wil ik Gerrit en Natascha bedanken voor de hulp bij het bereiden en polijsten van de vele samples. Verder ben ik Joop en Ruud van de glasinstrumentenmakerij veel dank verschuldigd voor het bewerken van enorme aantallen preparaten en membraanreactoren. Ook Cis bedank ik voor al haar belangstelling en hulp.

Ik had het geluk om met een viertal gemotiveerde, enthousiaste studenten te mogen samenwerken. Hun bijdrage aan mijn onderzoek is van grote waarde. Heidi, Anika, Marnix en Sjoerd, bedankt voor jullie grote inzet! Tevens wil ik Matthijs bedanken voor de samenwerking die geleid heeft tot hoofdstuk 3 van dit proefschrift. Bernard ben ik erkentelijk voor het schrijven van de software voor de uitwerking van de CR data en Jan bedank ik voor het op de valreep uitvoeren van mijn allerlaatste CR experimenten.

In de loop van de tijd hebben vier verschillende kamergenoten met mij opgescheept gezeten. Bij deze bedank ik Ben Bladergroen, Tomas, Fiona en Peter voor de gezellige tijd, de wetenschappelijke, en vele totaal niet-wetenschappelijke discussies. Met name Fiona en Peter wil ik bedanken voor alle steun en de prettige sfeer op onze kamer in de afgelopen 3 jaar! Nieck en Isabel bedank ik voor hun gastvrijheid tijdens de beginperiode van mijn promotie. Monse, voor haar energieke rondleiding door Mexico City en de rest van mijn (oud-)collega's voor alle hulp en gezelligheid in de afgelopen jaren.

Naast het werk als OIO is afleiding uiteraard broodnodig. Annemiek, László, Luc, Peter, Trudy, Barry en Jan-Luuk bedank ik voor de vele geweldige muzikale momenten en de gezelligheid. Tomas, voor de talloze plezierige en ontspannende tennis- en squashwedstrijden. Emile, Barry en Ingrid wil ik in het algemeen bedanken voor alle steun, goede gesprekken en lol. Emile, de geweldige trip naar de VS was memorabel! Verder betekent het einde van mijn promotietijd ook het einde van mijn tijd in huize "De Plantage". Ik wil mijn huisgenoten Hilde, Onno en Tom bedanken voor de gezelligheid, belangstelling en niet te vergeten de dagelijkse portie humor en totale non-sense.

Mijn ouders wil ik bedanken voor hun grote belangstelling, onvoorwaardelijke steun en liefde en die ze mij altijd hebben gegeven. Pa, ma, zonder jullie had ik dit niet kunnen bereiken!

En, Pa, ik heb het in mijn zak!

Tot slot, Alja, bedankt voor je liefde, hulp en medeleven in de afgelopen periode. Het gevoel dat jij mij geeft kan maar door een woord benaderd worden: compleetheid.

Marco

Levensloop

Marco van der Haar werd geboren op 15 september 1972 te Ermelo. Na zijn lagere-schooltijd in Marle genoot hij voortgezet onderwijs op College Noetsele te Nijverdal. Daar behaalde hij in 1989 zijn HAVO diploma, gevolgd door het VWO diploma in 1991. In hetzelfde jaar begon hij aan de Universiteit Utrecht met de studie Scheikunde. In deze periode liep hij stage bij het Shell Research en Technology Center in Amsterdam. Hij studeerde af bij de vakgroep Anorganische Chemie en Katalyse van prof. ir. J.W. Geus met als onderwerp de bepaling van de invloed van de drager en synthesewijze op de performance van kobalt katalysatoren voor de Fischer-Tropsch synthese. In 1996 studeerde hij af en aan het eind van hetzelfde jaar trad hij in dienst bij NWO als onderzoeker in opleiding aan de Universiteit Twente, waar hij onder begeleiding van dr. H.J.M. Bouwmeester en prof. dr. ir. H. Verweij onderzoek verrichtte aan dichte keramische membranen voor zuurstofscheiding. De resultaten van dit onderzoek staan beschreven in dit proefschrift.